People's Democratic Republic of Algeria
ministry of higher education and scientific research

**École Nationale Polytechnique**




**Control Engineering Department**

## Final Project Thesis

Thesis submitted for the degree of state engineer in control engineering

---

# State Estimation for Unmanned Aerial Vehicles Using IMU and UWB

---

**Oussama SIFOUR**

Under the supervision of **M.TADJINE** and **S.BERKANE**

Presented and defended publicly 04/07/2020

**Jury member :**

| | | | |
|---|---|---|---|
| President | R.ILLOUL | MCA | École Nationale Polytechnique- Algiers |
| Supervisors | M. TADJINE | Professor | École Nationale Polytechnique- Algiers |
| | S.BERKANE | PhD | Université du Québec en Outaouis- Canada |
| Examiner | M.CHAKIR | MCA | École Nationale Polytechnique- Algiers |

ENP 2020

RÉPUBLIQUE ALGÉRIENNE DÉMOCRATIQUE ET POPULAIRE
MINISTÈRE DE L'ENSEIGNEMENT SUPÉRIEUR ET DE LA RECHERCHE SCIENTIFIQUE

**École Nationale Polytechnique**

المدرسة الوطنية المتعددة التقنيات
Ecole Nationale Polytechnique

مخبر التحكم في العمليات الصناعية
Laboratoire de Commande des Processus

UQO UNIVERSITÉ DU QUÉBEC EN OUTAOUAIS

**Département d'Automatique**

## Mémoire de projet de fin d'études

pour l'obtention du diplôme d'ingénieur d'état en Automatique

---

# State Estimation for Unmanned Aerial Vehicles Using IMU and UWB

---

**Oussama SIFOUR**

Sous la supervision de **M.TADJINE** et **S.BERKANE**

Présenté et soutenu pibliquement le 04/07/2020

**Composition du Jury :**

| | | | |
|---|---|---|---|
| Président | R.ILLOUL | MCA | École Nationale Polytechnique- Alger |
| Promoteurs | M. TADJINE | Professeur | École Nationale Polytechnique- Alger |
| | S.BERKANE | PhD | Université du Québec en Outaouis- Canada |
| Examinateur | M.CHAKIR | MCA | École Nationale Polytechnique- Alger |

ENP 2020

**ملخص**

في هذه الأطروحة, تم النظر إلى مشكل القياس و التقدير إعتمادا على قسايات المدى و القياسات القسرية لطائرات دون طيار, عدة تقنيات لقياس التوجه تم تقديمها و دراستها و مقارنتها مع بعضها.
تم أيضا تقديم و دراسة طريقتين لقياس حالات الطائرات الغير متسارعة التي تعتمد على قياسات المدى و القياسات القسرية, تمت دراسة أيضا تقنيات الحصول على قياس الوضعية انطلاقا من قياسات المدى في مختلف الحالات أخيرا, تم تقديم و دراسة طريقتين لقياس حالات الطائرات المتساعة باستعمال قياسات المدى و القياسات القسرية, تمت مقارنة مختلف تقنيات القياس و التقدير في مختلف حالات الطيران الممكنة عبر عدة محاكات رقمية لاضهار فعالية التقنيات المدروسة

**الكلمات الدالة** : طائرات دون طيار, قياسات المدى, القياسات القسرية, قياس الحالة.

**Résumé**

Dans cette thèse, le problème d'estimation d'état des véhicules aériens sans pilote utilisant des mesures vectorielles et de distance a été étudié. Plusieurs observateurs non linéaires d'attitude s'appuyant sur les mesures de l'inertial measurement unit (IMU) ont été proposés et comparés.
Deux approches à état complet (orientation, position et vitesse) pour les véhicules non accélérés reposant sur des mesures IMU et UWB ont été proposées et comparées. Des méthodes de reconstruction pour les mesures de position ont été proposées lors de l'utilisation de moins de 4 emetteurs d'UWB.
En outre, deux observateurs non linéaires à état complet ont été proposés, discutés et comparés pour les véhicules accélérés s'appuyant sur des mesures IMU et de distance.
Enfin, toutes les méthodes d'estimation de l'état complet et l'observateur ont été comparées dans différents scénarios pour aider le lecteur à décider et à choisir une méthode d'estimation en fonction des performances requises, des conditions de vol et du scénario.

**Mots clés**: UAV, IMU, UWB, Estimation d'état.

**Abstract**

In this thesis, the state estimation problem for Unmanned aerial vehicles using vector measurements and range measurements was studied. Several nonlinear attitude observers relying on Inertial Measurements Unit (IMU) measurements were proposed and compared.
Two full state (orientation, position and velocity) approaches for non accelerated vehicles relying on IMU and UWB measurements were proposed and compared. Reconstruction methods for position measurements were proposed when using less than 4 UWB anchors.
Furthermore, two nonlinear full state observers for accelerated vehicles relying on IMU and range measurements were proposed, discussed and compared.
Finally, all the full state estimation methods and observer were compared in different scenarios to help the reader decide and choose an estimation method according to needed performance and flight condition and scenario.

**Key words**: UAV, IMU, UWB, State estimation.

# *Acknowledgment*

I would like to express my gratitude for my advisors **Pr. Mohamed TADJINE** and **Dr. Soulaimane BERKANE** for their help, patience and guidance through the thesis.

I want to thank **Pr. Mohamed TADJINE** for instilling in me a genuine passion for control engineering and for sharing his knowledge and experience as a teacher and a supervisor.

I want to thank **Dr. Soulaimane BERKANE** for being an excellent mentor and supervisor and sharing with me his considerable knowledge.

I would also like to thank my friends with whom I have spent three years at the control engineering department learning, exchanging and laughing.

Lastly, I wish also to thank the members of my family, in particular my mother and father and my sisters for their endless support and love.

*Dedicated to my mother and father, to my sisters, my friends and family and all those whom I care about...*

# Contents

# List of Figures

CHAPTER 1

# Introduction

## 1.1 Introduction

Unmanned Aerial Vehicles (UAVs) have gained a lot of interest over the last decade due to their simplicity as well as their flexibility to reach difficult places, maneuverability, stability and Take-Off and Landing capabilities. The popularity of UAVs has grown for both military and civil applications. They have been used in several applications such as surveillance, rescue, film making, structural inspection and maintenance. Their suitability and efficiency in accomplishing missions in the mentioned applications brought them rising attention from the public, turning them into an intriguing research topic. One of the trend topics in the development of UAVs is related to the state estimation problem. Determining the vehicle's state precisely is a basic requirement to achieve reliable control and autonomous flight. In this thesis, we focus on the full estimation of the UAV's states(attitude, poistion and velocity). Early works on state estimation rely mainly on Kalman type filters [20],[1]. Most common sensors deployed in UAVs are Inertial Measurements Unit (IMU) [12], cameras and range measurements such as GPS [7] or Ultra-Wide band sensors [4]. The purpose of this thesis is to propose and study different nonlinear observers for state estimation in different navigation scenarios and different flight conditions.

## 1.2 Motivation

The recent proliferation of Micro-Electro-Mechanical Systems (MEMS) components has lead to the development of a range of low cost and light weight sensors such as Inertial Measurement Unit (IMU), Global Positioning System (GPS), etc. The low power, light weight and potential for low cost manufacturing of these sensors made them cheaper and widely available.

The motivation behind this thesis relies on the use of these low cost sensors to reach a reliable estimation, as precisely determining the state of the UAV is the key step to achieve robust control and autonomous flight. However, these cheap sensors often output low resolution signals which are subject to high levels of noise. To achieve the main goal of this thesis, robust nonlinear observers need to be developed, studied and compared in different scenarios and flight conditions.

## 1.3 Litterature Review

As the UAVs states are not directly measurable, sensors are often used to estimate its value such as : magnetometer, accelerometer and gyroscope. The accelerometer provides a body referenced acceleration, the magnetometer provides a body referenced earth magnetic field measurement, and the gyroscope provides the body referenced angular velocity. The

straight integration of an IMU measurements would be a simple, yet ineffective way to determine the attitude of the UAV. This approach is ineffective as it leads to a drift over time in the attitude estimate as well as in the linear velocity and position estimates, due to the inherent gyro bias and numerical integration. Another ineffective method for attitude estimation is one that relies solely on inertial vector measurements such as those proposed in $[8] - [6]$. Again, this approach, referred to as static attitude determination, is ineffective in the presence of measurement noise. It is evident that sensor noise causes a major issue when trying to estimate the attitude of a rigid body, and thus, filtering techniques must be implemented. Filtering techniques combine the rigid body kinematic model and sensor measurements to produce a good estimate of the state of the rigid body. Such technique is the Kalman Filter (KF) [13] which consists of two steps : first the current state estimates are updated using the previous states and dynamical model of the system. Second, they are further updated using weighted noisy sensor measurements. The states estimated are then used in the next cycle. The KF has been originally designed for linear systems and does not apply directly to nonlinear systems. A common approach the deals with noisy nonlinear systems is known as the Extended Kalman Filter (EKF). This approach is not guaranteed to provide a good performance when the initial errors are wide, as it relies on system linearization. Further developments led to the Multiplicative [6] and Additive [24] Kalman Filters (MEKF and AEKF respectively). Although these methods provide acceptable attitude estimation, they are computationally expensive and as such, are not often implemented on small quadrotor UAVs, where the processing power is limited.

A computationally efficient alternative for attitude estimation relies upon the nonlinear dynamics of the system may instead be implemented. Many such complementary filters can be found in the literature $[10] - [10]$, some of which utilize the full Direction cosine Matrix (DCM) $[15], [10]$, and others relying only on the unit Quaternion representation $[10], [17]$. All of these nonlinear observers utilize the assumption that the accelerometer measures the gravity vector in the body frame, which is only valid under low transitional acceleration. If the UAV undergoes a large transitional acceleration, the estimation from these observers will become unreliable. To overcome this problem, nonlinear observers that also include the transnational state [7], [21], determined from say a GPS or UWB array, are utilized for UAVs expected to go through some high acceleration movements. These observers utilize an additional transitional state estimate function in the innovation term of the observer. A problem with any of these observers is that the earth's magnetic field becomes very difficult to measure once the motors of the UAV are activated, as these produce their own magnetic field further corrupting the measured vector. This problem can be mitigated with a calibration technique such as one described in [9]. Further through the vector decoupling strategy proposed with the observers of $[10], [11]$, this coupling problem can be minimized.

## 1.4 Thesis Contribution

The first two thesis contributions are based on previous work in the attitude estimation field such as [14] were the innovation term was borrowed and modified. The same approach was used to the full state estimation observers proposed in [4] and [5] in the last two contribution. To summarize, the thesis contribution are as follows :

- A sliding mode attitude observer that estimates the orientation directly on the Special Orthogonal group is proposed and studied in Chapter 3.
- A super twisting Observer for attitude estimation is proposed in Chapter 3.
- A reconstruction technique for position measurements when using 3 UWB anchors is proposed in Chapter 4.
- An algorithm that outputs the position measurements when using 2 UWB anchors and an Altimeter is proposed in Chapter 4.
- A full state estimation approach that uses Sliding mode observer and Kalman filter for non accelerated vehicles is studied in Chapter 5.
- A simplified and modificated version of a full state observer is proposed in Chapter 6.

## 1.5 Thesis Outline

This thesis is organised as follows :

- **Chapter 2** presents the notation, tools and mathematical background and preliminaries used throughout the thesis, as well as a rigid body model and dynamics.
- **Chapter 3** is devoted for the attitude estimation problem and studies various nonlinear attitude observers and compare between the performance of these observers.
- **Chapter 4** presents the UWB technology and methods to reconstruct the position measurements when using less than 4 UWB anchors.
- **Chapter 5** is devoted for full state estimation for UAVs undergoing near to zero linear accelerations and a comparison study between different full state estimation approaches.
- **Chapter 6** is devoted for full state estimation for UAVs performing all kind of accelerations and a comparison study between the full state observers.

- **Chapter 7** presents a general conclusion about the thesis work and results and future interests.

CHAPTER 2

# Mathematical Background

# 2.1 Introduction

In this chapter, we review some of the mathematical background that is used in the development and analysis of the estimation laws. A major component of this background involves the definitions of the attitude parameterizations used to describe the orientation of a rigid-body. A description of these attitude parameterizations and some of these properties are provided in Section 2.1. Section 2.2 defines the equations which govern the vehicle dynamics (system model), and Section 2.3 reviews some preliminary mathematical tools that will be helpful during the discussion of the estimation and control algorithms.

# 2.2 Attitude Representations

## 2.2.1 Coordinate Frames

To represent the orientation of a rigid body, we introduce two reference frames:

- **Inertial frame** $\mathcal{I}$: a frame rigidly attached to a position on the Earth.
- **Body-attached frame** $\mathcal{B}$: a frame which is rigidly attached to the vehicle center of gravity.

Throughout the thesis, we often refer to the orientation of the rigid-body, by which we mean the relative orientation of $\mathcal{B}$ with respect to $\mathcal{I}$. The goal of the attitude representation is to mathematically describe the orientation of the rigid-body.

## 2.2.2 Euler Angles Representaion

The most intuitive method for attitude parametrization is the Euler angles that parametrizes the attitude with three angles $(\phi, \theta, \psi)$, known as the roll, pitch and yaw. A rotation about the inertial frame $\hat{x}$ $\hat{y}$, and the $\hat{z}$ axis are shown below

$$\mathbf{R}_{\hat{x}}(\phi) = \begin{pmatrix} 1 & 0 & 0 \\ 0 & \cos\phi & -\sin\phi \\ 0 & \sin\phi & \cos\phi \end{pmatrix},$$
$$\mathbf{R}_{\hat{y}}(\theta) = \begin{pmatrix} \cos\theta & 0 & \sin\theta \\ 0 & 1 & 0 \\ -\sin\theta & 0 & \cos\theta \end{pmatrix},$$
$$\mathbf{R}_{\hat{z}}(\psi) = \begin{pmatrix} \cos\psi & -\sin\psi & 0 \\ \sin\psi & \cos\psi & 0 \\ 0 & 0 & 1 \end{pmatrix}.$$

As the orthogonal base vector is altered after each rotation, it is possible to represent any orientation. For example performing 3 rotations in the $x-y-z$ order results in the following rotation matrix.

$$\mathbf{R} = \mathbf{R}_{\hat{z}}(\psi)\mathbf{R}_{\hat{y}}(\theta)\mathbf{R}_{\hat{x}}(\phi) = \begin{pmatrix} c\phi c\psi - s\phi s\psi c\theta & -c\phi s\psi\omega\theta - s\phi\alpha\psi & s\psi s\theta \\ s\phi c\psi c\theta + c\phi s\psi & c\phi(\psi c\theta - s\phi s\psi & -c\psi s\theta \\ s\phi s\theta & c\phi s\theta & c\theta \end{pmatrix},$$

with $c(.)$ and $s(.)$ are cosin and sin functions. For small rotations about the three axes this matrix is given as :

$$\mathbf{R} = \begin{pmatrix} 1 & -\psi - \phi & 0 \\ \phi + \psi & 1 & -\theta \\ 0 & \theta & 1 \end{pmatrix}$$

which show that we can not represent a small rotation about the $\hat{y}$ axis. This problem is known as gimbal lock, and causes the rotation matrix to undergo a large change in an infinitcsimal amount of time, this issuc ariscs for rotations of $\pm\pi$ about the $\hat{y}$ axis as well.

### 2.2.3 Rotation Matrix

The direct-cosine, or rotation matrix, is a three-dimensional orthogonal matrix. A matrix $R \in \mathbb{R}^{3\times3}$ is considered a rotation matrix if it is contained within the set

$$\mathbb{SO}(3) := \left\{ R \in \mathbb{R}^{3\times3} | \det(R) = 1 | R^\top R = RR^\top = I_{3\times3} \right\}. \tag{2.1}$$

The set $\mathbb{SO}(3)$ forms a group with the linear matrix multiplication with identity element $I = I_3$ and inverse $R^{-1} = R^\top$. This set is often used since it offers a global and unique representation of the orientation of a frame of reference, and therefore we refer to this set as the rotation space. The Lie algebra of $\mathbb{SO}(3)$ is denoted by $\mathfrak{so}(3)$ and consists of all skew-symmetric 3 by 3 matrices

$$\mathfrak{so}(3) := \left\{ \Omega \in \mathbb{R}^{3\times3} : \Omega^\top = -\Omega \right\}. \tag{2.2}$$

The Lie algebra $\mathfrak{so}(3)$ is isomorphic to $\mathbb{R}^3$ through the map $[\cdot]\times : \mathbb{R}^3 \to \mathfrak{so}(3)$ defined by:

$$\omega \mapsto [\omega]_\times = \begin{bmatrix} 0 & -\omega_3 & \omega_2 \\ \omega_3 & 0 & -\omega_1 \\ -\omega_2 & \omega_1 & 0 \end{bmatrix}. \tag{2.3}$$

The rotation matrix $R \in \mathbb{SO}(3)$ can be used to map vector coordinates from one frame to another. For example, let $x_1$ denote the coordinates of a vector in frame $\mathcal{I}$, and $x_2$ denotes the coordinates of $x_1$ expressed in frame $\mathcal{B}$. Let $R$ denotes the rotation matrix

which describes the rotation from $\mathcal{I}$ to $\mathcal{B}$. Then, a well known property of the rotation matrix is:

$$x_2 = R^\top x_1.$$

The rotation matrix can also be expressed in terms of the axis-angle representation. For example, if we let $u \in \mathbb{R}^3$ denotes a unit-length vector of rotation and $\theta \in \mathbb{R}$ denotes the corresponding angle of rotation, then the corresponding rotation matrix $R(u, \theta) \in \mathbb{SO}(3)$ is given by the following transformation:

$$R(\theta, u) = \exp([\theta u]_\times) = I + \sin(\theta)[u]_\times + (1 - \cos(\theta))[u]_\times^2. \tag{2.4}$$

For a given matrix $R \in \mathbb{SO}(3)$, this parametrization is not unique. In fact, for attitudes of angle $\pi$, it is not difficult to show that $R(\pi, u) = R(-\pi, u)$ for all $u \in \mathbb{S}^2$ : the unit $n$-sphere embedded in $\mathbb{R}^3$.

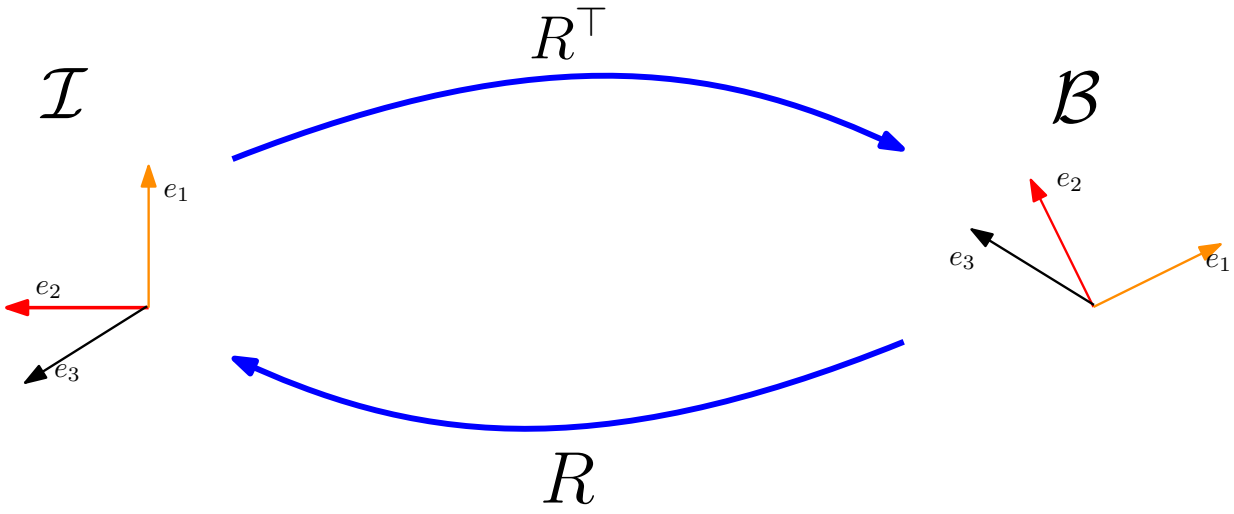


Figure 2.1: Rotation of $\mathcal{B}$ with respect to $\mathcal{I}$ frame.

### 2.2.4 Unit Quaternion

The unit quaternion representation of an attitude is a four element parametrization defined on the space

$$\mathbb{Q} = \left\{ Q = (q_0, q) \in \mathbb{R} \times \mathbb{R}^3 | {q_0}^2 + q^\top q = 1 \right\}.$$

A unit quaternion can be described in terms of the angle-axis representation as follows:

$$Q = \begin{pmatrix} q_0 \\ q_1 \\ q_2 \\ q_3 \end{pmatrix} = \begin{pmatrix} \cos(\gamma/2) \\ \sin(\gamma/2)\hat{k}_1 \\ \sin(\gamma/2)\hat{k}_2 \\ \sin(\gamma/2)\hat{k}_3 \end{pmatrix} = \begin{pmatrix} q_0 \\ q \end{pmatrix}, \tag{2.5}$$

where $\gamma$ is a rotation about the unit vector $\mathbf{u} := [\hat{u}_1; \hat{u}_2; \hat{u}_3]^\top$. The composition of two rotations described by two quatemions $Q_1$ and $Q_2$ is given by :

$$Q_1 \odot Q_2 = \begin{pmatrix} q_{01}q_{02} - q_1^\top q_2 \\ q_{01}q_2 + q_{02}q_1 + [q_1]_\times q_2 \end{pmatrix} \tag{2.6}$$

The unit quaternion $Q_I = [1; 0; 0; 0]^\top$ is the identity element, such that :

$$Q \odot Q^{-1} = Q^{-1} \odot Q = \begin{pmatrix} 1 \\ 0 \\ 0 \\ 0 \end{pmatrix}, \tag{2.7}$$

where

$$Q^{-1} = \begin{pmatrix} q_0 \\ -q \end{pmatrix}. \tag{2.8}$$

For a given vector $v \in \mathbb{R}^3$, where $v_I = Rv_B$ one can write

$$\bar{v}_I = Q \odot \bar{v}_B \odot Q^{-1}, \tag{2.9}$$

where $Q$ is the unit-quatemion associated with the rotation matrix $R$ and $\overline{v_I} = \begin{bmatrix} 0 & v_I^T \end{bmatrix}^\top$ and $\overline{v_B} = \begin{bmatrix} 0 & v_B^T \end{bmatrix}^\top$. Furthermore, the nine element rotation matrix can be expressed with the unit quatemion through the Rodriguez map $\mathcal{R}(Q) : Q\mathbb{SO}(3)$

$$\mathcal{R}(Q) = I_3 + 2q_0[q]_\times + [q]_\times^2. \tag{2.10}$$

The unit quaternion parametrization only requires a 4-element vector, making it computationally efficient for real world applications. It comes with the drawback that it is a non-unique representation of the attitude, since $R$ can be represented by either $Q$ or $-Q$ as evident from (2.10).

## 2.3 Rigid Body Dynamics

The motion of a rigid body navigating in three dimensional space can be broken into two main categories : transational motion and rotational motion. The transational dynamics are given by :

$$\dot{p}(t) = v(t), \tag{2.11}$$
$$\dot{v}(t) = ge_3 + R(t)a_B, \tag{2.12}$$

where $p(t) \in \mathbb{R}^3$ is the inertial position of the vehicle's center of gravity, $v(t) \in \mathbb{R}^3$ represents the inertial linear velocity, $R \in \mathbb{SO}(3)$ is the attitude matrix describing the orientation of a body-attached frame with respect to the inertial frame, $g$ is the norm of the acceleration due to gravity, $e_3 = [0; 0; 1]$ and $a_B(t) = R(t)a_I(t)$ is the "apparent acceleration", capturing all non-gravitational forces applied to the vehicle, expressed in the body-attached frame.

The rotational dynamic is derived from the orthogonality condition $RR^\top = I$ which gives

$$\frac{d}{dt}\left(R^\top R\right) = R^\top \dot{R} + (\dot{R})^\top R = 0. \tag{2.13}$$

It follows that $R(t)^\top \dot{R}(t) \in \mathfrak{so}(3)$ for all times $t \geq 0$ or, equivalently, there exists $\omega(t) \in \mathbb{R}^3$ such that $R(t)^\top \dot{R}(t) = [\omega(t)]_\times$. This leads to write

$$\dot{R}(t) = R(t)[\omega(t)]_\times, \tag{2.14}$$

which represents the attitude kinematics where $\omega(t)$ is referred to as the angular velocity vector. If $R$ is a rotation matrix describing the orientation of a body frame with respect to an inertial frame then $\omega(t)$ is the body-referenced (expressed in body frame coordinates) angular velocity of the body frame with respect to the inertial frame.

## 2.4 Numerical Integration on $\mathbb{SO}(3)$

Numerical integration methods that preserve some proprieties of differential manifolds have been widely discussed. Among these methods, The Lie-Euler integration method for the $\mathbb{SO}(3)$ Lie-group that preserves the determinant propriety of this group. Consider the following initial value problem on $\mathbb{SO}(3)$ :

$$\dot{R} = R[\omega]_\times, \qquad R(0) \in \mathbb{SO}(3). \tag{2.15}$$

The Lie-Euler formula for this problem is given by :

$$R_{n+1} = R_n \exp(h[\omega_n]_\times), \qquad R(0) \in \mathbb{SO}(3) \tag{2.16}$$

with $h$ being the integration step and the exponential map $\exp\left([x]_\times\right) \in \mathbb{SO}(3)$ is defined by the Rodriguez Formula on $\mathbb{SO}(3)$

$$\exp\left([x]_\times\right) = \begin{cases} I & x = 0 \\ I + \frac{\sin(\|x\|)}{\|x\|}[x]_\times + \frac{1-\cos(\|x\|)}{\|x\|^2}[x]_\times^2 & x \neq 0 \end{cases} \tag{2.17}$$

## 2.5 Mathematical Definitions and Identities

### 2.5.1 Metrics on $\mathbb{SO}(3)$

Roughly speaking, a metric (or distance) tells us how two elements of a given manifold are close to each other. More rigorously, a metric on $\mathbb{SO}(3)$ is a function $\mathbf{d} : \mathbb{SO}(3) \times \mathbb{SO}(3) \to \mathbb{R}_{\geq 0}$ that satisfies the following properties for all $R_1, R_2, R_3 \in \mathbb{SO}(3)$

- **Non-negativity :** $\mathbf{d}(R_1, R_2) \geq 0$.
- **Identity of indiscernibles :** $\mathbf{d}(R_1, R_2) = 0$ if and only if $R_1 = R_2$.
- **Symmetry :** $\mathbf{d}(R_1, R_2) = \mathbf{d}(R_2, R_1)$.
- **Triangle inequality :** $\mathbf{d}(R_1, R_3) \leq \mathbf{d}(R_1, R_2) + \mathbf{d}(R_2, R_3)$.

One possible way to measure the distance between two rotation matrices on $\mathbb{SO}(3)$ is to use the Frobenious norm on the embedding Euclidean space $\mathbb{R}^{3\times 3}$ as follows:

$$\mathbf{d}_E(R_1, R_2) = \|R_1 - R_2\|_F, \tag{2.18}$$

which defines the Euclidean (or Chordal) distance on $\mathbb{SO}(3)$. It can be verified that $\mathbf{d}_E(\cdot, \cdot)$ satisfies the following property

$$\mathbf{d}_E(R_1, R_2) = \mathbf{d}_E\left(I, R_1 R_2^\top\right) = \sqrt{2\,\mathrm{tr}\left(I - R_1 R_2^\top\right)} \leq \sqrt{8}, \tag{2.19}$$

where the fact that $R_1 R_2^\top \in \mathbb{SO}(3)$, and hence $\mathrm{tr}(R_1 R_2) \geq -1$, has been used to obtain the upper bound of $\mathrm{d}_E(\cdot, \cdot)$. Throughout this work, the following normalized attitude norm on $\mathbb{SO}(3)$ is used

$$|R|_I = \frac{\mathrm{d}_E(I, R)}{\sqrt{8}} = \frac{\|I - R\|_F}{\sqrt{8}} = \frac{\sqrt{\mathrm{tr}(I - R)}}{\sqrt{4}}. \tag{2.20}$$

### 2.5.2 Stability

Various types of stability may be discussed for the solutions of differential equations describing dynamical systems. The most important type is that concerning the stability of solutions near to a point of equilibrium. This may be discussed by the theory of *Aleksandr Lyapunov*. In simple terms, solution will stay arbitrary near $x_0$ if they start sufficiently near$x_0$. More strongly, if $x_0$ is Lyapunov stable and all solutions that start out near $x_0$ converge to $x_0$, then $x_0$ is asymptotically stable. The notion of exponential stability guarantees a minimal rate of decay, i.e., an estimate of how quickly the solutions converge. For more formal stability definitions the reader is referred to Khalil (2002).

**Theorem 1.** *(Khalil 2002): Let $f(x)$ be a locally Lipschitz function defined over a domain $D \subset R^n$, which contains the origin, and $f(0) = 0$. Let $V(x)$ be a continuously differentiable function defined over $D$ such that*

$$V(0) = 0 \text{ and } V(x) > 0 \text{ for all } x \in D \text{ with } x \neq 0 \tag{2.21}$$

$$\dot{V}(x) \leq 0 \text{ for all } x \in D \tag{2.22}$$

*Then, the origin is a stable equilibrium point of $\dot{x} = f(x)$. Moreover, if*

$$\dot{V}(x) < 0 \text{ for all } x \in D \text{ with } x \neq 0 \tag{2.23}$$

*then origin is asymptotically stable. Furthermore, if $D = R^n, (3.7)$ and (3.9) hold for all $x \neq 0$, and*

$$\|x\| \to \infty \Rightarrow V(x) \to \infty \tag{2.24}$$

*then the origin is globally asymptotically stable.*

**Theorem 2.** *(Khalil 2002) Let $f(x)$ be a locally Lipschitz function defined over a domain $D \subset R^n$, which contains the origin, and $f(0) = 0$. Let $V(x)$ be a continuously differentiable function defined over $D$ such that*

$$k_1\|x\|^a \leq V(x) \leq k_2\|x\|^a. \tag{2.25}$$

$$\dot{V}(x) \leq -k_3\|x\|^a. \tag{2.26}$$

*for all $x \in D$, where $k_1, k_2, k_3$, and $a$ are positive constants. Then, the origin is an exponentially stable equilibrium point of $\dot{x} = f(x)$. If the assumptions hold globally, the origin will be globally exponentially stable.*

### 2.5.3 Useful Mathematical Identities

In this subsection, useful relations and lemmas, which will be used throughout the thesis are provided.

For any $M, N \in \mathbb{R}^{3\times3}, x, y \in \mathbb{R}^3$ and $\alpha \in \mathbb{R}$ one has:

$$\operatorname{tr}\left(M^{\top}\right) = \operatorname{tr}(M), \tag{2.27}$$
$$\operatorname{tr}(M+N) = \operatorname{tr}(M) + \operatorname{tr}(N), \tag{2.28}$$
$$\operatorname{tr}(\alpha M) = \alpha \operatorname{tr}(M), \tag{2.29}$$
$$\operatorname{tr}(MN) = \operatorname{tr}(NM), \tag{2.30}$$
$$\operatorname{tr}(MN) = 0 \quad \left(\text{if } M = M^{\top} \text{ and } N = -N^{\top}\right), \tag{2.31}$$
$$\det(MN) = \det(M)\det(N), \tag{2.32}$$
$$\det\left(I + xy^{\top}\right) = 1 + x^{\top}y. \tag{2.33}$$

Using these propertics of the trace function, the following identities are ensily derived in a straightforward manner. For all $x, y \in \mathbb{R}^3$ and $R, P \in \mathbb{SO}(3)$ one has

$$\operatorname{tr}\left(xy^{\top}\right) = x^{\top}y, \tag{2.34}$$
$$\operatorname{tr}\left(yx^{\top}\left(I - RP^{\top}\right)\right) = \frac{1}{2}\left\|R^{\top}x - P^{\top}y\right\|^2 - \frac{1}{2}\|x-y\|^2. \tag{2.35}$$

For any $x, y \in \mathbb{R}^3$ one has

$$[x]_{\times}y = x \times y, \tag{2.36}$$
$$[x]_{\times}y = -[y]_{\times}x, \tag{2.37}$$
$$[x]_{\times}^3 = -\|x\|^2[x]_{\times}, \tag{2.38}$$
$$[x]_{\times}[y]_{\times} = -\left(x^{\top}y\right)I + yx^{\top}, \tag{2.39}$$
$$x \times y = 2\psi\left(yx^{\top}\right), \tag{2.40}$$
$$[x \times y]_x = yx^{\top} - xy^{\top}, \tag{2.41}$$
$$\ll A, B \gg_f = \operatorname{tr}(A^{\top}B), \tag{2.42}$$
$$\left\langle\langle [x]_{\times}, [y]_{\times}\right\rangle\rangle_f = 2x^{\top}y. \tag{2.43}$$

Where $\ll ., . \gg_f$ represents the Forbenius inner product. Moreover, for any $x, y \in \mathbb{R}^3, M \in \mathbb{R}^{3\times 3}$ and $R \in \mathbb{SO}(3)$ the following relations hold

$$\left\langle\langle M, [x]_{\times}\right\rangle\rangle_f = \left\langle\langle \pi_a(M), [x]_{\times}\right\rangle\rangle_f, \tag{2.44}$$
$$[(Mx)\times(My)]_{\times} = M[x\times y]_{\times}M^{\top}, \tag{2.45}$$
$$M[x]_{\times} + [x]_{\times}M^{\top} = \left[\left(\operatorname{tr}(M)I - M^{\top}\right)x\right]_{\times}, \tag{2.46}$$
$$\psi(MR) = R^{\top}\psi(RM), \tag{2.47}$$
$$R[x]_{\times}R^{\top} = [Rx]_{\times}. \tag{2.48}$$

where $\pi_a, \pi_s$ denote, respectively, the anti-symmetric and symmetric projection operators in square matrix space defined as follows :

$$\pi_a(H) = \frac{1}{2}\left(H - H^T\right), \quad \pi_s(H) = \frac{1}{2}\left(H + H^T\right).$$

CHAPTER 3

# Attitude Estimation

## 3.1 Introduction

In this chapter, different kinds of observers of the rotation matrix $R$ are introduced and compared in Section 3.7. In control theory, an observer gives an estimate of an internal state of a system from measurements of the input and output of the system. In this case, the measurements are provided by sensor readings from the Inertial Measurement Unit (IMU) as elaborated in the first section. Feedback control of the system is applied to the observers' estimation, because the measurements depend on the accuracy of the equipment. In this case, the state of the attitude $R \in \mathbb{SO}(3)$ of the vehicle is estimated. The vehicle's position depends on the orientation. Therefore, it is essential that the state estimate of the orientation is as accurate as possible. Four different kinds of attitude estimation and reconstruction are elaborated. First, The TRIAD reconstruction algorithm is introduced in section 3.3. Complementary filter and a sliding mode-based observer are studied respectively in section 3.4 and 3.5. Finally the second order sliding mode or Super-twisting observer is presented in section 3.6.

## 3.2 IMU Measurements and Observability

### 3.2.1 Inertial Measurements Unit (IMU)

An Inertial Measurement Unit (IMU) is an electronic device (sensor) that measures and reports a body's specific force, angular rate, and sometimes its orientation using a combination of accelerometers, gyroscopes, and sometimes magnetometers.

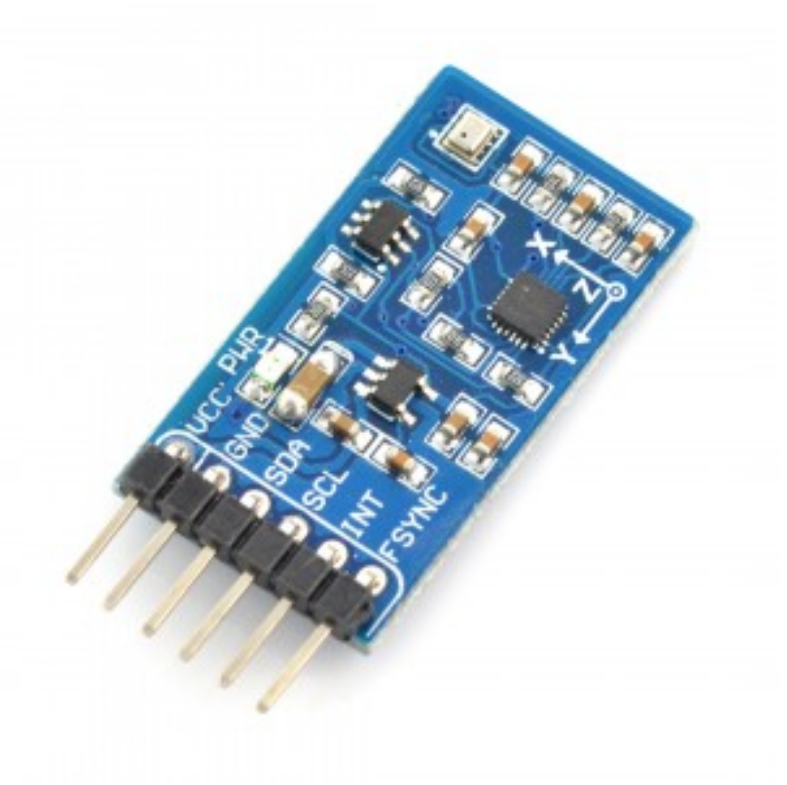


Figure 3.1: MEMS Inertial Measurements Unit

### Accelerometer

An accelerometer is an electromechanical device used to measure acceleration forces. Such forces may be static, like the continuous force of gravity or, as it is the case with many mobile devices, dynamic to sense movement or vibrations. Acceleration is the measurement of the change in velocity, or speed divided by time.

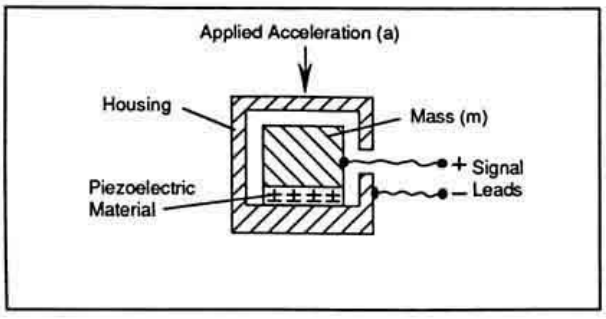


Figure 3.2: accelerometer functionning schemes

### Gyroscope

A gyroscope is a device used to measure the angular velocity of an object. It is made of a spinning wheel or disc in which the axis of rotation (spin axis) is free to assume any orientation by itself. When rotating, the orientation of this axis is unaffected by the tilting or the rotation of the mounting, according to the conservation of angular momentum.

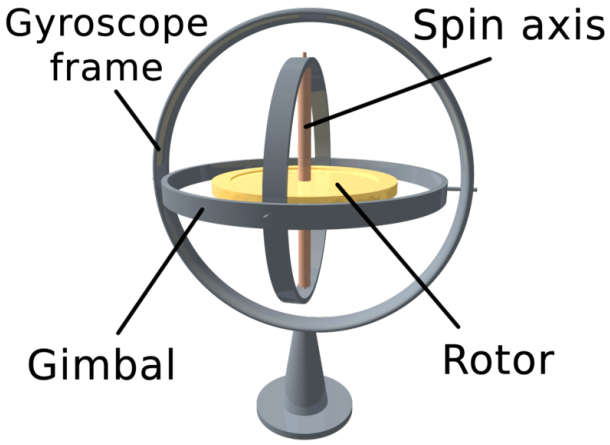


Figure 3.3: Gyroscope

When MEMS (Micro-Electromechanical Systems) technology emerged, a miniaturized MEMS-Gyroscope based on the Foucault pendulum coupled with a vibrating element has been made.

### Magnetometer

A magnetometer is a device that measures direction, strength, or relative change of a magnetic field at a particular location. Measurement of the magnetization of a material (like a ferromagnet) is an example of its use. A compass can be considered as a magnetometer that measures the direction of an ambient magnetic field, in this case, Earth's magnetic field.

In this work,IMUs that provide measurements of angular velocity, body-attached frame apparent acceleration and body-attached frame magnetic field are assumed available. These sensors are modelled as follows:

$$\omega^y = \omega + \eta_\omega, \tag{3.1}$$

$$m_B = R^\top m_I + \eta_{mag}, \tag{3.2}$$

$$a_B = R^\top a_I + \eta_{acc}, \tag{3.3}$$

where $m_I$ is the constant and known earth's magnetic field and $a_I$ a time-varying unknown apparent acceleration. $\eta_\omega$,$\eta_{mag}$ and $\eta_{acc}$ are respectively gyroscope, magnetometer and accelerometer noises.

### 3.2.2 Observability Assumption

In this subsection, observability assumptions needed to design a converging attitude observer is discussed. The following is a general assumption used in attitude estimation field:

**Assumption 1.** There exists a constant $c0 > 0$ such that $\|m_I \times a_I\| \geq c_0$ for all $t \geq 0$.

Assumption 1 is guaranteed if the time-varying apparent acceleration $a_I(t)$ is non-vanishing and is always non-collinear with the constant magnetic field vector $m_I$. Note that $(a_I(t) = 0)$ corresponds to the rigid body part of a free-fall case which is not likely under normal flight conditions.

**Assumption 2.** There exists a constant $c_3 \geq 0$ such that $\|\omega(t)\| \leq c_4$.

Assumption 2 is due to real physical constraints on the system trajectory which are needed in the stability analysis.

**Assumption 3.** The linear acceleration of the vehicle is near to zero $a_I \approx -ge_3$.

### 3.2.3 Objective

The objective is to design a robust attitude observer that takes measurements (3.1)-(3.3) and outputs reliable orientation estimation.

## 3.3 Attitude Reconstruction

Utilizing a widely available Inertial Measurement Unit (IMU), that gives the two non co-linear vector measurements $a_B$ and $m_B$ given by (3.1)-(3.3) and relying on Assumption 3. One can consider that the initial counterpart $a_I$ of the vector $a_B$ is known and corresponds to the earth's gravitational vector $a_I = [0; 0; g]^\top$. To reconstruct the attitude a third vector $w_B$ can be defined as follows:

$$w_B = [a_B]_\times m_B \tag{3.4}$$

Likewise :

$$w_I = [a_I]_\times m_I \tag{3.5}$$

Arranging the three vectors side by side gives the following relation that will be used to determine the $R$ matrix.

$$\begin{bmatrix} a_I & m_I & w_I \end{bmatrix} = R^\top \begin{bmatrix} a_B & m_B & w_B \end{bmatrix} \tag{3.6}$$

which can be solved :

$$R^\top = \begin{bmatrix} a_B & m_B & w_B \end{bmatrix} \begin{bmatrix} a_I & m_I & w_I \end{bmatrix}^{-1} \tag{3.7}$$

### 3.3.1 Numerical Simulation

In this subsection, we implement the attitude observers defined in previous section to estimate the vehicle orientation directly on $\mathbb{SO}(3)$ using IMU measurements. Consider a vehicle navigating with the following angular velocity applied to :

$$\omega(t) = \begin{bmatrix} 0.3\cos(\pi t/10) \\ 0.5\cos(2\pi t/10 + \pi/4) \\ 0.8\cos(4\pi t/10) \end{bmatrix} \tag{3.8}$$

With an initial attitude $R(0) = \exp(\frac{\pi}{2}[e_3]_\times)$. The inertial earth's magnetic field is taken as$m_I = [0.42; 0.2949; 0.15]^\top$Gauss, and the earth's gravity is $g = 9.81 m/s^2$. The initial conditions of the observer is $\hat{R}(0) = I_3$. The measurement noises are modelled as a Gaussian white noises with variances, $\sigma_\omega = 0.16(deg/s^2)$, $\sigma_{acc} = 3.10^{-4}(m/s^2)$ and $\sigma_{mag} = 0.025(Gauss)$.

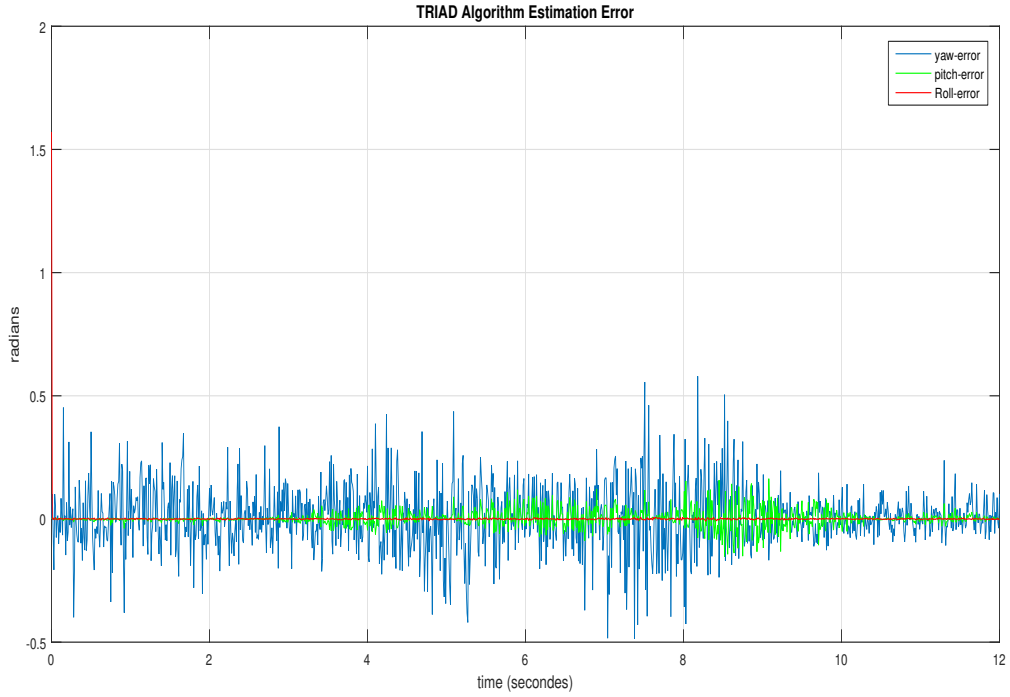


Figure 3.4: attitude estimation error using TRIAD Algorithm

Although this method seems simplistic, in real time implementations calculating the inverse of a matrix is a computationally heavy task, and should be avoided if possible. Further this method offers no form of filtering for noisy measurements and as such will not produce reliable result as seen in the figure above.

## 3.4 Complementary Filter

The complimentary filter is a reliable type of attitude observer filters in the field of orientation estimation, as it uses the non-linear dynamic of the system, instead of linearizing the system around some point, and it proved to be a good filter against noises. This filter provides an estimation of the rotation matrix $R$ from two vector measurements ($a_B$, $m_B$, and $\omega^y$) from the IMU. The observer is given by :

$$\begin{cases} \dot{\hat{R}} = \hat{R}[\omega^y + k_p\sigma_R]_\times, \\ \sigma_R = \rho_1(a_B \times \hat{R}^\top a_I) + \rho_2(m_B \times \hat{R}^\top m_I), \end{cases} \tag{3.9}$$

where $\hat{R}$ is the estimated rotation matrix and the innovarion term $\sigma_R$ represents an error between the true attitude $R$ and the estimated attitude $\hat{R}$ and it's easily seen that this innovation term will vanish as $\hat{R} \to R$ over time.

The goal of this observer is driving the natural estimation error defined as : $\tilde{R} = R\hat{R}^\top$ to the identity $I_{3_\times}$ over time and it can be illustrated by the following schemes :

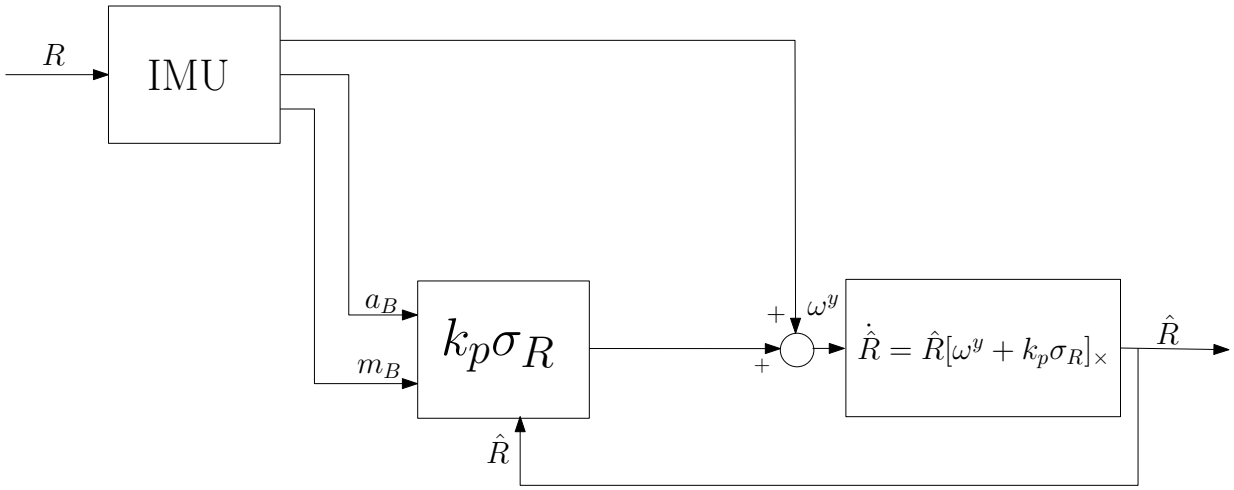


Figure 3.5: complimentary filter for attitude using IMU schemes

### 3.4.1 Stability Analysis

**Theorem 3.** *Consider the rotation kinematics (2.15) for a time varying $R(t) \in \mathbb{SO}(3)$ and with measurements given by (3.1)-(3.3). Let $\hat{R}(t)$ denotes the solution of the observer (3.9). taking in cosideration the error $\tilde{R} = R\hat{R}^\top$. Then*

- *All trajectories converge to the set $\mathbb{U} = \{I_3\} \times \{\tilde{R} \in \mathbb{SO}(3) : \tilde{R} = R(\pi, \epsilon(M_0))\}$, where $\epsilon(M_0)$ represents the eigenvectors of $M_0$*
- *The set $\bar{\mathbb{U}} = \{\tilde{R} \in \mathbb{SO}(3) : \tilde{R} = R(\pi, \mathbb{S}^2)\}$ is invariant and a repeller.*
- *The equilibrium $\tilde{R} = I_3$ is locally exponentially stable and almost globally asymptotically stable.*

*Proof.* 1 Let us consider the following Lyapunov function candidate :

$$\mathbf{V}(\tilde{R}) = \frac{1}{4}\operatorname{tr}(M_0 - M_0\tilde{R}). \tag{3.10}$$

And taking in consideration that the innovation term $\sigma_R$ can also be written as follows :

$$\sigma_R = \rho_1(a_B \times \hat{R}^\top a_I) + \rho_2(m_B \times \hat{R}^\top m_I). \tag{3.11}$$

The skew-matrix of the innovation term satisfies :

$$[\sigma_R]_\times = \hat{R}^\top M_0 R - R^\top M_0 \hat{R}. \tag{3.12}$$

Multiplyin both sides by $\hat{R}$ and $\hat{R}^\top$ will result in:

$$\hat{R}[\sigma_R]_\times \hat{R}^\top = M_0 R\hat{R}^\top - \hat{R}R^\top M_0, \tag{3.13}$$

$$[\hat{R}\sigma_R]_\times = M_0\tilde{R} - \tilde{R}^\top M_0. \tag{3.14}$$

Finally, $\sigma_R$ satisfies :

$$\sigma_R = \hat{R}^\top \operatorname{vex}(2\pi_a(M_0\tilde{R})). \tag{3.15}$$

$M_0$ is a symmetric semi-definite positive matrix defined as follows :

$$M_0 = \rho_1 a_I a_I^\top + \rho_2 m_I m_I^\top. \tag{3.16}$$

And the dynamic of the error $\tilde{R} = R\hat{R}^\top$ is given by:

$$\dot{\tilde{R}} = \dot{R}\hat{R}^\top + R\dot{\hat{R}}^\top, \tag{3.17}$$
$$= R[\omega]_\times \hat{R}^\top + R[\omega + k_p\sigma_R]_\times{}^\top \hat{R}^\top, \tag{3.18}$$
$$= R[k_p\sigma_R]_\times{}^\top \hat{R}^\top, \tag{3.19}$$
$$= k_p\tilde{R}[\hat{R}\sigma_R]_\times^\top, \tag{3.20}$$
$$= -k_p\tilde{R}[\mathrm{vex}(2\pi_a(M_0\tilde{R})]_\times. \tag{3.21}$$

Then, the time derivative of $\mathbf{V}$ can be given by:

$$\dot{\mathbf{V}}(\tilde{R}) = \frac{-1}{4}\,\mathrm{tr}(M_0\dot{\tilde{R}}), \tag{3.22}$$
$$= \frac{-1}{4}\,\mathrm{tr}(M_0\tilde{R}[\hat{R}k_p\sigma_R]_\times^\top), \tag{3.23}$$
$$= \frac{-k_p}{4}\,\mathrm{tr}(\pi_a(M_0\tilde{R})[\hat{R}\sigma_R]_\times^\top), \tag{3.24}$$
$$= \frac{-k_p}{4} \ll [\hat{R}\sigma_R]_\times, \pi_a(M_0\tilde{R}) \gg_f, \tag{3.25}$$
$$= \frac{-k_p}{2} \ll [\hat{R}\sigma_R]_\times, [\hat{R}\sigma_R]_\times \gg_f, \tag{3.26}$$
$$= -k_p\langle[\hat{R}\sigma_R]_\times, [\hat{R}\sigma_R]_\times\rangle, \tag{3.27}$$
$$= -k_p\|\sigma_R\|^2. \tag{3.28}$$

$\mathbf{V}$ is a positive definite function and its derivative is negative semi definite function, according to Lasalle theorem trajectories will converge to the largest invariant set $\Omega = \{\tilde{R} \in \mathbb{SO}(3) : \dot{\mathbf{V}}(\tilde{R}) = 0\} = \{\tilde{R} \in \mathbb{SO}(3) : \mathrm{vex}(2\pi_a(M_0\tilde{R})) = 0\}$ using Quaternion proprietie from [2].

$$\mathrm{vex}(2\pi_a(M_0\tilde{R})) = 2(q_0 I - [q]_\times)E(M_0)q = 0. \tag{3.29}$$

where $E(M_0) = \frac{1}{2}(\mathrm{tr}(M_0)I_3 - M_0)$ which is a positive definite matrix.

$2(q_0 I - [q]_\times)E(M_0)q = 0$ results in two cases :

- case 1

$$q = 0 \implies \mathrm{vex}(2\pi_a(M_0\tilde{R})) = 0 \implies \tilde{R} = I_3. \tag{3.30}$$

- case 2

$$q \neq 0 \implies q^\top \mathrm{vex}(2\pi_a(M_0\tilde{R})), \tag{3.31}$$
$$= 2q_0 q^\top E(M_0)q = 0, \tag{3.32}$$
$$\implies q_0 = \cos(\theta/2) = 0 \implies \theta = \pi. \tag{3.33}$$

The second case also implies that

$$-2[q]_\times E(M_0)q = 0, \tag{3.34}$$
$$\implies E(M_0)q = \lambda q. \tag{3.35}$$

$q$ is an eigenvector of $E(M_0)$ which means it's an eigenvector of $M_0$ also and since $q = \sin(\theta/2)u$ then $u$ is an eignervector of $M_0$ this prooves that the second case results in $\tilde{R} = R(\pi, \epsilon(M_0))$.. and that all trajectories will converge to the set $\mathbb{U}$: solution of (3.30) □

*Proof.* 2 Let us consider the following function :

$$\mathbf{W} = 1 + \mathrm{tr}(\tilde{R}). \tag{3.36}$$
$$= 4{q_0}^2. \tag{3.37}$$

The derivative of $\mathbf{W}$ is :

$$\dot{\mathbf{W}} = -k_p tr(\dot{\tilde{R}}), \tag{3.38}$$
$$= -k_p tr(\tilde{R}[\mathrm{vex}(M_0\tilde{R})]_\times), \tag{3.39}$$
$$= -k_p tr(\pi_a(\tilde{R})[\mathrm{vex}(M_0\tilde{R})]_\times), \tag{3.40}$$
$$= \frac{k_p}{2}\mathrm{vex}(\pi_a(\tilde{R}))^\top \mathrm{vex}(M_0\tilde{R})]_\times), \tag{3.41}$$
$$= \frac{k_p}{2}(2q_0 q)^\top (2(q_0 I_3 - [q]_\times)E(M_0)q), \tag{3.42}$$
$$= 2k_p {q_0}^2 q^\top E(M_0)q. \tag{3.43}$$

We know that $q_0 = 0 \ \ \forall \tilde{R} \in \bar{\mathbb{U}} = \{\tilde{R} \in \mathbb{SO}(3) : \tilde{R} = R(\pi, \mathbb{S}^2)\}$ this implies that the set $\bar{\mathbb{U}}$ is invariant since $\mathbf{W} = 0$ and $\dot{\mathbf{W}} = 0$ and $\forall \tilde{R} \notin \bar{\mathbb{U}}$ the function $\mathbf{W}$ is positive and it's derivative $\dot{\mathbf{W}}$ is positive also thanks to the fact $q^\top E(M_0)q > 0$.Which implies that the set $\bar{\mathbb{U}}$ is a repeller but it's also Lebesgue measure zero $\implies$ $\tilde{R} = I_3$ is an almost globally asymptotically stable set. □

*Proof.* 3 to prove that $\tilde{R} = I_3$ is locally exponentially stable let us consider the linearized error dynamics around $\tilde{R} = I_3$ :

$$\tilde{R} = I_3 + [x]_\times : \quad x = \theta u \tag{3.44}$$

it's derivative satisfies :

$$\dot{\tilde{R}} = [\dot{x}]_\times, \tag{3.45}$$
$$= -k_p \tilde{R}[\mathrm{vex}(2\pi_a(M_0\tilde{R}))]_\times, \tag{3.46}$$
$$= -k_p(I_3 + [x]_\times)[E(M_0)x]_\times. \tag{3.47}$$
$$= -k_p[E(M_0)x]_\times, \tag{3.48}$$

this results in:

$$\dot{x} = k_p E(M_0) x, \tag{3.49}$$

which proves that $x = 0$ ($\tilde{R} = I_3$) is exponentially stable since $E(M_0)$ is positive definite. □

### 3.4.2 Numerical Simulation

In this subsection, we implement the nonlinear attitude observers defined in previous section to estimate the vehicle orientation directly on $\mathbb{SO}(3)$ using IMU measurements. Consider a vehicle navigating with the following angular velocity applied to :

$$\omega(t) = \begin{bmatrix} 0.3\cos(\pi t/10) \\ 0.5\cos(2\pi t/10 + \pi/4) \\ 0.8\cos(4\pi t/10) \end{bmatrix}; \tag{3.50}$$

With an initial attitude $R(0) = \exp([\pi/6\pi/5\pi/5]_\times)$. The inertial earth's magnetic field is taken as$m_I = [0.42; 0.2949; 0.15]^\top$Gauss, and the earth's gravity is $g = 9.81 m/s^2$. The initial conditions of the observer is $\hat{R}(0) = I_3$. The observer parameters are taken as $\rho_1 = 2, \rho_2 = 2/6$ and $k_p = 2$. The measurement noises are modelled as a Gaussian white noises with variances, $\sigma_\omega = 0.16(deg/s^2)$,$\sigma_{acc} = 3.10^{-4}(m/s^2)$ and $\sigma_{mag} = 0.025(Gauss)$.

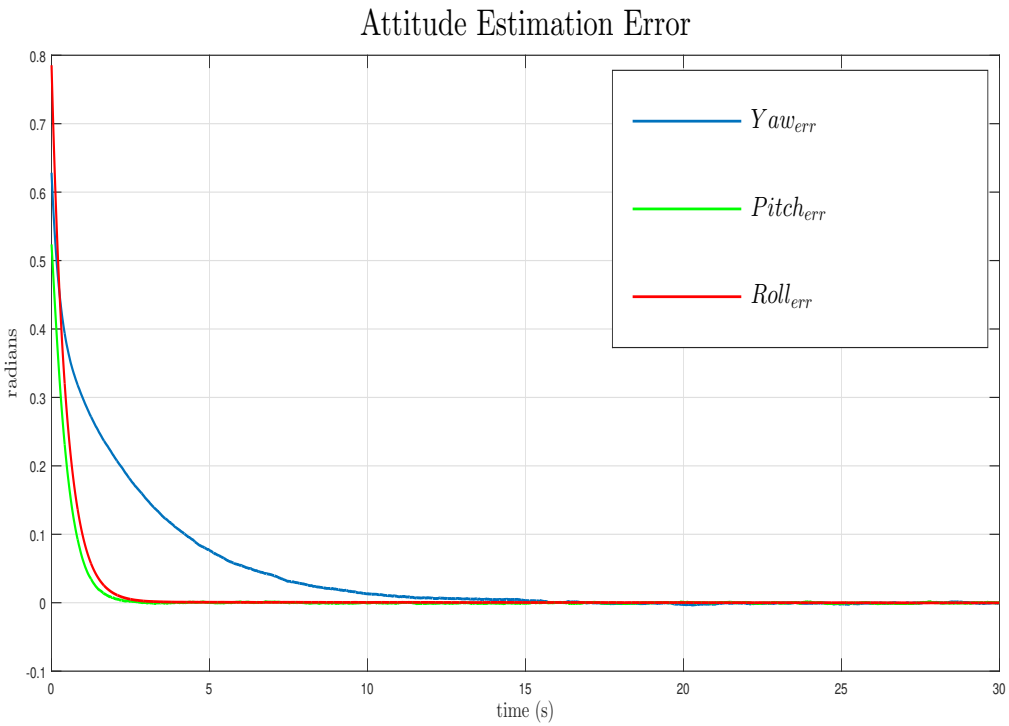


Figure 3.6: attitude estimation error using nonlinear complimentary filter

## 3.5 Sliding Mode Observer

The idea of the sliding mode observer is to use the innovation term of the complimentary filter as a sliding manifold and design a correction term $u$ that drives the attitude error to the following manifold on $\mathbb{R}^3$ :

$$s = k_1(m_B \times \hat{R}^\top m_I) + k_2(a_B \times \hat{R}^\top a_I) = 0 \tag{3.51}$$

which ensures that the motion on the manifold forces $\hat{R} \to R$ as $t \to \infty$. Consider the following positive definite scalar function:

$$\mathbf{W}(s) = \frac{1}{2}\|s\|^2. \tag{3.52}$$

The time derivative of $\mathbf{W}$ satisfies :

$$\dot{\mathbf{W}}(s) = s^\top(\sum_{n=1}^{2} k_i([\dot{R}^\top v_i]_\times \hat{R} v_i + [R^\top v_i]_\times \dot{\hat{R}}^\top v_i)), \tag{3.53}$$

where $v_i = m_I$ and $v2 = a_I$ using proprieties (2.36) and (2.41) $\dot{\mathbf{W}}(s)$ equals:

$$\dot{\mathbf{W}}(s) = s^\top(\sum_{n=1}^{2} k_i([[\omega]_\times{}^\top R^\top v_i]_\times \hat{R}^\top v_i + [R\top v_i]_\times [\omega + k_p u]_\times{}^\top \hat{R} v_i)). \tag{3.54}$$

This will result in:

$$\dot{\mathbf{W}}(s) = s^\top [\omega + k_p u]_\times{}^\top + s^\top(\sum_{n=1}^{2} k_p k_i (R^\top v_i u^\top \hat{R}^\top v_i - u v_i^\top \tilde{R} v_i)). \tag{3.55}$$

Choosing $u = sign(s)$ and defining the vector $\alpha = R^\top m_I u^\top m_I \in \mathbb{R}^3$ and $\beta = R^\top a_I u^\top a_I \in \mathbb{R}^3$, and the scalars $\lambda_1 = m_I^\top \tilde{R} m_I$ and $\lambda_2 = a_I^\top \tilde{R} a_I$, and taking in consideration the propriety $x^\top [y]_\times x = 0, \forall x, y \in \mathbb{R}^3$, the derivative of $\mathbb{W}(s)$ satisfies:

$$\dot{\mathbf{W}}(s) = k_p(k_1 s^\top \alpha + k_2 s^\top \beta) - k_p|s|(k_1\lambda_1 +¸2\lambda_2), \tag{3.56}$$

$$= \frac{k_p}{2}(k_1 tr([s]_\times [\alpha]_\times + k_2 tr([s]_\times [\beta]_\times) - k_p|s|(k_1\lambda_1 +¸2\lambda_2), \tag{3.57}$$

$$= \frac{k_p}{2}(k_1 tr([s]_\times{}^\top [\alpha]_\times + k_2 tr([s]_\times{}^\top [\beta]_\times) - k_p|s|(k_1\lambda_1 +¸2\lambda_2). \tag{3.58}$$

$\lambda_1^*$ and $\lambda_2^*$ denotes respectively, the maximum values that $m_i^\top \tilde{R} m_I$ and $a_I^\top \tilde{R} a_I$ can take, and taking in consideration the inequality $\mathrm{tr}(A^\top B) \leq \|A\|_1 \|B\|_1$, the derivative satisifies :

$$\dot{\mathbf{W}}(s) \leq \frac{k_p}{2}(k_1\|[s]_\times\|_1\|[\alpha]_\times\|_1 + k_2\|[s]_\times\|_1\|[\beta]_\times\|_1) - k_p|s|(k_1\lambda_1^* +_\epsilon 2\lambda_2^*), \tag{3.59}$$

$$\leq k_p(k_1|s||\alpha| + k_2|s||\beta|) - k_p|s|(k_1\lambda_1^* +_\epsilon 2\lambda_2^*), \tag{3.60}$$

$$\leq k_p(k_1(|\alpha| - \lambda_1^*) + k_2(|\beta| - \lambda_2^*))|s|, \tag{3.61}$$

$$\leq -|s|, \qquad \forall \frac{k_1}{k_2} \geq \frac{|\alpha| - \lambda_1^*}{\lambda_2^* - |\beta|}. \tag{3.62}$$

Note that $|\beta|, |\alpha|, \lambda_1^*$, and $\lambda_2^*$ are finite scalars and depend directly on $m_I$ and $a_I$ vectors.

choosing $u = sign(s)$ with a proper tuning of $k_1$ and $k_2$ to satisfy the condition (3.62), guarantees the reachability of the surface in a finite time starting from any point, meaning that the attitude error will reach the sliding manifold $s = 0$ in a finite time and stays there where the dynamic on $s = 0$ is forced to drive $\hat{R} \to R$ i.e. $\tilde{R}$ tend to the identity matrix $i_3$ as $t$ tend to $\infty$.

Note that introducing the *sign* function causes discontinuity problem in the system dynamics, the idea is to apply a continuous function which has approximately the same shape as the *sign* function. Let use a continuous function defined on $\mathbb{R} \to ]-1, 1[$ in the following vector :

$$u = \Psi(s), \tag{3.63}$$

with $\Psi(s)$ defined :

$$\Psi(s) = \frac{2}{\pi}\begin{bmatrix}\arctan(ms_1)\\ \arctan(ms_2)\\ \arctan(ms_3)\end{bmatrix} \tag{3.64}$$

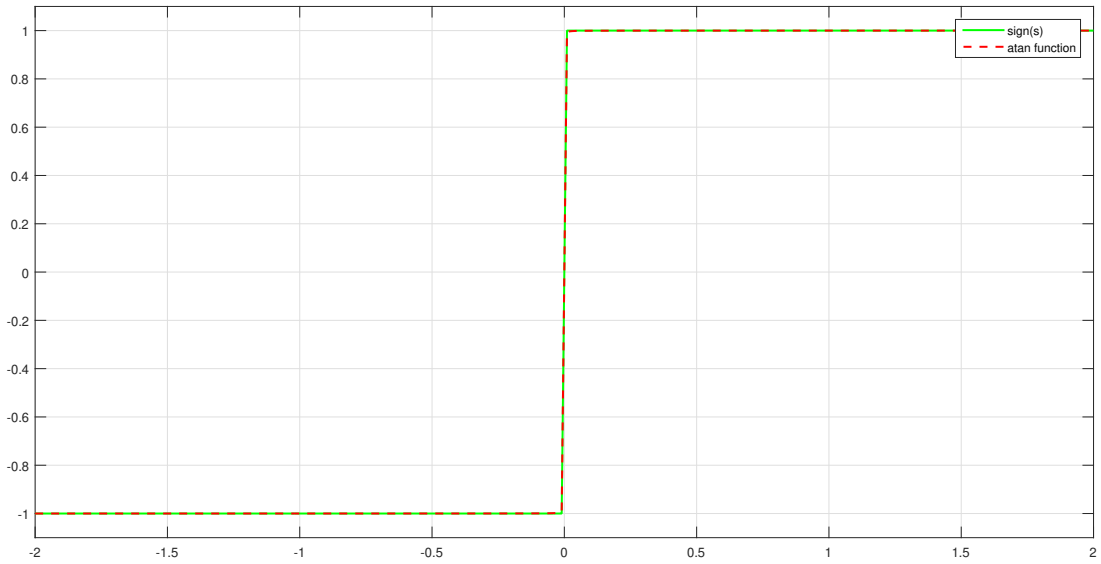


Figure 3.7: the graph of $\frac{2\arctan(ms)}{pi}$ function with $m = 10^4$ versus the graph of $sign(s)$ function

choosing $m$ big enough preserves the robustness of the $sign$ function and satisfy the reachability condition established above.

The observer will then be given by :

$$\begin{cases} \dot{\hat{R}} = \hat{R}[\omega^y + k_p\Psi(s)]_\times, \\ s = k_1 m_B \times \hat{R}^\top m_I + k_2 a_B \times \hat{R}^\top a_I, \\ \Psi(s) = \frac{2}{\pi}\begin{bmatrix}\arctan(ms_1) & \arctan(ms_2) & \arctan(ms_3)\end{bmatrix}^\top. \end{cases} \tag{3.65}$$

### 3.5.1 Stability Analysis

**Theorem 4.** *Consider the rotation kinematics (2.15) for a time varying $R(t) \in \mathbb{SO}(3)$ and with measurements given by (3.1)-(3.3). Let $\hat{R}(t)$ denotes the solution of the sliding mode observer (3.65). taking in consideration the error $\tilde{R} = R\hat{R}^\top$. Then*

- *All trajectories converge to the set $\mathbb{U} = \{I_3\} \times \{\tilde{R} \in \mathbb{SO}(3) : \tilde{R} = R(\pi, \epsilon(M_0))\}$.*
- *The set $\bar{\mathbb{U}} = \{\tilde{R} \in \mathbb{SO}(3) : \tilde{R} = R(\pi, \epsilon(M_0)\}$ is unstable.*
- *The equilibrium $\tilde{R} = I_3$ is locally exponentially stable and it's almost globally asymptotically stable.*

*Proof.* 1 Let us consider the following Lyapunov candidate function :

$$\mathbf{V} = \frac{1}{4}\operatorname{tr}(M_0 - M_0\tilde{R}). \tag{3.66}$$

the time derivative of $\mathbf{V}$ is given by:

$$\begin{aligned}
\dot{\mathbf{V}} &= \frac{-1}{4}\operatorname{tr}(M_0\dot{\tilde{R}}), && (3.67)\\
&= \frac{-k_p}{4}\operatorname{tr}(M_0\tilde{R}[\hat{R}u]_\times^\top), && (3.68)\\
&= \frac{-k_p}{4}\operatorname{tr}(\pi_a(M_0\tilde{R})[\hat{R}u]_\times^\top), && (3.69)\\
&= \frac{-k_p}{4} \ll [\hat{R}u]_\times, \pi_a(M_0\tilde{R}) \gg_f, && (3.70)\\
&= \frac{-k_p}{2} \ll [\hat{R}u]_\times, [\operatorname{vex}(2\pi_a(M_0\tilde{R}))]_\times \gg_f, && (3.71)\\
&= -k_p < [\hat{R}u]_\times, [\hat{R}s]_\times >, && (3.72)\\
&= -k_p s^\top \Psi(s), && (3.73)\\
&= \frac{-2k_p}{\pi}(s_1 \arctan(ms_1) + s_2 \arctan(ms_2) + s_3 \arctan(ms_3)). && (3.74)
\end{aligned}$$

$\mathbf{V}$ is a positive definite function and it's derivative is negative semi definite function thanks to the fact that $x \arctan(mx) \geq 0$. According to Lasalle theorem, trajectories will converge to the largest invariant set $\Omega = \{\tilde{R} \in \mathbb{SO}(3) : \dot{\mathbf{V}}(\tilde{R}) = 0\}$ . $\mathbf{V}(\tilde{R}) = 0$ means that $s = 0$ or $\Psi(ms) = 0$ and since the $\arctan(x) = 0$ only if $x = 0$. The set $\Omega = \{\tilde{R} \in \mathbb{SO}(3) : s = 0\} = \{\tilde{R} \in \mathbb{SO}(3) : \operatorname{vex}(2\pi_a(M_0\tilde{R})) = 0\}$. same as the previous observer and using Quaternion proprieties :

$$\operatorname{vex}(2\pi_a(M_0\tilde{R})) = 2(q_0 I - [q]_\times)E(M_0)q = 0. \tag{3.75}$$

where $E(M_0) = \frac{1}{2}(\text{tr}(M_0)I_3 - M_0)$ which is a positive definite matrix.

$2(q_0 I - [q]_\times)E(M_0)q = 0$ results in two cases :

- case 1

$$q = 0 \implies \text{vex}(2\pi_a(M_0\tilde{R})) = 0 \implies \tilde{R} = I_3. \tag{3.76}$$

- case 2

$$q \neq 0 \implies q^\top \text{vex}(2\pi_a(M_0\tilde{R})), \tag{3.77}$$
$$= 2q_0 q^\top E(M_0)q = 0, \tag{3.78}$$
$$\implies q_0 = \cos(\theta/2) = 0 \implies \theta = \pi. \tag{3.79}$$

The second case also implies that

$$-2[q]_\times E(M_0)q = 0, \tag{3.80}$$
$$\implies E(M_0)q = \lambda q. \tag{3.81}$$

$q$ is an eigenvector of $E(M_0)$ which means it's an eigenvector of $M_0$ also. and since $q = sin(\theta/2)u$. $u$ is an eignervector of $M_0$ this proves that the second case results in $\tilde{R} = R(\pi, \epsilon(M_0))$.. and that all trajectories will converge to the set $\mathbb{U}$: solution of (3.75) □

*Proof.* 2 For rotation of $\pi$ around the unit vector $u \in \epsilon(M_0)$, the attitude error matrix is given by :

$$\tilde{R} = R(\pi, u)\exp([x]_\times), \quad x \approx 0. \tag{3.82}$$

for small rotations this can be written as :

$$\tilde{R} \approx R(\pi, u)(I_3 + [x]_\times). \tag{3.83}$$

the linearized dynamics are :

$$\dot{\tilde{R}} = R(\pi, u)[\dot{x}]_\times. \tag{3.84}$$

on can write the skew matrix of $\dot{x}$ as follows :

$$[\dot{x}]_\times = -k_p R(\pi, u)^\top \tilde{R}[\hat{R}\Psi(s)]_\times, \tag{3.85}$$
$$= k_p R(\pi, u)^\top R(\pi, u)(I_3 + [x]_\times)[\text{vex}(2\pi_a(M_0\tilde{R})]_\times, \tag{3.86}$$
$$= \frac{-k_p}{2}(I_3 + [x]_\times)(M_0\tilde{R} - \tilde{R}^\top M_0), \tag{3.87}$$
$$= \frac{-k_p}{2}(I_3 + [x]_\times)(M_0(I_3 + [x]_\times) - (I_3 - [x]_\times)M_0), \tag{3.88}$$
$$= \frac{-k_p}{2}(M_0 R(\pi, u)[x]_\times + [x]_\times R(\pi, u)M_0). \tag{3.89}$$

Taking $M^* = M_0 R(\pi, u)$ :

$$[\dot{x}]_\times = \frac{-k_p}{2}[(\mathrm{tr}(M^*)I_3 + (M^*)^\top)x]_\times, \tag{3.90}$$

$$= -k_p[E(M^*)x]_\times. \tag{3.91}$$

this result in the following linear system :

$$\dot{x} = -k_p E(M^*)x. \tag{3.92}$$

To study the stability of this linearized system, we'll determine the sign of the eigenvalues of $E(M^*)$ matrix.

$$u^\top E(M^*)u = \frac{u^\top}{2}(\mathrm{tr}(M^*)I_3 - M_0 R(\pi, u))u. \tag{3.93}$$

And since $u \in \epsilon(M_0), M_0 u = \lambda u$, where $\lambda$ are the eigenvalues of $M_0$.

$$u^\top E(M^*)u = \frac{1}{2}(\mathrm{tr}(M^*) - \lambda), \tag{3.94}$$

$$= \frac{1}{2}(\mathrm{tr}(M_0(2uu^\top - I_3)) - \lambda), \tag{3.95}$$

$$= \frac{1}{2}(-\mathrm{tr}(M_0)), \tag{3.96}$$

$$\leq 0. \tag{3.97}$$

Thanks to the fact that $M_0$ is a positive semi-definite matrix, which means $E(M^*)$ has at least one negative eigenvalues $\implies$ $-E(M^*)$ has at least one positive eigenvalue. This the equilibrium set $\bar{\mathbb{U}}$ is unstable but it's also Lebesgue measure zero $\implies$ $\tilde{R} = I_3$ is an almost globally asymptotically stable set.

□

*Proof.* 3

To prove that $\tilde{R} = I_3$ is locally exponentially stable let us consider the linearized error dynamics around $\tilde{R} = I_3$ :

$$\tilde{R} = I_3 + [x]_\times : \quad x = \theta u. \tag{3.98}$$

it's derivative satisfies :

$$\dot{\tilde{R}} = [\dot{x}]_\times, \tag{3.99}$$

$$= -k_p \tilde{R}[\hat{R}\Psi(s)]_\times, \tag{3.100}$$

$$= -k_p(I_3 + [x]_\times)[\hat{R}\Psi(m\hat{R}^\top \mathrm{vex}(2\pi_a(M_0\tilde{R})))]_\times, \tag{3.101}$$

$$= -k_p(I_3 + [x]_\times)[\hat{R}\Psi(m\hat{R}^\top E(M_0)x)]_\times. \tag{3.102}$$

And for $x \approx 0$ the function $\arctan(x) \approx x$ this results in:

$$[x]_\times = \frac{-2mk_p}{\pi}(I_3 + [x]_\times)[E(M_0)x]_\times, \tag{3.103}$$

$$\dot{x} = \frac{-2mk_p}{\pi}E(M_0)x. \tag{3.104}$$

which proves that $x = 0$ ($\tilde{R} = I_3$) is exponentially stable since $E(M_0)$ is positive definite. □

### 3.5.2 Numerical Simulation

In this subsection, we implement the nonlinear attitude observers defined in previous section to estimate the vehicle orientation directly on $\mathbb{SO}(3)$ using IMU measurements. Consider a vehicle navigating with the following angular velocity applied to :

$$\omega(t) = \begin{bmatrix} 0.3\cos(\pi t/10) \\ 0.5\cos(2\pi t/10 + \pi/4) \\ 0.8\cos(4\pi t/10) \end{bmatrix} \tag{3.105}$$

With an initial attitude $R(0) = \exp(\frac{\pi}{2}[e_3]_\times)$. The inertial earth's magnetic field is taken as$m_I = [0.42; 0.2949; 0.15]^\top$Gauss, and the earth's gravity is $g = 9.81m/s^2$. The inital conditions of the observer is $\hat{R}(0) = I_3$. The observer parameters are taken as $k_1 = 2/6, k_2 = 2$,$m = 10^4$ and $k_p = 2$. The measurement noises are modelled as a Gaussian white noises with variances, $\sigma_\omega = 0.16(deg/s^2)$,$\sigma_{acc} = 3.10^{-4}(m/s^2)$ and $\sigma_{mag} = 0.025(Gauss)$.

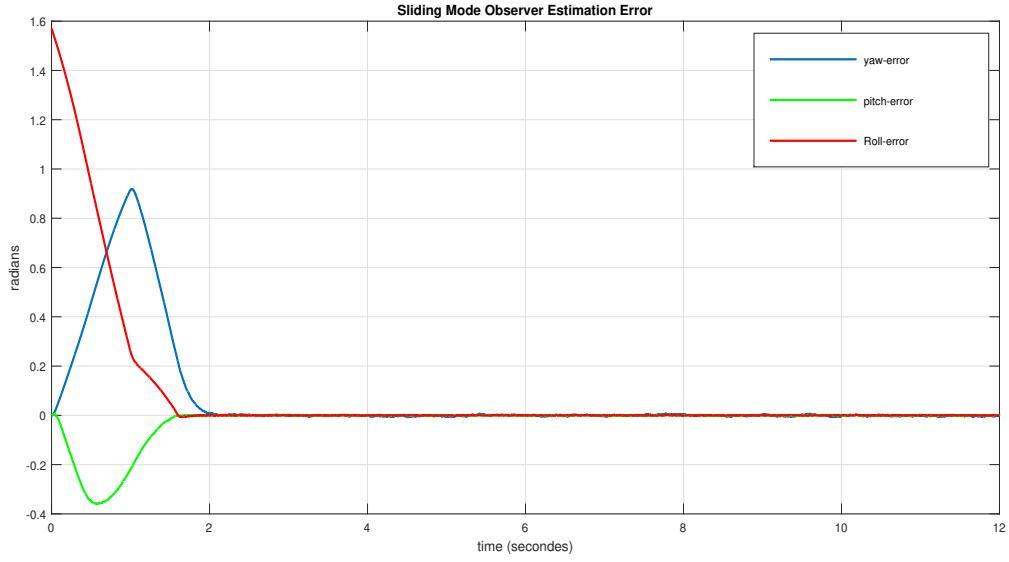


Figure 3.8: attitude estimation error using nonlinear sliding mode observer

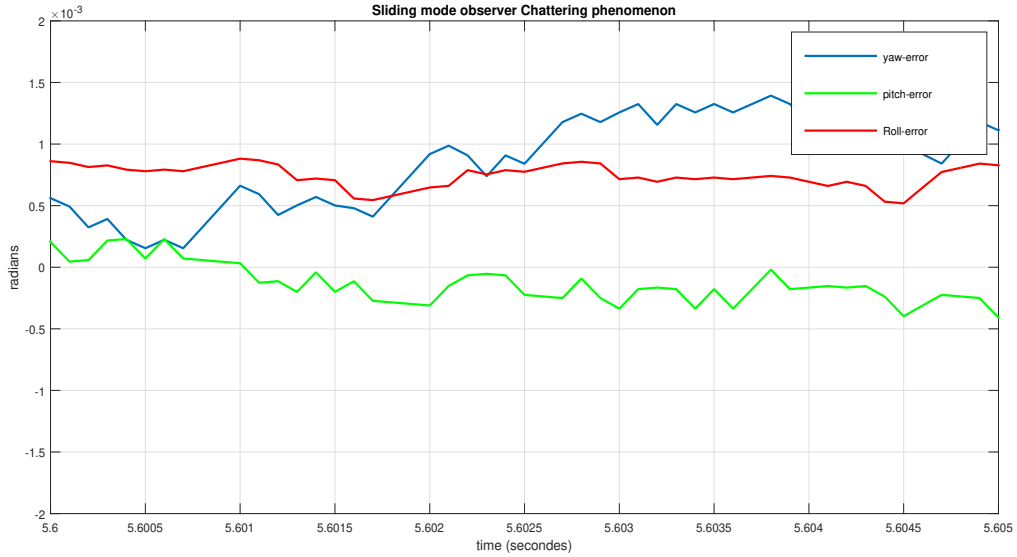


Figure 3.9: chattering phenomenon using nonlinear sliding mode observer

## 3.6 Super Twisting Sliding Mode

The sliding mode technique is essentially based on the resolution of differential equations with a discontinuous right hand side which is introduced in previous section. Historically, the twisting mode algorithm is the first 2nd order sliding mode algorithm known. The Super-Twisting Algorithm (STA) or Super-Twisting observer is a well-known second order sliding mode (SOSM) algorithm. It was first designed as an absolutely continuous control law, allowing to compensate Lipschitz perturbations exactly and ensuring finite time convergence. This algorithm is widely used to substitute discontinuous controllers by continuous ones and to attenuate the chattering phenomenon caused by the first order sliding mode (as we can see in the Numerical Simulation section). It features are twisting around the origin of the 2nd order sliding plane. The trajectories perform an infinite number of rotations while converging in finite time to the origin. In the super-twisting algorithm the trajectories on the 2nd order sliding plane are also characterized by twisting around the origin as illustrated in the following figure.

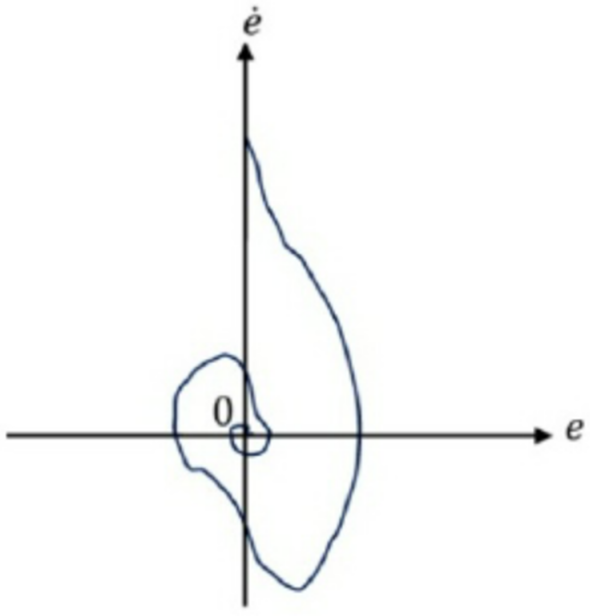


Figure 3.10: Super twisting phase trajectory

The super twisting observer algorithm is given by :

$$\begin{cases} \dot{\hat{R}} = \hat{R}[\omega^y + k_p u]_\times, \\ u = u_1 + u_2, \\ u_1 = -k_3 |s|^{\frac{1}{2}} sign(s), \\ \dot{u}_2 = -k_4 sign(s), \\ s = k_1(m_B \times \hat{R}^\top m_I) + k_2(a_B \times \hat{R}^\top a_I) = 0, \end{cases} \tag{3.106}$$

where $s$ is the sliding surface the same used for the first order sliding mode in the previous section and $k_i \quad i = 1 \dots 4$ are tunning scalars. The finite time stability is often used to proove the convergence of the Super-twisting algorithm in a finite time.

### 3.6.1 Numerical Simulation

In this subsection we implement the nonlinear attitude observers defined in previous section to estimate the vehicle orientation directly on $\mathbb{SO}(3)$ using IMU measurements. Consider a vehicle navigating with the following angular velocity applied to :

$$\omega(t) = \begin{bmatrix} 0.3\cos(\pi t/10) \\ 0.5\cos(2\pi t/10 + \pi/4) \\ 0.8\cos(4\pi t/10) \end{bmatrix} \tag{3.107}$$

With an initial attitude $R(0) = \exp(\frac{\pi}{2}[e_3]_\times)$. The inertial earth's magnetic field is taken as$m_I = [0.42; 0.2949; 0.15]^\top$Gauss, and the earth's gravity is $g = 9.81 m/s^2$. The initial conditions of the observer is $\hat{R}(0) = I_3$. The observer parameters are taken as $k_1 = 2/6, k_2 = 2$,$k_3 = -1.3$,$k_4 = -1.5$,$m = 10^4$ and $k_p = 2$. The measurement noises are modelled as a Gaussian white noises with variances, $\sigma_\omega = 0.16(deg/s^2)$,$\sigma_{acc} = 3.10^{-4}(m/s^2)$ and $\sigma_{mag} = 0.025(Gauss)$.

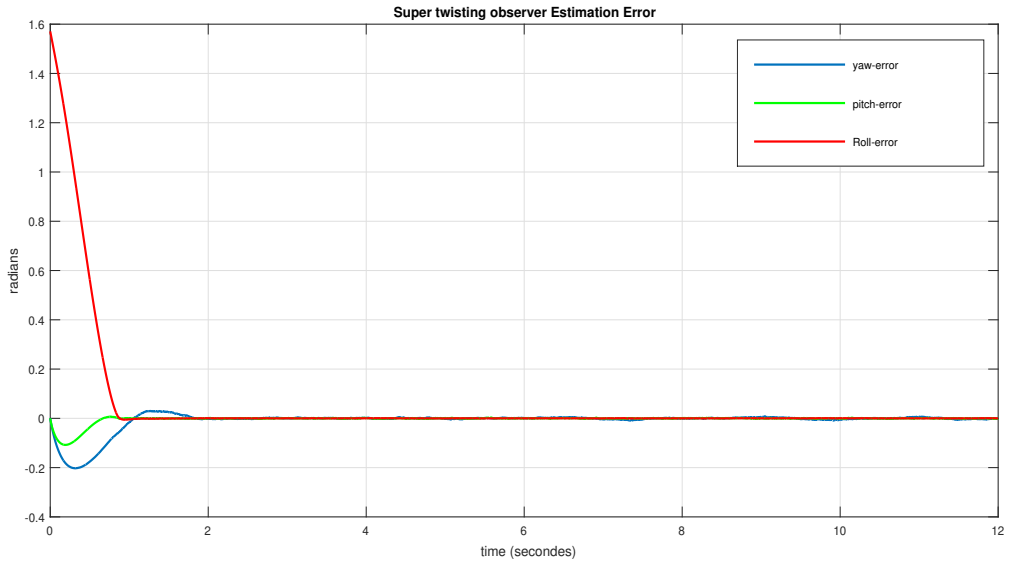


Figure 3.11: attitude estimation error using nonlinear sliding mode observer

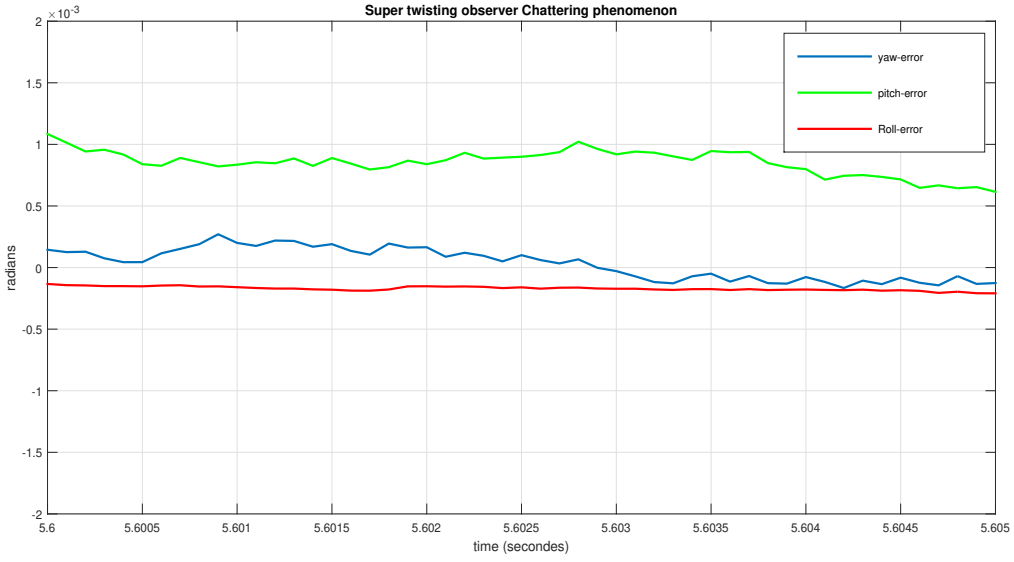


Figure 3.12: chattering phenomenon using nonlinear sliding mode observer

## 3.7 Comparaison and Robustness Study

In this section, we will compare the previous attitude observers and test their robustness by corrupting the Gyroscope measurements i.e.: adding (10%, 30%..) of the measurements to the measured values, increasing the noise and adding perturbations. The behaviour of the attitude observers will be compared in a single graph by plotting the trace function $\Phi(\tilde{R}) = \text{tr}(I_3 - \tilde{R})$. First let us put together the performance of the three nonlinear observers in normal conditions to compare the convergence speed. Consider a vehicle navigating with the following angular velocity applied to :

$$\omega(t) = \begin{bmatrix} 0.8\cos(\pi t/10) \\ \cos(2\pi t/10 + \pi/4) \\ 1.2\cos(4\pi t/10) \end{bmatrix} \tag{3.108}$$

With an initial attitude $R(0) = \exp(\frac{\pi/2}{4}[e_3]_\times)$. The inertial earth's magnetic field is taken as$m_I = [0.42; 0.2949; 0.15]^\top$Gauss, and the earth's gravity is $g = 9.81m/s^2$. The inital conditions of the observer is $\hat{R}(0) = I_3$. The observer parameters are taken as $k_1 = 1/12, k_2 = 1.5$,$k_3 = -1.3$,$k_4 = -1.5$,$\rho_1 = 1.5$,$\rho_2 = 1/12$,$m = 10^4$ and $k_p = 2$. The measurement noises are modelled as a Gaussian white noises with variances, $\sigma_\omega = 0.16(deg/s^2)$,$\sigma_{acc} = 3.10^{-4}(m/s^2)$ and $\sigma_{mag} = 0.025(Gauss)$.

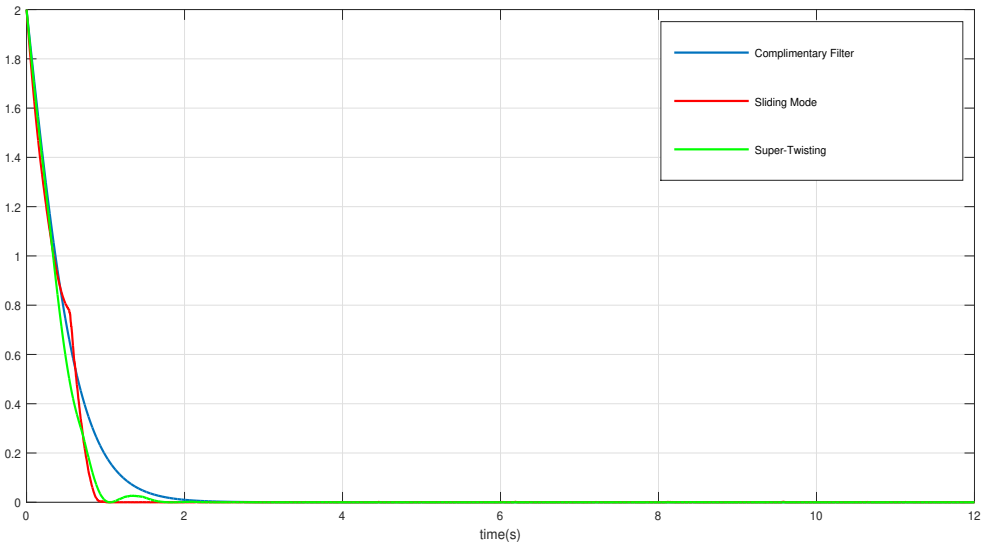


Figure 3.13: convergence speed of the attitude estimation error using the three nonlinear observers versus time

### 3.7.1 Noise and Bias Filtering

In this subsection, we will test the filtering of the nonlinear observers by multiplying the noise variance of the accelerometer, gyroscope and magnetometer.

$$\omega^y = \omega + \alpha\eta_\omega, \tag{3.109}$$
$$m_B = R^\top m_I, + \alpha\eta_{mag}, \tag{3.110}$$
$$a_B = R^\top a_I + \alpha\eta_{acc}. \tag{3.111}$$

First let's consider the cases $\alpha = 10$ (Multiplying the variance noise ten times) then $\alpha = 20$. and considering the same observer's constants and simulation scenario as the previous subsection :

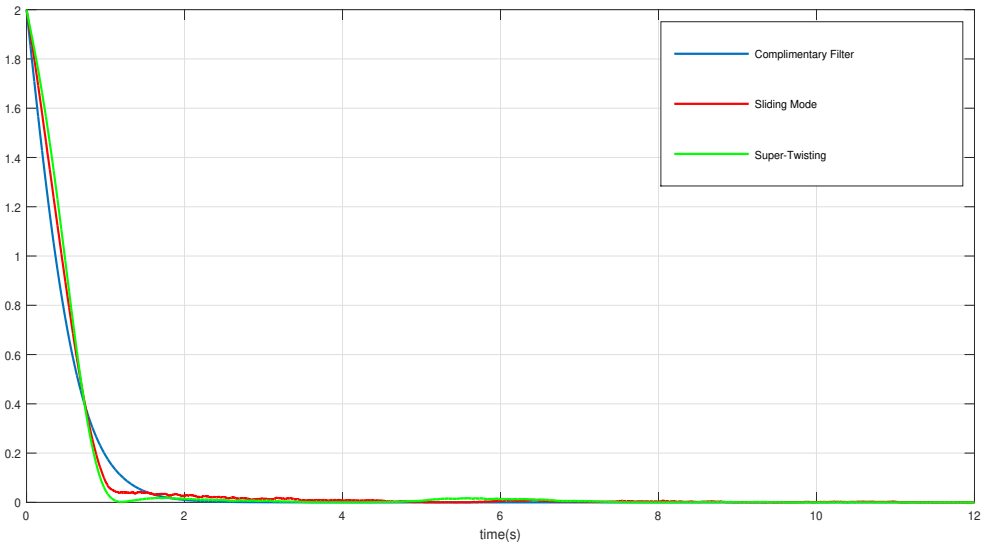


Figure 3.14: Comparison between the three observers when noise variances is 10 times bigger

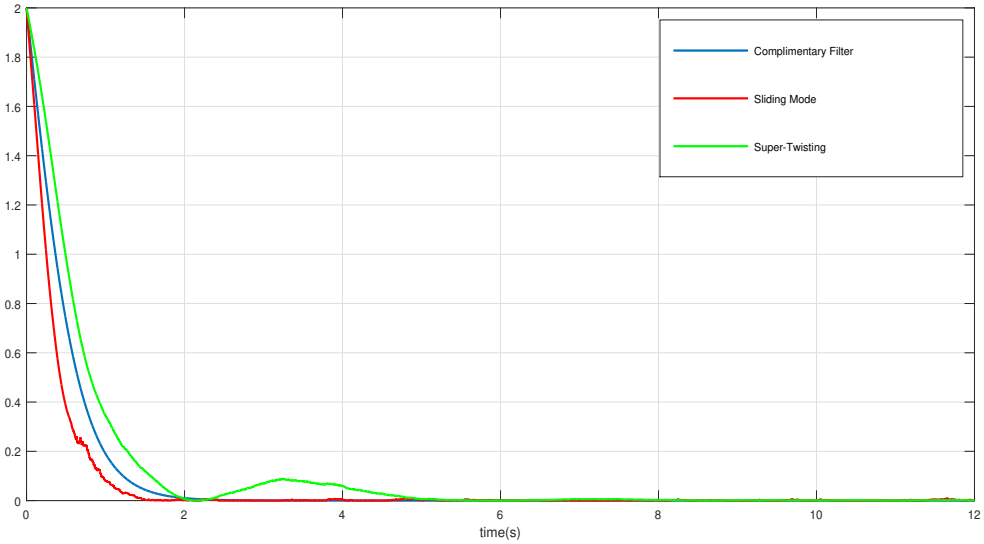


Figure 3.15: Comparison between the three observers when noise variances is 20 times bigger

Note that the noise variances $\sigma_\omega = 0.16(deg/s^2)$,$\sigma_{acc} = 3.10^{-4}(m/s^2)$ and $\sigma_{mag} = 0.025(Gauss)$ are taken from the data-sheet of a cheap commercial IMU.

We can see that the Complimentary filter offers a very good noise filtering and tops the other two observers. However, if the Gyroscope measurements are corrupted by a constant gyro bias $b_\omega = 5(deg/sec)$ at the form of :

$$\omega^y = \omega + b_\omega + \eta_\omega, \tag{3.112}$$
$$m_B = R^\top m_I, + \eta_{mag}, \tag{3.113}$$
$$a_B = R^\top a_I + \eta_{acc}. \tag{3.114}$$

We can see that the complimentary filter implemented in the section 3.4 offers no form of bias elimination and the estimated attitude is not reliable. However, the sliding mode observer and the super twisting observers eliminates the gyro bias and offers a very reliable estimation of the attitude.

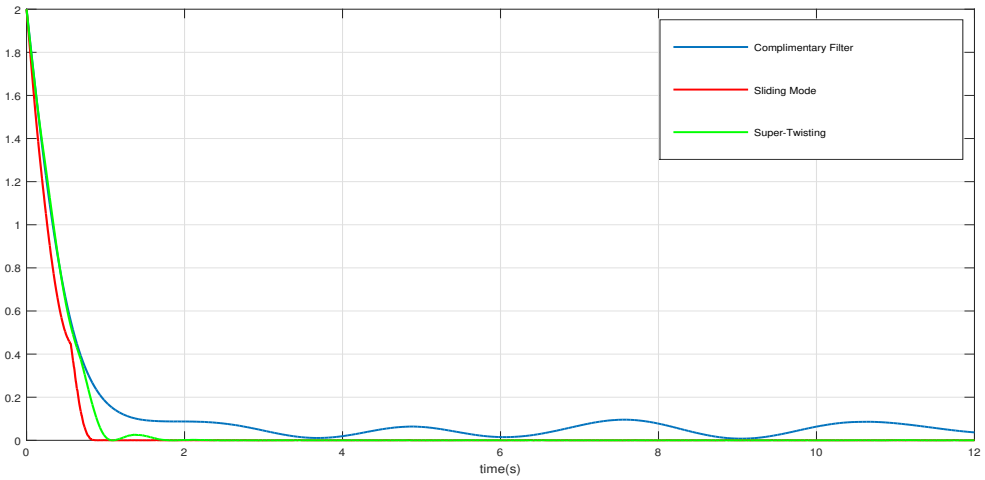


Figure 3.16: Comparison between the three observers when a constant $b_\omega$ is added

### 3.7.2 Corrupted Measurements

In this subsection, we will compare the previous attitude observers and test their robustness by corrupting the Gyroscope measurements by adding 10%, 30% and finally 50% of the gyroscope measurements to the measured angular velocity. Let us consider the same simulation scenario and same observers constants :

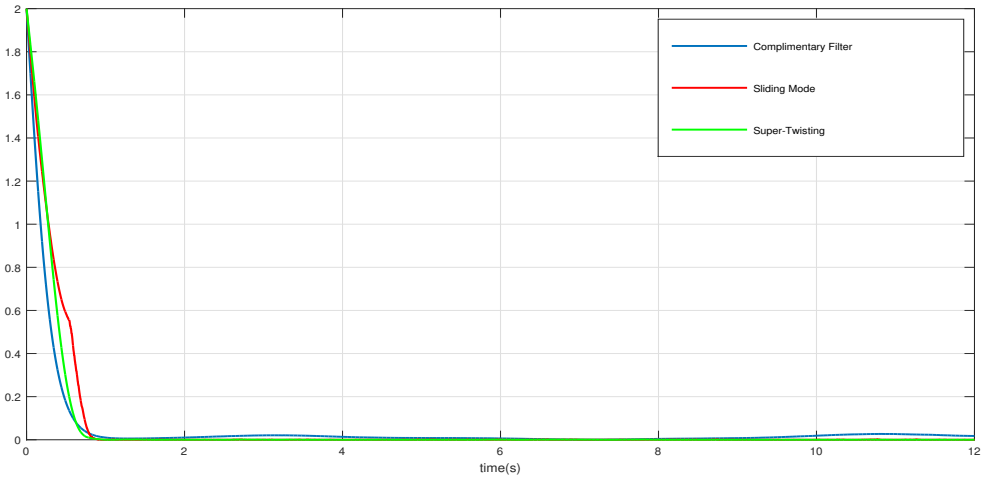


Figure 3.17: Comparison between the three observers when Gyroscope measurements are corrupted by 10% of the measured value

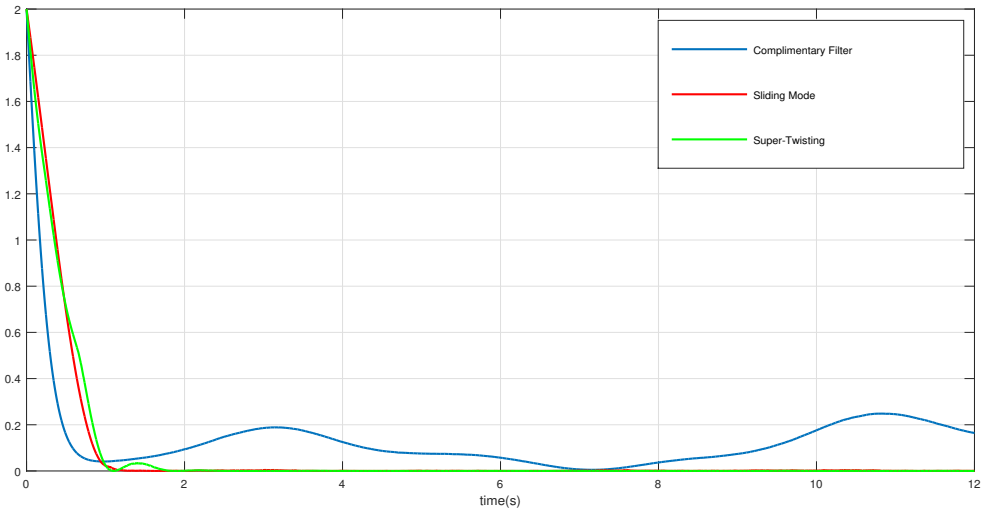


Figure 3.18: Comparison between the three observers when Gyroscope measurements are corrupted by 30% of the measured value

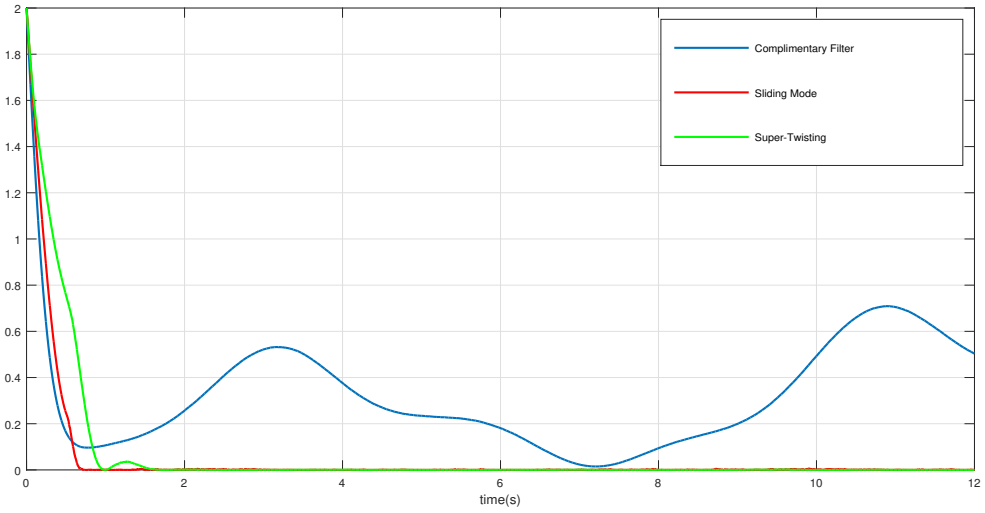


Figure 3.19: Comparison between the three observers when Gyroscope measurements are corrupted by 50% of the measured value

### 3.7.3 Initial Values

In this subsection, we will compare the observers behaviour by considering a large initial angle error. Let us consider the initial values : $R(0) = \exp\left((\pi - 0.1)[e_3]_\times\right)$, and $\hat{R}(0) = I_3$ with same simulation scenario and same observer constants as before the results are as follows :

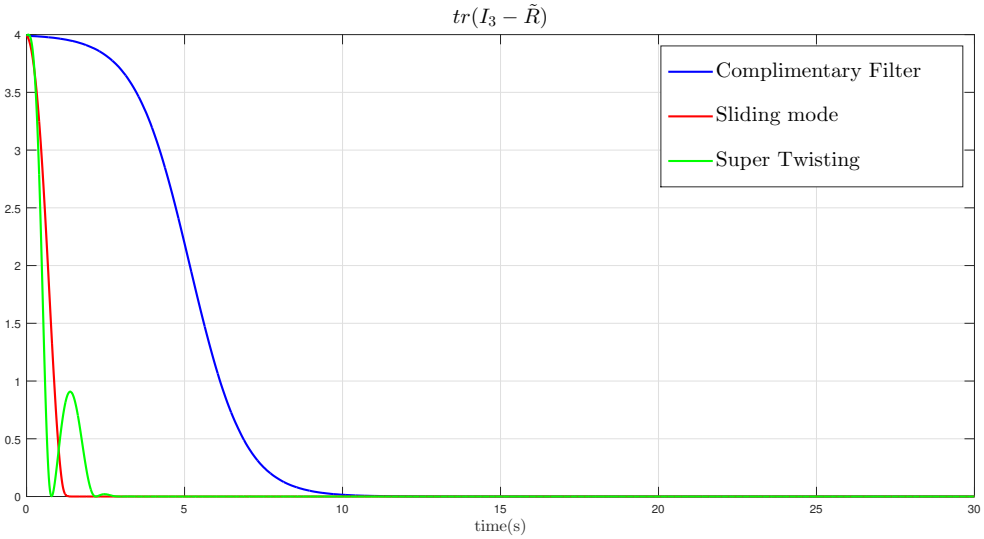


Figure 3.20: Comparison between the three observers when the initial angle error is close to $\pi$

## 3.8 Conclusion

In this chapter we proposed three nonlinear attitude observers and a TRIAD reconstruction method. All of the proposed methods require the use of vector measurements. The stability of the nonlinear complimentary filter and the sliding mode observer were discussed and proved. The three observers were compared :

- First, by amplifying the noise and adding a constant bias. The complimentary filter showed a very good noise filtering while the other two observers gave acceptable results. However, the sliding mode observer and Super-twisting observer eliminated the constant gyro bias while the complimentary filter offers no form of bias elimination. Note that a bias-attitude complimentary filter (Mahony and Hamel 2007) can be used to solve this problem but that will require more time to converge and more computational resources. A possible solution can be studied also for the noise filtering using the sliding mode and the Super-twisting observers, this possible solution

consist of using a Volterra estimator[19] to filter the measurements from the IMU before using them in the sliding mode or Super-twisting observers since this type of filters has been studied recently and showed a very good noise elimination.

- Second, the observer's performances were compared by corrupting the angular velocity measurements obtained from the gyroscope. The sliding mode and Super-twisting observers showed a very good results while the complimentary filter gave unreliable estimation.

- Third, the observer's performances were compared by increasing the angle initial error close to $\pi$. The sliding mode and super-twisting observers showed a faster convergence than the complimentary filter. Note that the difference in the converging speed is also present in the case of small initial angle error as seen in figure(3.13).

CHAPTER 4

# Position Reconstruction Using UWB Range Measurements

## 4.1 Introduction

Inertial navigation systems (INS) are widely deployed in many autonomous and robot platforms [22]. INS systems use measurements from accelerometers, gyroscopes and sometimes magnetomers to provide an estimate of the position, velocity and orientation of a vehicle. These sensors are often available inside a single low-cost unit called an Inertial Measurement Unit (IMU). The use of INS alone for navigation might lead to unreliable state estimates since measurement errors and unknown initial conditions lead to drifts in the estimation over long time horizons [1]. For this reason, INS are usually aided by other sensors such as Global Positioning Systems (GPS) which allow to correct the position estimates over time, thus, restricting the estimation errors to small bounds, or Ultra-Wide Band (UWB) sensors which is a radio technology that can use a very low energy level for short-range, high-bandwidth communications over a large portion of the radio spectrum. Range measurements using UWB radio technology is getting popular in indoor applications. The idea is to deploy $n$ source points (anchors) of transmitter modules at known locations and a receiver module installed on board the UAV. By communicating signals between the receiver and the transmitters, it is possible to calculate the ranges (distances) between the receiver and the anchors and determine the position of the UAV. Generally $n \geq 4$ anchors are used to determine the vehicle's position without ambiguity. In this chapter we will discuss different methods to reconstruct the position information from UWB sensors for different scenarios.

## 4.2 Ultra-Wide Band technology

UWB is a wireless technology intended for digital data transmission over short distances at low power density. The name reflects that the technology occupies a large bandwidth of the radio frequency spectrum. In unlicensed applications, the UWB uses short-duration pulses over a spectrum of frequencies between $3.1GHz$ to $10.6GHz$. The Ultra-Wide Band dates back to the beginning of radio when G. Marconi used spark-gap transmitters in transatlantic radio communication. The technology evolved considerably in the mid 20th century as it proved to be very useful in short range positioning for indoor environment applications.

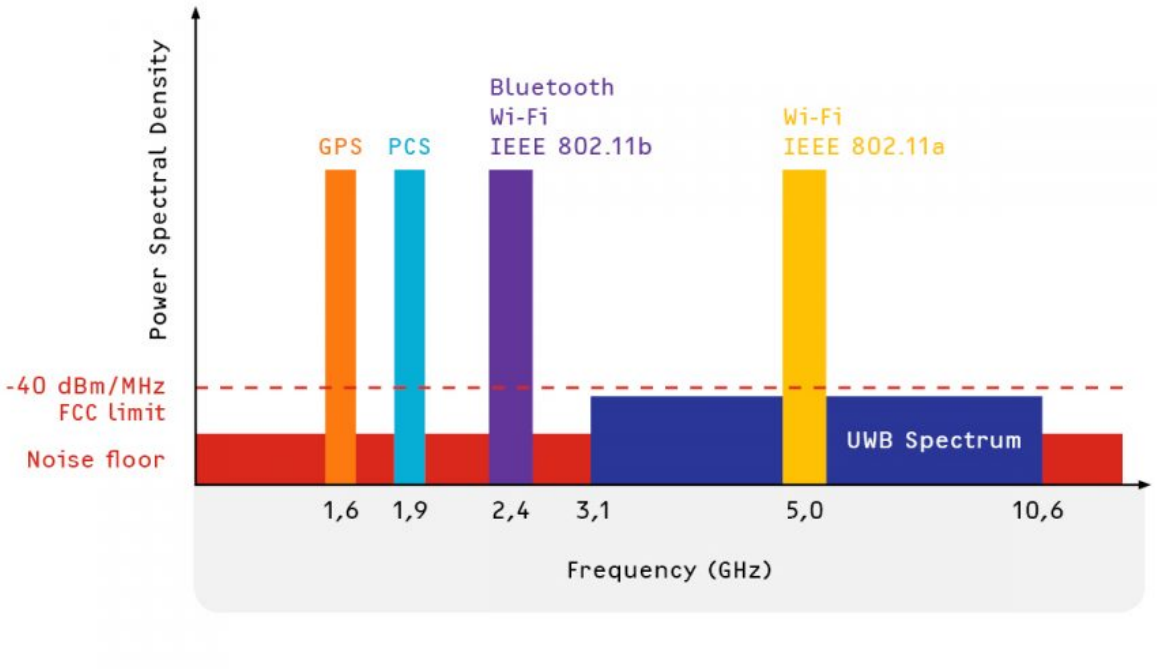


Figure 4.1: UWB frequency spectrum figure from [18]

## 4.3 Position Reconstruction Using $n \geq 4$ Range Measurements

We assume that we have $n \geq 4$ non-coplanar UWB anchors (source points) with known constant locations (positions), denoted as $d_i$ .The corresponding UWB range measurements are given by :

$$d_i = \|p - p_i\|, i = 1, \ldots, 4 \tag{4.1}$$

we can proceed as follows.First define the following measurable scalars :

$$y_i = \frac{1}{2}(d_i^2 - d_1^2 - \|p_i\|^2 + \|p_1\|^2), i = 2, \ldots, 4. \tag{4.2}$$

Then, one can show that $y_i = (p_1 - p_i)^\top p, i = 2, \ldots, 4$. By defining $y = [y_2, \ldots, y_n]^\top$, one can obtains :

$$y = \begin{bmatrix} (p_1 - p_2)^\top \\ \vdots \\ (p_1 - p_n)^\top \end{bmatrix} p, \tag{4.3}$$

which encodes the position information provided by the range measurements.

## 4.4 Position Reconstruction Using 3 Range Measurements

The idea is to deploy 3 UWB anchors (source points) in a non colinear form. These 3 points make a plan given by an equation of this type : $ax + by + cz + d = 0$. Then restrict the vehicle movement to either above the plan only or under the plan only and make sure that the vehicle will not cross the plan formed by the three source points during it's operating time. To illustrate this method first, let us assume that the ground surface corresponds to $z = 0$ plane in the reference frame, which limits the unmanned vehicle movement only in the $z > 0$ area.

Now assume we have 3 source points (UWB anchors) deployed at these locations $p_1(0, 0, 0)$, $p_2(1, 0, 0)$ and $p_3(0, 1, 0)$, the corresponding range measurements denoted by $d_i, i = 1, 2, 3$ and where $p = [x, y, z]^\top$ are given by:

$$x^2 + y^2 + z^2 = d_1^2 \tag{4.4}$$
$$(x - 1)^2 + y^2 + z^2 = d_2^2 \tag{4.5}$$
$$x^2 + (y - 1)^2 + z^2 = d_3^2 \tag{4.6}$$

subtracting (4.5) from (4.4) and (4.6) from (4.4), we obtain:

$$x = \frac{1}{2}(d_1^2 - d_2^2 + 1), \tag{4.7}$$
$$y = \frac{1}{2}(d_1^2 - d_3^2 + 1) \tag{4.8}$$

and :

$$z^2 = d_1^2 - x^2 - y^2. \tag{4.9}$$

Note that $d_1^2 - x^2 - y^2 = f(d_1, d_2, d_3) = q_1^2 - \frac{1}{4}(d^2 - d_2^2 + 1)^2 - \frac{1}{4}(d^2 - d_3^2 + 1)^2$ is always a positive value because of the existence of intersection point between the three spheres defined at (4.4)-(4.5) and (4.6) which corresponds to ($p$ UAV center). The positiveness $z^2$ can also

be shown by determining the minimum value of $f(d_1, d_2, d_3)$ under the different triangular inequalities constraint of the triangles formed by the anchors and the UAV using Lagrange method, which results in finding that, the nature of the point$(d_1, d_2, d_3) = (0, 1, 1)$ in a minimum of $f$ under the previous constraints. The positiveness of $z^2$ means that $z$ will always have positive and negative values, and taking the assumption established before into consideration, we can reconstruct the output vector $y$ by always taking the positive value of $z$.

## 4.5 Position Reconstruction Using 2 Range Measurements and Altimeter

### 4.5.1 Barometric Altimeter Sensor

Altimeters are devices designed to calculate the height of a vehicle above the surface directly below it. This height may be Above Ground Level (AGL) or Above Sea Level (ASL).

Different types of altimeter use different technologies to calculate the altitude, including pressure-density to altitude relation. The altitude can be calculated by comparing the atmospheric pressure at the current height with the pressure at ground level. In general terms, the greater the altitude the lower the pressure. However, air pressure is affected not only by altitude, air pressure may also fluctuate due to changes in the weather which may cause changes in both pressure and temperature. These variables must be taken into account during the calibration process in order to obtain an accurate reading from a barometric altimeter. To calculate altitude, a barometric altimeter uses the following equation:

$$z = \log(P_0/P). \tag{4.10}$$

where :

$\mu$ : is a constant that depends on the acceleration of gravity and the molar mass of the air,

$T$ : is absolute temperature,

$P$ : is the pressure at the altitude $z$,

$Po$ : is the pressure at the ground level.

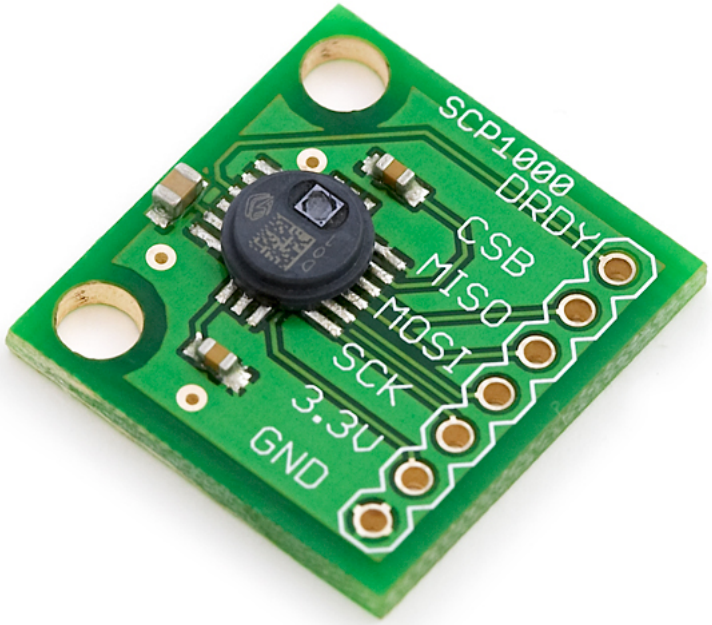


Figure 4.2: MEMS Barometric Altimeter

### 4.5.2 Inertial Navigation System (INS)

An Inertial Navigation System (INS) is a device that uses accelerometer data with gyroscope data to calculate the position, velocity and orientation of the vehicle. The INS algorithmes are based on the Dead Reckoning method which consists of calculating the current position by using a previously determined position. The orientation and the transitional states are obtained from integrating the measurements of the IMU (gyroscope and accelerometer) and using a stochastic estimation method to filter the noise such as Kalman filter. However, All inertial navigation systems suffer from integration drift, small errors in the measurement of acceleration and angular velocity are integrated into progressively larger errors in velocity, which are compounded into still greater errors in position. Since the new position is calculated from the previous calculated position and the measured acceleration and angular velocity, these errors accumulate roughly proportionally to the time since the initial position was input. Even the best accelerometers, with a standard error of $10(/sec^2)$, would accumulate a large significant error within minutes. Therefore, the position must be periodically corrected by input from some other type of position measurements such as GPS or UWB.

### 4.5.3 Reconstruction Method

We assume available 2 UWB source points deployed at these locations $p_1(0,0,0)$ and $p_2(1,0,0)$, an altimeter sensor that provides $z$ position and an INS (Inertial Navigation System) algorithm that uses accelerometer and gyroscope data from and Inertial Measurement Unit (IMU) to output linear velocity, and position measurements, these measurements are given by:

$$x^2 + y^2 + z^2 = d_1^2, \tag{4.11}$$
$$(x-1)^2 + y^2 + z^2 = d_2^2, \tag{4.12}$$
$$z_{mes} = z + \eta_{alt}, \tag{4.13}$$
$$v_{ins} = v + \delta_v, \tag{4.14}$$
$$p_{ins} = p + \delta_p, \tag{4.15}$$

where $\eta_{alt}$ is the altimeter noise, $p_{ins}$ and $v_{ins}$ are position and velocity measurements provided by the INS algorithm, $\delta_v$ and $\delta_p$ are integration drifts. From (4.11) and (4.12) and altimeter measurements, we can obtain:

$$x = \frac{1}{2}(d_1^2 - d_2^2 + 1), \tag{4.16}$$
$$y^2 = d_1^2 - x^2 - z^2. \tag{4.17}$$

Same as the previous method, $y$ here has a positive and a negative value. We propose the following algorithm to reconstruct the $y$ position measurement and here $y_1$ and $y_2$ are solutions for equation (4.17) and $y_{ins}$ is the measurement output from the INS algorithm. :

**Algorithm 1:** y position measurement reconstruction

**Result:** y
initialization;
**while** $t \leq t_f$ **do**
  **if** $abs(y_1 - y_{ins}) < abs(y_2 - y_{ins})$ **then**
    $y{=}y_1$
    $y_{ins} = y_1$
  **else**
    $y{=}y_1$
    $y_{ins} = y_1$
  **end**
  $y_{ins} = y_{ins} + h.v_{yins}$
**end**

This algorithm takes INS outputs and compares it with the two values of $y$ from (4.17), since the difference between the INS outputs and real $y$ value is the integration drift. The

algorithm corrects $y_{ins}$ each step to ensure that the difference between the real $y$ value and $y_{ins}$ is the drift due to one integration step denoted $h$.

## 4.6 Conclusion

In this chapter we presented the UWB technology for range measurements and the vehicle position measurements reconstruction using 4 or more anchors. We also proposed two solution to reconstruct the position information when less than 4 anchors are available. The first method imposes some limitation to the vehicle's movement area while the second method works in all cases. However, both methods don't perform well when the range measurements are very noisy, a possible and interesting solution is to filter the measurements using Volterra observer [19] before using them in the two reconstruction algorithms.

CHAPTER 5

# State Estimation for Non-Accelerated Vehicles

## 5.1 Introduction

In this chapter, we study two estimation approaches for UAV that performs low linear accelerations, a Complimentary filter with linear Kalman filter in section 5.2.1 and an attitude Sliding Mode observer with linear Kalman filter in section 5.2.2. Both estimation approaches provide position, linear velocity and orientation obtained directly on the rotation group to avoid singularities or ambiguities. The observers uses IMU measurements along with range sensors that provides position information. A comparison study is provided in section 5.3.

## 5.2 Complete State Estimation

In this section, we want to estimate the full state of the vehicle (position, velocity and attitude) under the following main assumption :

**Assumption 1.** The vehicle is near to hover and performs near to zero accelerations $a_B \approx -gR^\top e_3$.

Assumption 1 means that the rotational dynamics is decoupled from the transitional dynamics, which means we can estimate the attitude of the vehicle using one of the observers defined in Chapter 3, then use the estimated attitude to estimate the transitional states (position and velocity).

### 5.2.1 Complimentary Filter and Kalman Filter

Decoupling the attitude estimation from the position and linear velocity estimation allow us to estimate the attitude first then use the estimated attitude to estimate the transitional states, this approach is given as follows :

$$\begin{cases} \dot{\hat{R}} = \hat{R}[\omega^y + k_p\sigma_R]_\times, \\ \sigma_R = \rho_1(a_B \times R^\top a_I) + \rho_2(m_B \times R^\top m_I). \end{cases} \tag{5.1}$$

And

$$\begin{cases} \dot{p} = v, \\ \dot{v} = u, \end{cases} \tag{5.2}$$

where

$$u = ge_3 + \hat{R}a_B. \tag{5.3}$$

We can safely represent the transitional system as follows :

$$\begin{cases} \dot{x} = Ax + Bu, \\ y = Cx, \end{cases} \tag{5.4}$$

where $x = [p^\top; v^\top]^\top$ and $A = \begin{bmatrix} 0_{3\times3} & I_3 \\ 0_{3\times3} & 0_{3\times3} \end{bmatrix}$, $B = \begin{bmatrix} 0_{3\times3} \\ I_3 \end{bmatrix}$ and $C = \begin{bmatrix} I_3 & 0_{3\times3} \end{bmatrix}$

The Kalman filter of the transitional system is given by :

$$\begin{cases} \dot{\hat{x}} = A\hat{x} + Bu + LC(x - \hat{x}), \\ \hat{y} = C\hat{x}, \end{cases} \tag{5.5}$$

and

$$L = PC^\top R^{-1}, \tag{5.6}$$

$$\dot{P} = AP + PA^\top - PCR^{-1}CP + Q \tag{5.7}$$

with $P$ being the solution of the differential Riccati equation thanks to the fact that the pair (A,C) is uniformly observable, the Riccati equation is well conditioned and the solution converges to a constant. and $R$ and $Q$ are the process and covariance matrices.

### Numerical Simulation

In this section, we implement the estimation approach defined in the previous section to estimate the vehicle's full state using UWB and IMU measurements. Consider a vehicle navigating in inertial frame following this low accelerated trajectory:

$$p(t) = \begin{bmatrix} 1.5 + \frac{1}{2}\sin(2\pi t/T) \\ 2.5 + \frac{1}{2}\cos(2\pi t/T) \\ 1.25 + \frac{1}{4}\cos(2\pi t/T) \end{bmatrix}, T = 100. \tag{5.8}$$

The angular velocity applied to the vehicle is given by:

$$\omega(t) = \begin{bmatrix} 0.3\cos(\pi t/10) \\ 0.5\cos(2\pi t/10 + \pi/4) \\ 0.8\cos(4\pi t/10) \end{bmatrix} \tag{5.9}$$

With an initial attitude $R(0) = \exp([r_0]_\times), r_0 = [\pi/6; \pi/5; \pi/5]^\top$. The inertial earth's magnetic field is taken as $m_I = [0.42; 0.2949; 0.15]^\top$Gauss, and the earth's gravity is $g = 9.81m/s^2$. The inital conditions of the observer are $\hat{x} = [0; 0; 0; 0; 0; 0]^\top$. $\hat{R}(0) = I_3$ and $P(0) = I_6$ with $Q = 0.01 \times I_3$ and $V = 0.2 \times I_6$, and the parameters are taken as $\rho_1 = 2$,

$\rho_2 = \rho_1/6$,and $k_p = 1$. The measurement noises are modelled as a Gaussian white noises with variances, $\sigma_\omega = 0.16(deg/s^2)$,$\sigma_{acc} = 3.10^{-4}(m/s^2)$ and $\sigma_{mag} = 0.025(Gauss)$.

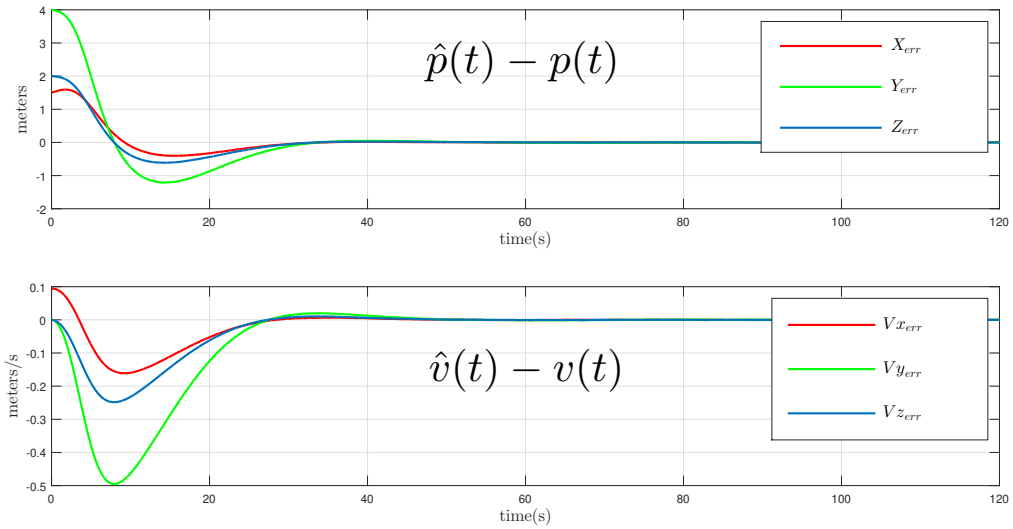


Figure 5.1: Position and velocity estimation errors versus time using Complimentary filter with Kalman filter

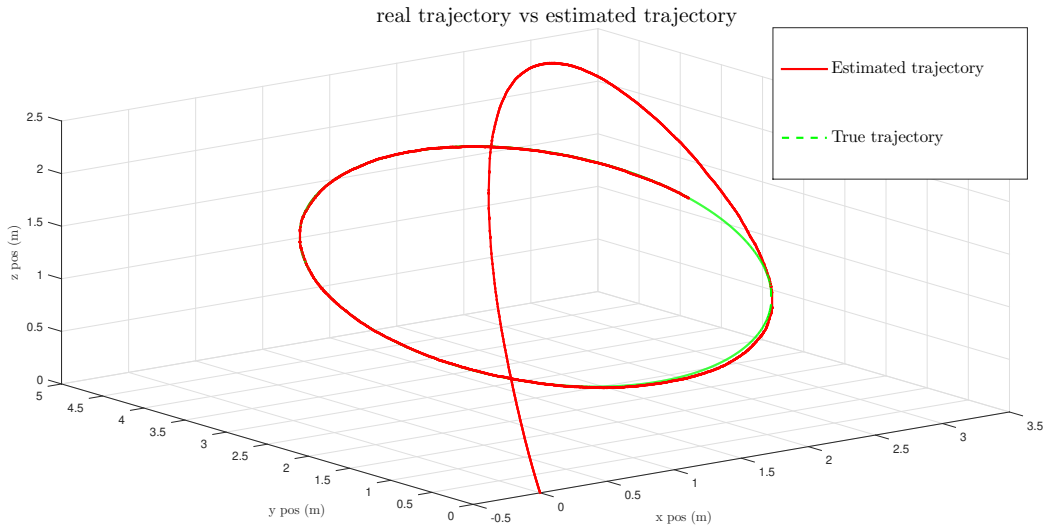


Figure 5.2: Estimated trajectory versus true trajectory using Complimentary filter with Kalman filter

### 5.2.2 Sliding Mode Observer and Kalman Filter

Same as the previous observer, the rotational dynamics are decoupled from the transitional dynamics. Here we use the Sliding mode defined in the section 3.5 to estimate the orientation, then we estimate the rotational states using Kalman filter, the estimation approach is given as follow:

$$\begin{cases} \dot{\hat{R}} = \hat{R}[\omega^y + k_p \Psi(\sigma)]_\times, \\ \sigma = \rho_1(a_B \times R^\top a_I) + \rho_2(m_B \times R^\top m_I), \\ \Psi(\sigma_R) = \frac{2}{\pi}\Big[\arctan(m\sigma_1) \quad \arctan(m\sigma_2) \quad \arctan(m\sigma_3)\Big]^\top. \end{cases} \tag{5.10}$$

The Kalman filter of the transitional system is given by :

$$\begin{cases} \dot{\hat{x}} = A\hat{x} + Bu + LC(x - \hat{x}), \\ \hat{y} = C\hat{x}. \end{cases} \tag{5.11}$$

and

$$L = PC^\top R^{-1}, \tag{5.12}$$

$$\dot{P} = AP + PA^\top - PCR^{-1}CP + Q. \tag{5.13}$$

#### Numerical Simulation

In this subsection, we implement the estimation approach defined in the previous section to estimate the vehicle's full state using UWB and IMU measurements. Consider a vehicle navigating in inertial frame following this low accelerated trajectory:

$$p(t) = \begin{bmatrix} 1.5 + \frac{1}{2}\sin(2\pi t/T) \\ 2.5 + \frac{1}{2}\cos(2\pi t/T) \\ 1.25 + \frac{1}{4}\cos(2\pi t/T) \end{bmatrix}, T = 100. \tag{5.14}$$

The angular velocity applied to the vehicle is given by:

$$\omega(t) = \begin{bmatrix} 0.3\cos(\pi t/10) \\ 0.5\cos(2\pi t/10 + \pi/4) \\ 0.8\cos(4\pi t/10) \end{bmatrix}. \tag{5.15}$$

With an initial attitude $R(0) = \exp([r_0]_\times), r_0 = [\pi/6; \pi/5; \pi/5]^\top$. The inertial earth's magnetic field is taken as$m_I = [0.42; 0.2949; 0.15]^\top$Gauss, and the earth's gravity is $g = 9.81 m/s^2$. The inital conditions of the observer are $\hat{x} = [0; 0; 0; 0; 0; 0]^\top$. $\hat{R}(0) = I_3$ and

$P(0) = I_6$ with $Q = 0.01 \times I_3$ and $V = 0.2 \times I_6$, and the parameters are taken as $\rho_1 = 2$, $\rho_2 = \rho_1/6$,and $k_p = 1$. The measurement noises are modelled as a Gaussian white noises with variances, $\sigma_\omega = 0.16(deg/s^2)$,$\sigma_{acc} = 3.10^{-4}(m/s^2)$ and $\sigma_{mag} = 0.025(Gauss)$.

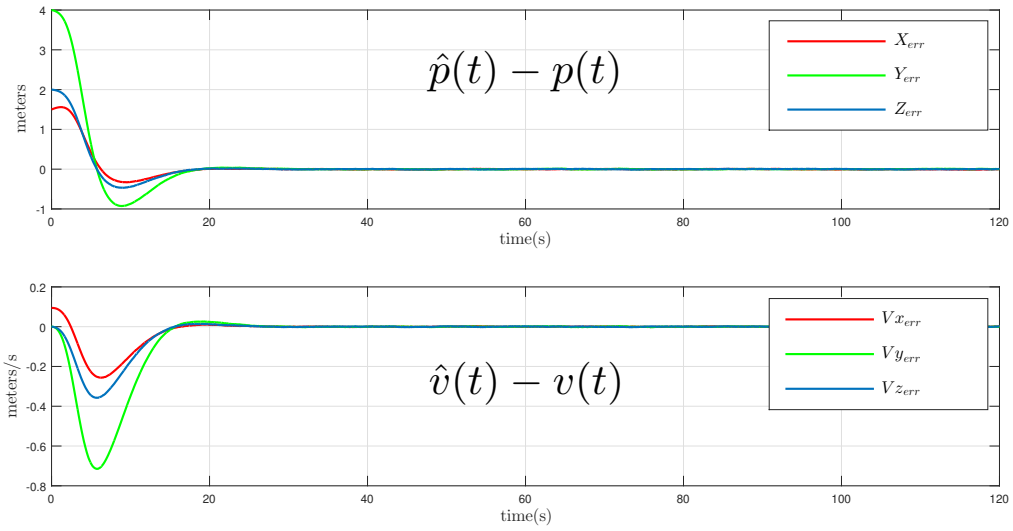


Figure 5.3: Position and velocity estimation errors versus time using Complimentary filter with Kalman filter

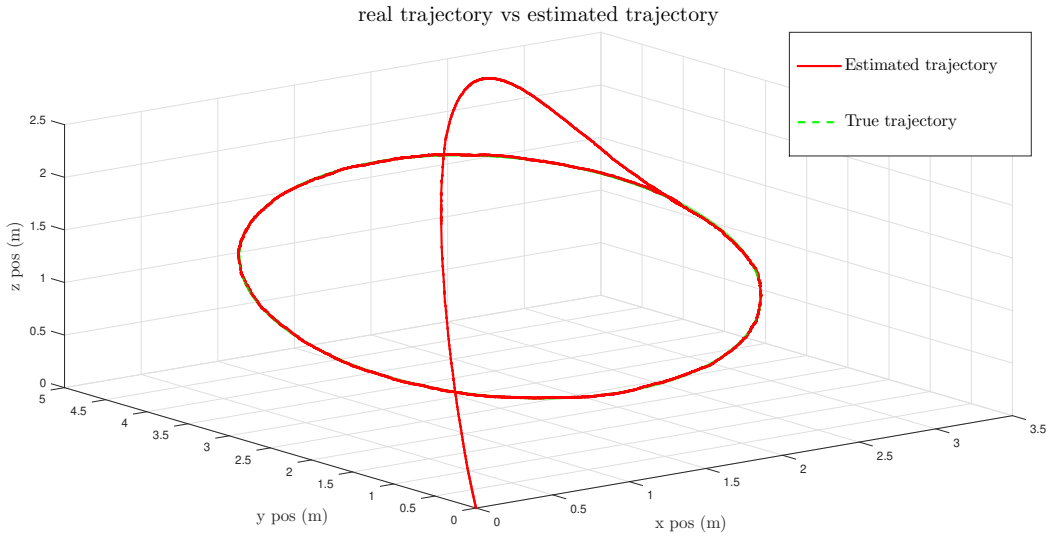


Figure 5.4: Estimated trajectory versus true trajectory using Complimentary filter with Kalman filter

## 5.3 Comparison Study

In this section, we will compare the previous full state estimation approaches and test their robustness by increasing the acceleration performed by the vehicle and see the performance of the two estimation approaches. It is easily seen that decreasing $T$ in the following trajectory will result in performing bigger acceleration. First let us consider the case where $T = 100s$ :

$$p(t) = \begin{bmatrix} 1.5 + \frac{1}{2}\sin(2\pi t/T) \\ 2.5 + \frac{1}{2}\cos(2\pi t/T) \\ 1.25 + \frac{1}{4}\cos(2\pi t/T) \end{bmatrix}, T = 100. \tag{5.16}$$

The angular velocity applied to the vehicle is given by:

$$\omega(t) = \begin{bmatrix} 0.3\cos(\pi t/10) \\ 0.5\cos(2\pi t/10 + \pi/4) \\ 0.8\cos(4\pi t/10) \end{bmatrix}. \tag{5.17}$$

First let us see the noise filtering :

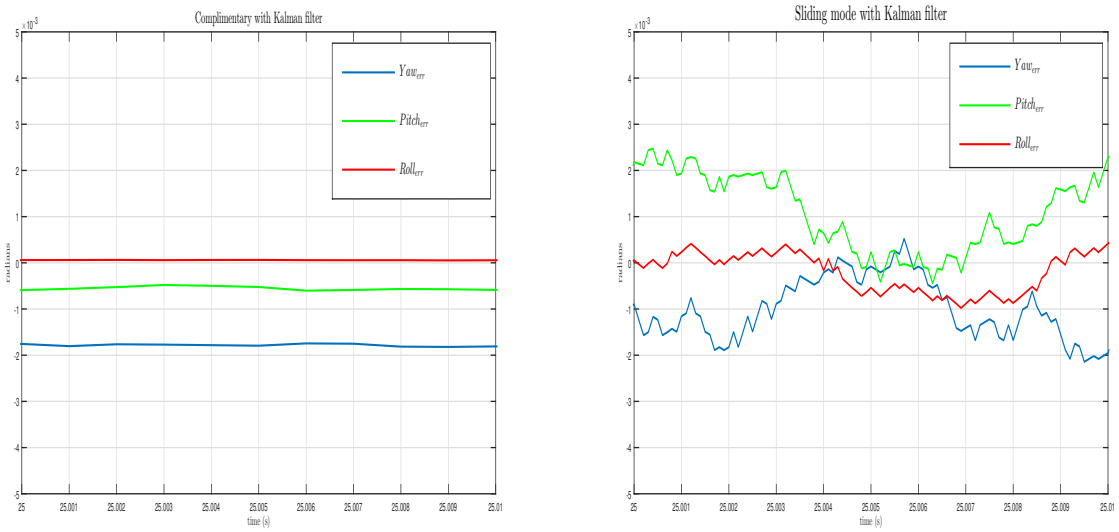


(a) Complimentary with Kalman

(b) Sliding mode with Kalman

Figure 5.5: Noise filtering comparison between Sliding mode with Kalman filter observer and Complimentary with Kalman filter

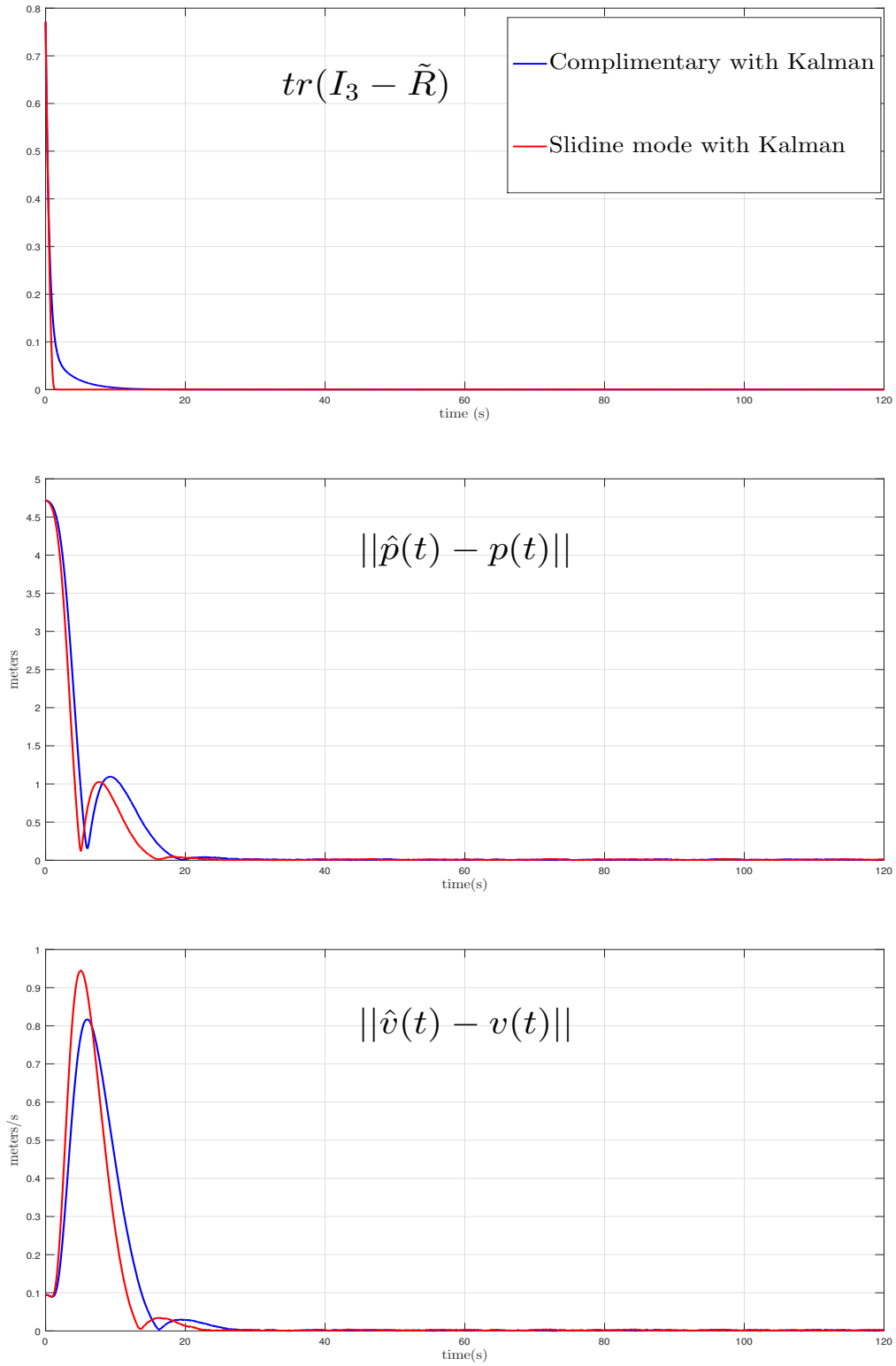


Figure 5.6: Comparison between Sliding mode with Kalman filter observer in red and Complimentary with Kalman filter in blue in case of T=100

The case when $T = 30s$ will result in a faster trajectory :

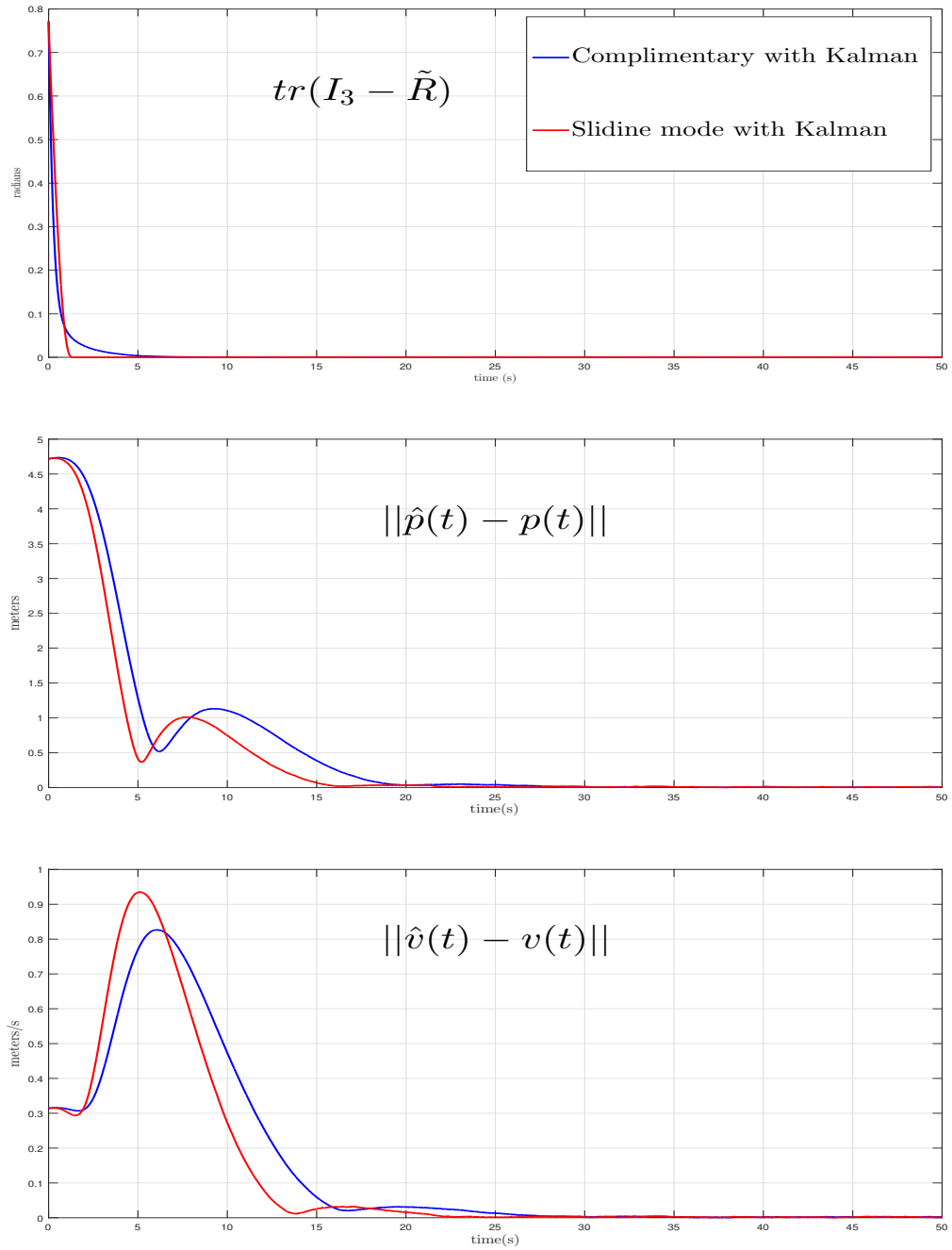


Figure 5.7: Comparison between Sliding mode with Kalman filter observer in red and Complimentary with Kalman filter in blue in case of T=100

Finally the case when $T = 10s$ :

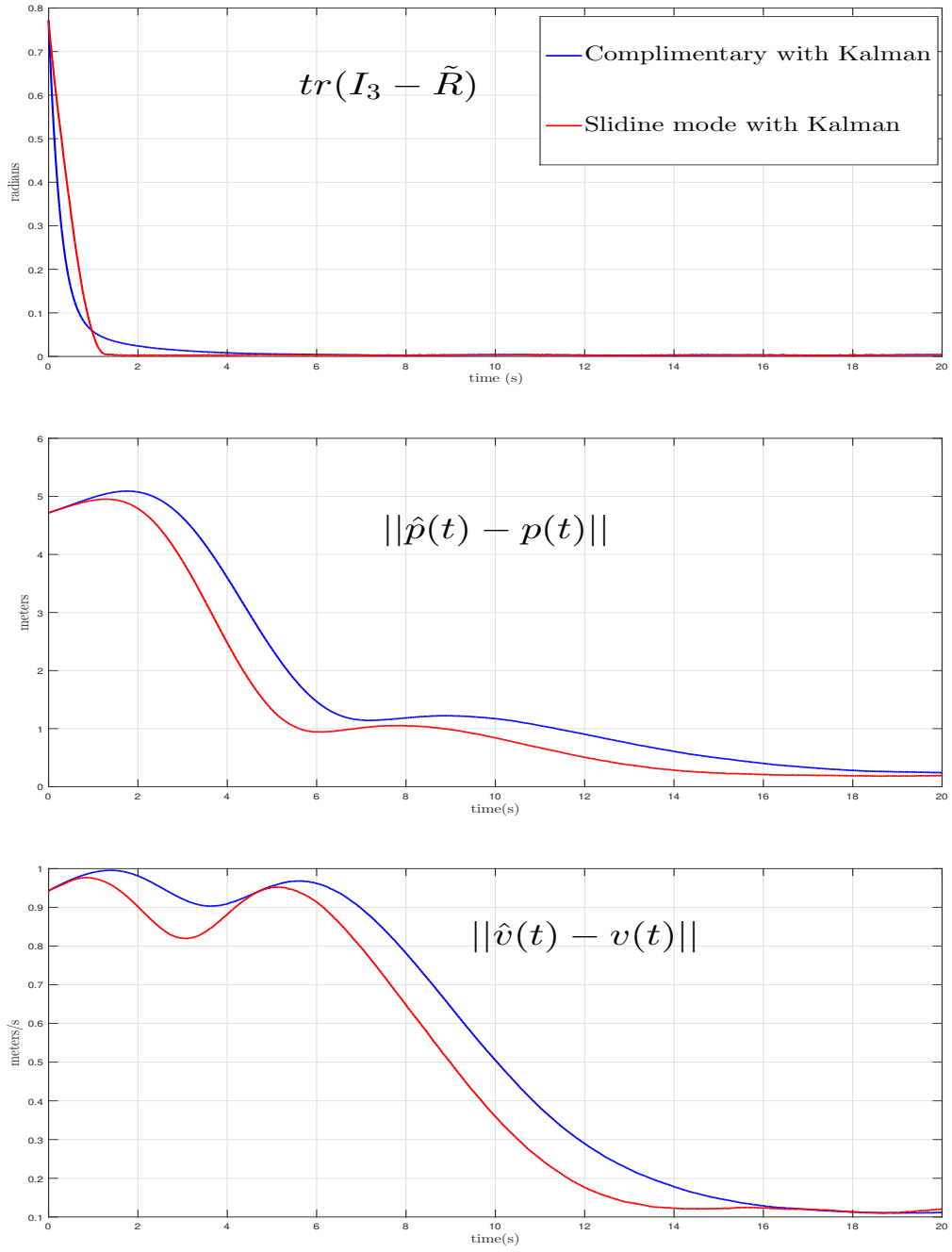


Figure 5.8: Comparison between Sliding mode with Kalman filter observer in red and Complimentary with Kalman filter in blue in case of T=100

## 5.4 Conclusion

In this chapter, we proposed two estimation approaches for UAV that performs low linear accelerations. The two estimation approaches require the use of vector measurements. The two observers were compared by increasing the vehicle's linear acceleration. The sliding mode observer with Kalman filter converges faster than the Complimentary filter with Kalman filter for all the accelerations. However, the Complimentary filter with Kalman filter have a better noise handling in attitude estimations than the Sliding mode with Kalman filter due to the chattering phenomenon that occurs when using the Sliding mode observer.

CHAPTER 6

# Stat Estimation for Accelerated Vehicles

## 6.1 Introduction

Early works on UAV state observation use stochastic observers such as Kalman filter to navigate. However, these stochastic observers rely on linearization assumption and may not be reliable in certain cases when the initial errors are important. Recently, nonlinear deterministic observers are studied as they offer robustness and stability properties provided by Lyapunov theorems while dealing with the interconnection between the rotational and transitional state due to performing accelerated trajectory. Moreover, compared to stochastic estimators, the nonlinear deterministic estimators are usually less computationally demanding.

In this chapter, we propose two nonlinear deterministic observers a Riccati high-order observer in section 6.3 and a constant gain observer in section 6.4. Both observers provide position, linear velocity and orientation obtained directly on the rotation group to avoid singularities or ambiguities. The observers use IMU measurements along with range sensors that provides position information. The asymptotic stability of the two observers is proved using Lyapunov-based stability tools.

## 6.2 System Model and Measurements

### 6.2.1 System Model

$$\dot{p} = v, \tag{6.1}$$
$$\dot{v} = ge_3 + Ra_B, \tag{6.2}$$
$$\dot{R} = R[\omega]_\times, \tag{6.3}$$

where $p \in \mathbb{R}^3$ is the inertial position of the vehicle's center of gravity, $v \in \mathbb{R}^3$ represents the inertial linear velocity, $R \in \mathbb{S}O(3)$ is the attitude matrix describing the orientation of a body-attached frame with respect to the inertial frame, $\omega$ is the angular velocity of the body-attached frame with respect to the inertial frame expressed in the body-attached frame, g in the norm of the acceleration due to gravity,$e_3 = [0, 0, 1]^T$ and $a_B = R^T a_I$ is the "apparent acceleration", capturing all non gravitational forces applied to the vehicle, expressed in the body-attached frame.

### 6.2.2 Measurements

We assume available an IMU that provides measurements of the angular velocity, the body-attached frame apparent acceleration and the body-attached frame magnetic field. These sensors are modelled :

$$\omega^y = \omega + \eta_\omega, \tag{6.4}$$
$$a_B = R^\top a_I + \eta_{acc}, \tag{6.5}$$
$$m_B = R^\top m_I + \eta_{mag}, \tag{6.6}$$

where $m_I$ is the constant and known earth's magnetic field, $a_I$ is a time-varying unknown apparent acceleration, $\eta_\omega$, $\eta_{acc}$ and $\eta_{mag}$ are respectively gyroscope, accelerometer and magnetometer noises. We also assume that we have measurements of the following output vector :

$$y = p. \tag{6.7}$$

### 6.2.3 Objective

The objective is to design a converging state observer to estimate position, velocity and orientation of the vehicle relying on measurements (6.4)-(6.6) under these assumptions :
**Assumption 1.** There exists a constants $c_0$ such that
$\|m_I \times a_I\| \geq c_0$ for all $t \geq 0$.

**Assumption 2.** There exist constants $c_1, c_2, c_3 > 0$ such that $c1 \leq \|a_I(t)\| \leq c_2$ and $\|\dot{a}_I(t)\| \leq c_3$ for all $t \geq 0$.

**Assumption 3.** There exists a constant $c_4 \geq 0$ such that $\|\dot{\omega}_I(t)\| \leq c_4$.

These assumptions are due to real physical constraints on the system.

## 6.3 Riccati High-Order State Observer

In this section, we design a time-varying gain observer by considering the extended transnational state $x := \left[p^\top, v^\top, a_I^\top\right]^\top \in \mathbb{R}^9$. In view of (6.1) – (6.3) and (6.4) – (6.6), the dynamics of $x$ are written as follows :

$$\dot{x} = \bar{A}x + Bge_3 + \underline{B}\dot{a}_I, \tag{6.8}$$
$$y = Cx, \tag{6.9}$$

where the matrices $\bar{A}, \bar{B}, \underline{B}$ and $C$ are defined as follows:

$$\bar{A} = \begin{bmatrix} 0_{3\times3} & I_3 & 0_{3\times3} \\ 0_{3\times3} & 0_{3\times3} & I_3 \\ 0_{3\times3} & 0_{3\times3} & 0_{3\times3} \end{bmatrix}, \quad \bar{B} = \begin{bmatrix} 0_{3\times3} \\ I_3 \\ 0_{3\times3} \end{bmatrix}, \quad \underline{B} = \begin{bmatrix} 0_{3\times3} \\ 0_{3\times3} \\ I_3 \end{bmatrix}, C = \begin{bmatrix} I_3 & 0_{3\times3} & 0_{3\times3} \end{bmatrix}. \tag{6.10}$$

We have simplified the observer given in [4] by ignoring the gyro bias estimator, it is given as follows :

$$\hat{x} = \underline{B}\hat{R}a_B + \hat{z}, \tag{6.11}$$
$$\dot{\hat{z}} = \bar{A}\hat{z} + \bar{B}\left(ge_3 + \hat{R}a_B\right) + K(t)(y - C\hat{x}) + \sigma_1, \tag{6.12}$$
$$\dot{\hat{R}} = \hat{R}\left[\omega^y + k_1\sigma_2\right]_\times, \tag{6.13}$$

with initial conditions $\hat{x}(0) \in \mathbb{R}^6, R(0) \in \mathbb{SO}(3)$. The innovation terms $\sigma_1 \in \mathbb{R}^9$ and $\sigma_2 \in \mathbb{R}^3$ are defined as follows:

$$\sigma_1 = -k_1\underline{B}\left[\hat{R}\sigma_2\right]_\times \hat{R}a_B, \tag{6.14}$$
$$\sigma_2 = \rho_1\left(m_B \times \hat{R}^\top m_I\right) + \rho_2\left(a_B \times \hat{R}^\top \mathrm{sat}_{\hat{c}_2}\left(\hat{a}_I\right)\right), \tag{6.15}$$
$$\hat{a}_I = \hat{R}a_B + \underline{B}^\top\hat{z}, \tag{6.16}$$

where $k_1, k_2, \rho_1, \rho_2$and $\hat{c}_2$ are positive with $\hat{c}_2 > c_2$, the gain matrix is chosen as $K(t) = \gamma L_\gamma P(t) C^\top Q(t)$, with $L_\gamma = blockdiag\left(I_3, \gamma I_3, \gamma^2 I_3\right)$, $sat_{\hat{c}_2}(\hat{a}_I) = min(1, \hat{c}_2/\|\hat{a}_I\|)\hat{a}_I$ and $P(t)$ is solution to the following continuous differential Riccati-like equation:

$$\frac{1}{\gamma}\dot{P} = \bar{A}P + P\bar{A}^\top - PC^\top Q(t)CP + V(t)$$

where $\gamma \geq 1, P(0) \in \mathbb{R}^{9\times9}$ positive define, $Q(t) \in \mathbb{R}^{3\times3}$ and $V(t) \in \mathbb{R}^{9\times9}$ are continuous, bounded and uniformly positive definite matrices. Note that choosing $\gamma = 1$ yields the

traditional continuous Riccati equation used in the Kalman filter where $Q^{-1}(t)$ and $V(t)$ are interpreted as the covariance matrices for the output $y$ and the process, respectively. The introduction of the scalar $\gamma$ allows for the asymptotic stability of the interconnection of the transnational and rotational parts of the nonlinear observer.

### 6.3.1 Stability Analysis

Let us define the following error variables:

$$\tilde{x} = x - \hat{x}, \tag{6.17}$$
$$\tilde{R} = R\hat{R}^{\top}, \tag{6.18}$$
$$\zeta = L_{\gamma}^{-1}\tilde{x}. \tag{6.19}$$

Now consider the following positives definite functions:

$$\mathbf{V}(\zeta) = \frac{1}{\gamma}\zeta^{\top}P^{-1}\zeta. \tag{6.20}$$

$$\mathbf{W}(\zeta, \tilde{R}) = \mathbf{V}(\zeta) + \frac{1}{4}\operatorname{tr}(M_0 - M_0\tilde{R}). \tag{6.21}$$

One can show the following result by following the proof steps of the same observer found in [4] :

$$\dot{\mathbf{W}} \leq -k_p\|\sigma_2\|^2 - \frac{\gamma\beta_1 v_m}{2\beta_2^2}\mathbf{V}(\zeta). \quad \forall\|\zeta\|^2 \geq \frac{4c_g\beta_2^2}{\gamma^3\beta_1 v_m} \tag{6.22}$$

**W** shows that the proposed nonlinear observer guarantees the convergences and the asymptotic stability of the zero estimation errors, for $t \geq T$ and angles errors less than $180°$.

### 6.3.2 Numerical Simulation

In this section, we implement the Riccati high-gain observer defined in section 6.3 to estimate the vehicle full state using 3 range measurements. Consider a vehicle navigating in inertial frame following this trajectory:

$$p(t) = \begin{bmatrix} \sin(\pi/3)\sin(2kt)/2 \\ \cos(\pi/3)\sin(2kt)/2 \\ 3+\cos(kt) \end{bmatrix}, k = 0.5. \tag{6.23}$$

The angular velocity applied to the vehicle is given by:

$$\omega(t) = \begin{bmatrix} 0.3\cos(\pi t/10) \\ 0.5\cos(2\pi t/10+\pi/4) \\ 0.8\cos(4\pi t/10) \end{bmatrix}. \tag{6.24}$$

With an initial attitude $R(0) = \exp(\frac{\pi}{2}[e_2]_\times)$. The inertial earth's magnetic field is taken as$m_I = [0.42; 0.2949; 0.15]^\top$Gauss, and the earth's gravity is $g = 9.81m/s^2$. The initial conditions of the observer are $\hat{z} = [1;1;1;1;1;1;1;1;1;1]^\top$. $\hat{R}(0) = I_3$ and $P(0) = I_9$ with $Q = 0.1 \times I_3$ and $V = 0.15 \times I_9$, and the parameters are taken as $\rho_1 = 2/6$, $\rho_2 = 2$, $k_1 = k_2 = 2$, $\gamma = 4$ and $\hat{c}_2 = 15$. The measurement noises are modelled as a Gaussian white noises with variances, $\sigma_\omega = 0.16(deg/s^2)$,$\sigma_{acc} = 3.10^{-4}(m/s^2)$ and $\sigma_{mag} = 0.025(Gauss)$.

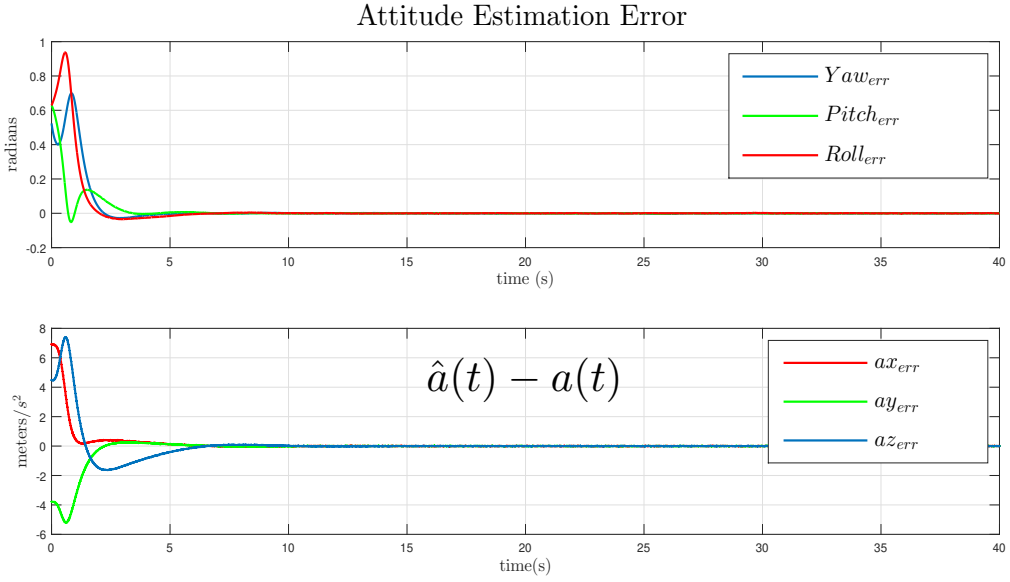


Figure 6.1: Attitude and acceleration estimation errors versus time using Riccati high-order observer

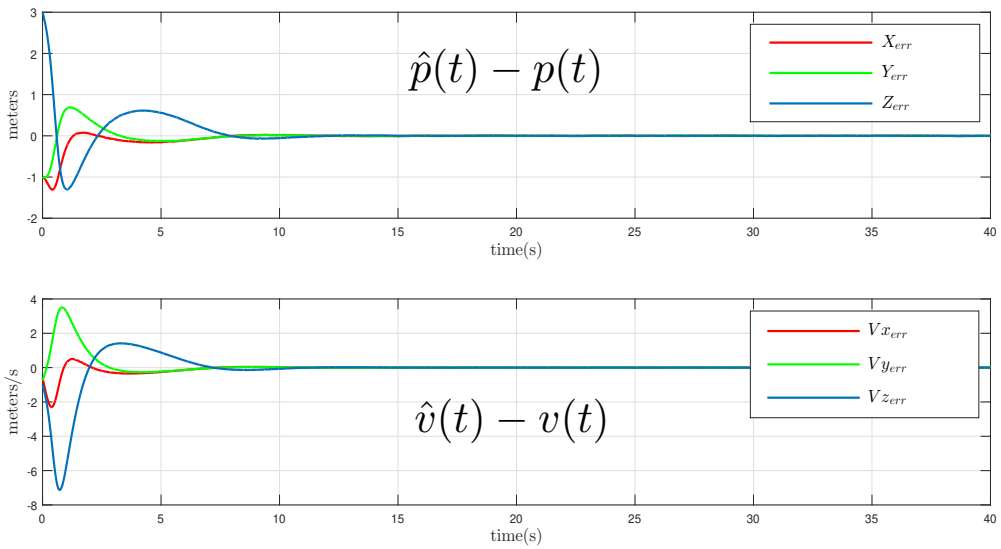


Figure 6.2: Position and velocity estimation errors versus time using Riccati high-order observer

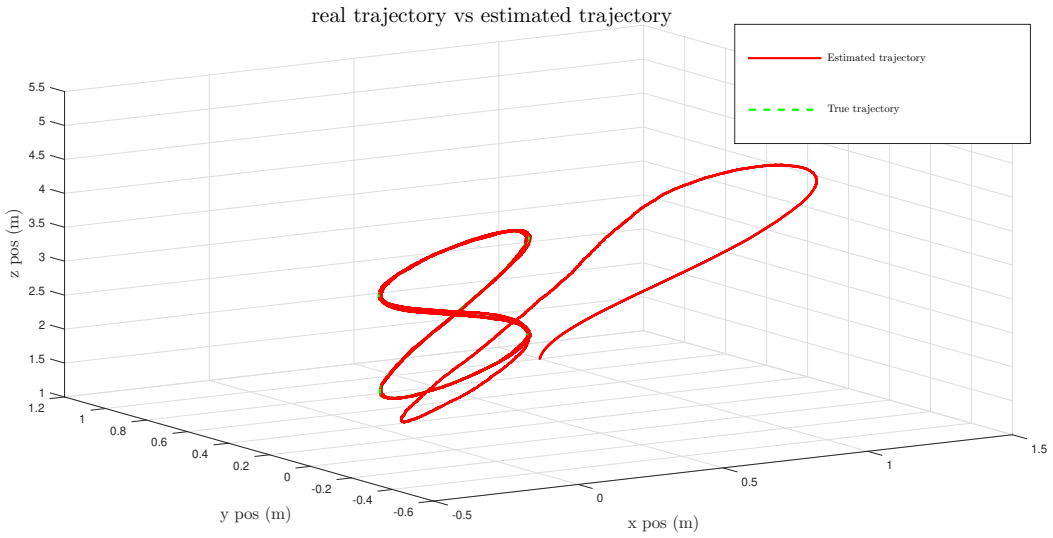


Figure 6.3: Estimated trajectory versus true trajectory using Riccati high-order observer

## 6.4 Constant Gain State Observer :

In this section, we study a constant gain observer to estimate the full state $(p, v, R)$ consisting of position, velocity and attitude. We define the combined following state $x = [p^\top, v^\top]^\top \in \mathbb{R}^6$, the dynamics of $x$ are written as follows :

$$\dot{x} = Ax + B(ge_3 + Ra_B), \tag{6.25}$$
$$y = Cx, \tag{6.26}$$

where

$$A = \begin{bmatrix} 0_{3\times3} & I_3 \\ 0_{3\times3} & 0_{3\times3} \end{bmatrix}, \tag{6.27}$$
$$C = \begin{bmatrix} I_3 & 0_{3\times3} \end{bmatrix}, \tag{6.28}$$
$$B = \begin{bmatrix} 0_{3\times3} & I_3 \end{bmatrix}^\top. \tag{6.29}$$

We propose the following modified version of the nonlinear observer found in [5]:

$$\dot{\hat{x}} = A\hat{x} + B(ge_3 + \hat{R}a_B) + K(y - C\hat{x}) + \sigma_1, \tag{6.30}$$
$$\dot{\hat{R}} = R[\omega^y + k_1\Psi(\sigma_2)]_\times \tag{6.31}$$

with initial conditions $\hat{x}(0) \in \mathbb{R}^6$ and $\hat{R}(0) \in \mathbb{SO}(3)$. The innovation terms $\sigma_1 \in \mathbb{R}^6$ and $\sigma_2 \in \mathbb{R}^3$ are defined as follows:

$$\sigma_1 = -k_1(A - KC)^{-1}B[\hat{R}\Psi(\sigma_2)]_\times \hat{R}a_B, \tag{6.32}$$
$$\sigma_2 = \rho_1(m_B \times \hat{R}^\top m_I) + \rho_2(a_B \times \hat{R}^\top \mathbf{sat}_{\hat{c}2}(a_I)), \tag{6.33}$$
$$\Psi(\sigma_2) = \frac{2}{\pi}\begin{bmatrix} \arctan(m\sigma_{21}) & \arctan(m\sigma_{22}) & \arctan(m\sigma_{23}) \end{bmatrix}^\top, \tag{6.34}$$
$$\hat{a}_I = \hat{R}a_B + B^\top K(y - C\hat{x}). \tag{6.35}$$

The scalars $k_1$, $\rho_1$, $\rho_2$ and $\hat{c}_2$ are positive tuning parameters with $\hat{c}_2 > c_2$ (defined in assumption (2)), $K \in \mathbb{R}^{6\times6}$ is a constant gain matrix chosen as $K = \gamma L_\gamma K_0$ such that $A - K_0C$ is Hurwitz, $L_\gamma = blockdiag(I_3, \gamma I_3)$ and $\gamma > 1$.

Introducing the $\Psi(\sigma_2)$ function eliminates any constant gyroscope bias measurements $(b_\omega)$ that may come with the IMU measurements at the form of $\omega^y = \omega + b_\omega + \eta_\omega$. Note that eliminating the gyro bias using the observer found in ref8 requires adding a gyro bias estimator which results in a slower convergence of the estimation error. However, chattering phenomenon occurs when using the sliding mode based-observer, as shown in the simulation section.

### 6.4.1 Stability Analysis

Let us define the following estimation errors

$$\tilde{R} = R\hat{R}^\top, \tag{6.36}$$
$$\tilde{x} = x - \hat{x}. \tag{6.37}$$

We also define the auxiliary variable:

$$\zeta = L_\gamma^{-1}(A - KC)\tilde{x} + L_\gamma^{-1}B(I_3 - \tilde{R})^\top a_I. \tag{6.38}$$

it is straightforward to verify the following facts:

$$a_I - \hat{a}_I = B^\top L_\gamma \zeta, \tag{6.39}$$
$$L_\gamma^{-1}KCL\gamma = \gamma K_0 C, \tag{6.40}$$
$$L_\gamma^{-1}AL_\gamma = \gamma A, \tag{6.41}$$
$$L_\gamma^{-1}B = \frac{1}{\gamma}B. \tag{6.42}$$

in view of (6.40)-(6.49) and (6.50)-(6.51), and the previous facts. One can derive the following dynamics:

$$\dot{\tilde{x}} = (A - KC)\tilde{x} + B(I_3 - \tilde{R})^\top a_I - \sigma_1, \tag{6.43}$$
$$\dot{\tilde{R}} = k_1\tilde{R}[\hat{R}\sigma_2]_\times^\top, \tag{6.44}$$
$$\dot{\zeta} = \gamma(A - K_0C)\zeta + \frac{1}{\gamma}B(I_3 - \tilde{R})^\top \dot{a}_I. \tag{6.45}$$

Now consider the following positive definite function:

$$\mathbf{V}(\zeta) = \frac{1}{\gamma}\zeta^\top P\zeta. \tag{6.46}$$

where $P$ is solution of the Lyapunov equation $P(A + K_0C) + (A - K_0C)^\top P = -I_3$ which exists and is positive definite thanks to the fact that $(A - K_0C)$ is Hurwitz. Denote $\beta_1$ and $\beta_2$ the smallest and biggest eigenvalues of $P$, respectively. The time derivative of $\mathbf{V}$ is:

$$\dot{\mathbf{V}}(\zeta) = -\|\zeta\|^2 + \frac{2}{\gamma^2}\zeta^\top PB(I_3 - \tilde{R})^\top \dot{a}_I. \tag{6.47}$$

In view of Assumption 2, it follows that:

$$\|(I_3 - \tilde{R})^\top \dot{a}_I\| \leq \sqrt{8\,\mathrm{tr}(I_3 - \tilde{R})}\|\dot{a}_I\|, \tag{6.48}$$
$$\leq \sqrt{8 \times 3}c_3, \tag{6.49}$$
$$:= c_g. \tag{6.50}$$

Then, the derivative of $\mathbf{V}$ satisfies :

$$\dot{\mathbf{V}}(\zeta) \leq -\|\zeta\|^2 + \frac{2c_g\beta_2}{\gamma^2}\|\zeta\|, \tag{6.51}$$

$$\leq \frac{-1}{2}\|\zeta\|^2 + \|\zeta\|(\frac{2\beta_2 c_g}{\gamma^2} - \frac{1}{2}\|\zeta\|), \tag{6.52}$$

$$\leq \frac{-1}{2}\|\zeta\|^2, \quad \forall\|\zeta\| \geq \frac{4\beta_2 c_g}{\gamma^2}, \tag{6.53}$$

$$\leq \frac{-\gamma}{2\beta_2}\mathbf{V}(\zeta). \quad \forall\|\zeta\| \geq \frac{4\beta_2 c_g}{\gamma^2} \tag{6.54}$$

Let $c_\zeta$ and $T$ be any two positive constant scalars. Consider the set $\Omega = \{\zeta : \mathbf{V}(\zeta) \leq \gamma^{-3}{c_\zeta}^2\beta_1\}$. For any $\zeta \in \Omega$ one has $\|\zeta\|^2 \leq \gamma\beta_1^{-1}\mathbf{V}(\zeta) \leq (c_\zeta\gamma^{-1})^2$. On the other hand, if $\zeta \notin \Omega$ and if we pick $\gamma \geq 4{\beta_1}^{-\frac{1}{2}}{\beta_2}^{\frac{3}{2}}c_g{c_\zeta}^{-1}$ then :

$$\|\zeta\|^2 \geq {\gamma_2}^{-1}\mathbf{V}(\zeta) > \gamma^{-2}{c_\zeta}^2\beta_1{\beta_2}^{-1} \geq 16{\beta_2}^2{c_g}^2\gamma^{-4}. \tag{6.55}$$

It follows that for all $\zeta \notin \Omega$ one has $\dot{\mathbf{V}}(\zeta) \leq -\frac{\gamma}{2\beta_2}\mathbf{V}(\zeta)$, Which means $\zeta$ must enter $\Omega$ before the following time:

$$T^* = \frac{2\beta_2}{\gamma}\ln(\frac{\gamma\mathbf{V}(\zeta(0))}{\beta_1 c_\zeta^2}). \tag{6.56}$$

which can be tuned arbitrary small by increasing the value of $\gamma$. The following result immediately follows:

$\forall c_\zeta, T > 0, \forall\zeta(0).\exists\gamma_1 \geq 1$ s.th $\gamma \geq \gamma_1 \implies \|\zeta(t)\| \leq \gamma^{-1}c_\zeta, \forall t \geq T.$

Now consider the following Lyapunov function candidate :

$$\mathbf{W}(\zeta, \tilde{R}) = \mathbf{V}(\zeta) + \mathbf{V}_2(\tilde{R}). \tag{6.57}$$

Where $\mathbf{V}_2(\tilde{R}) = \frac{1}{2}\operatorname{tr}(M_0 - \tilde{R}M_0)$ and $M_0 = \rho_1 m_I {m_I}^\top + \rho_2 a_I {a_I}^\top$.

One can verify that :

$$\dot{\mathbf{W}} \leq -k_1\sigma_2^\top\Psi_{(2)} - \frac{-\gamma}{2\beta_2}\mathbf{V}(\zeta). \quad \forall\|\zeta\| \geq \frac{4\beta_2 c_g}{\gamma^2} \tag{6.58}$$

$\mathbf{W}$ shows that the proposed nonlinear observer guarantees the convergences and the asymptotic stability of the zero estimation errors, for $t \geq T$ and angles errors less than $180°$.

### 6.4.2 Numerical Simulation

#### Navigation Using 3 UWB Anchors

In this section, we implement the nonlinear observers defined in section 6.4 to estimate the vehicle full state using 3 range measurements. Consider a vehicle navigating in inertial frame following this trajectory:

$$p(t) = \begin{bmatrix} \sin(\pi/3)\sin(2kt)/2 \\ \cos(\pi/3)\sin(2kt)/2 \\ 3+\cos(kt) \end{bmatrix}, k = 0.5. \tag{6.59}$$

The angular velocity applied to the vehicle is given by:

$$\omega(t) = \begin{bmatrix} 0.3\cos(\pi t/10) \\ 0.5\cos(2\pi t/10+\pi/4) \\ 0.8\cos(4\pi t/10) \end{bmatrix}. \tag{6.60}$$

With an initial attitude $R(0) = \exp(\frac{\pi}{2}[e_2]_\times)$. The inertial earth's magnetic field is taken as$m_I = [0.42; 0.2949; 0.15]^\top$Gauss, and the earth's gravity is $g = 9.81 m/s^2$. The initial conditions of the observer are $\hat{x} = [0,0,2,0,0,0]^\top$. $\hat{R}(0) = I_3$ and $K_0 = PC^\top Q$ with $P$ is the solution of the algebraic Riccati equation $PA + A^\top P + V - PCQ^{-1}C^\top P = 0$ with $Q = 1.5 \times I_3$ and $V = 0.15 \times I_6$, and the parameters are taken as $\rho_1 = 2/6, \rho_2 = 2, k_1 = 0.5, \gamma = 5$ and $\hat{c}_2 = 15$. The measurement noises are modelled as a Gaussian white noises with variances, $\sigma_\omega = 0.16(deg/s^2)$,$\sigma_{acc} = 3.10^{-4}(m/s^2)$ and $\sigma_{mag} = 0.025(Gauss)$.

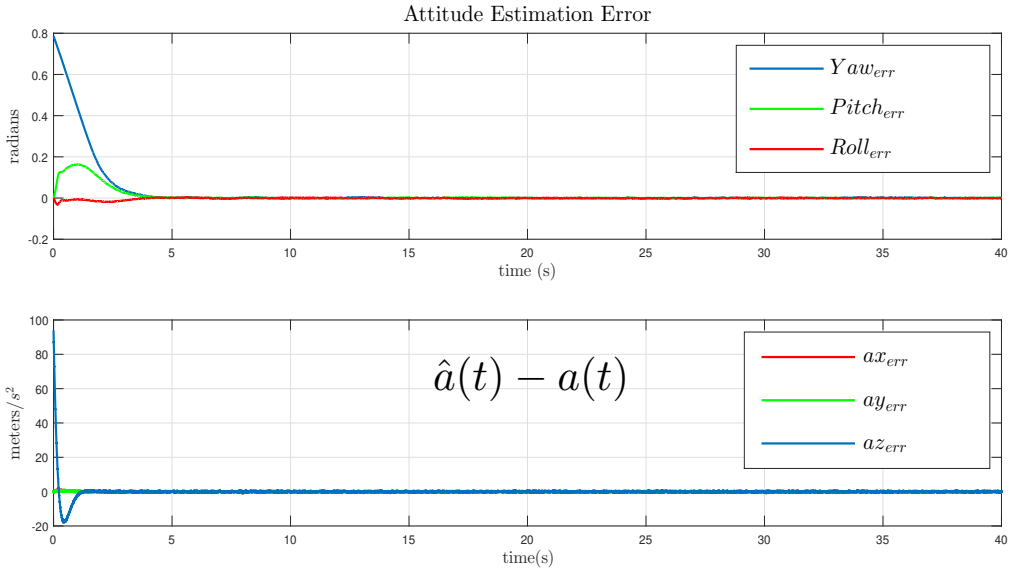


Figure 6.4: Attitude and acceleration estimation error versus time with the constant gain observer using 3 range measurements

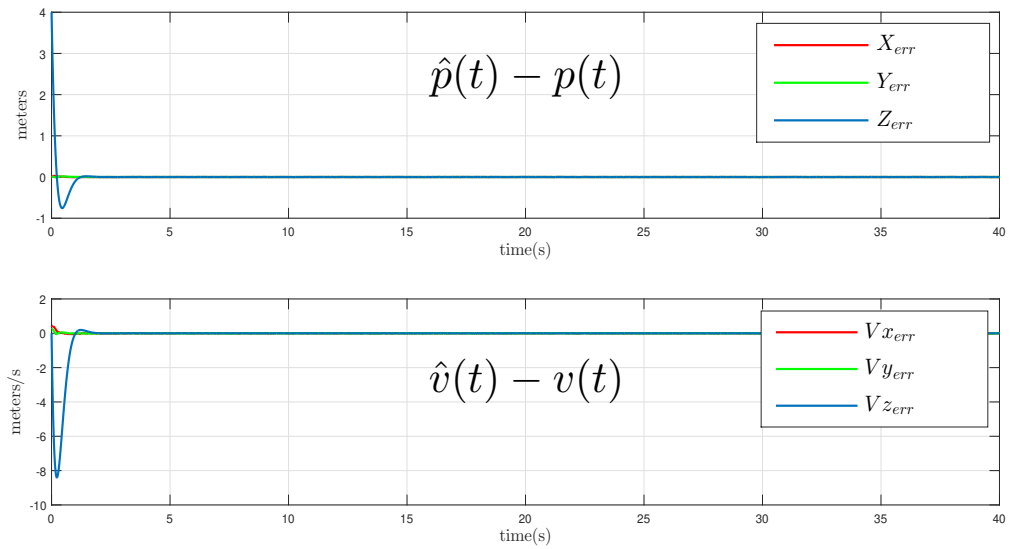


Figure 6.5: Position and velocity error versus time with the constant gain observer using 3 range measurements

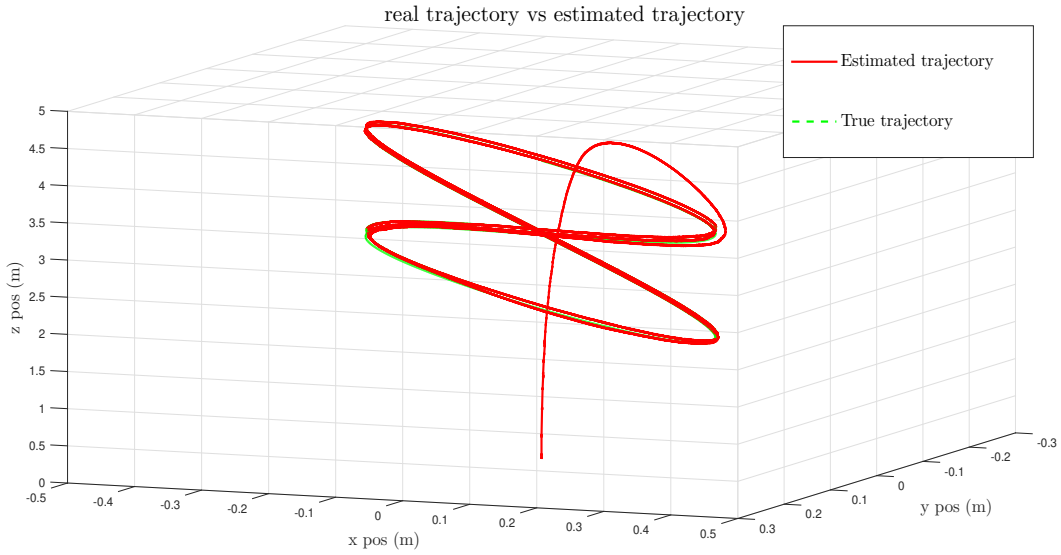


Figure 6.6: estimated trajectory with the constant gain observer using 3 range measurements

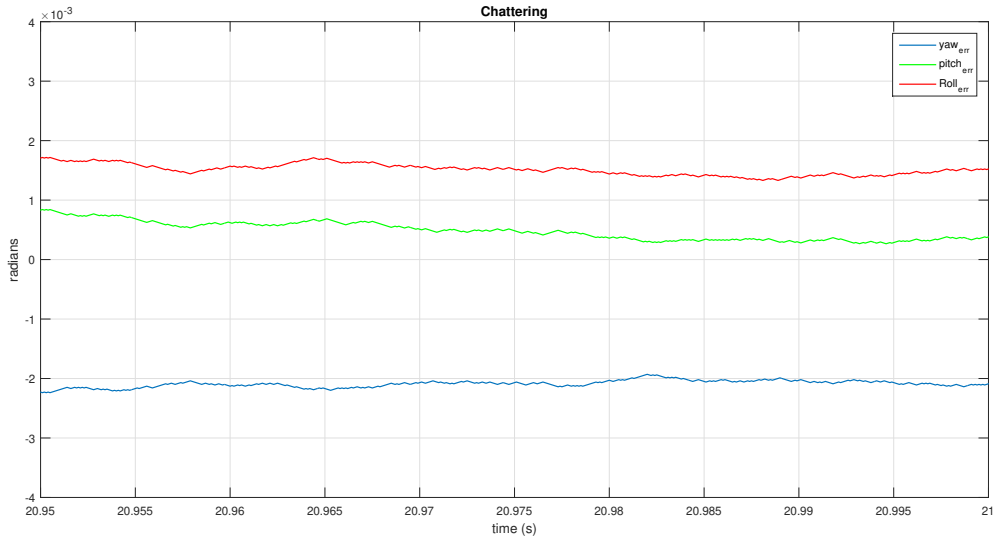


Figure 6.7: Attitude Chattering phenomenon

### Navigation using 2 UWB and an altimeter

Same as the previous subsection, we implement the observers defined in section 6.4 to estimate the vehicle full state using 2 range measurements and an altimeter. Consider a vehicle navigating in inertial frame following this trajectory:

$$p(t) = \begin{bmatrix} 1.5 + 1.5\sin(2\pi t/T) \\ 2.5 + 1.5\cos(2\pi t/T) \\ 1.25 + \frac{1.5}{2}\sin(2\pi t/T) \end{bmatrix}, T = 30. \tag{6.61}$$

The angular velocity applied to the vehicle is given by:

$$\omega(t) = \begin{bmatrix} 0.3\cos(\pi t/10) \\ 0.5\cos(2\pi t/10 + \pi/4) \\ 0.8\cos(4\pi t/10) \end{bmatrix}, \tag{6.62}$$

and taking the same conditions and constants.

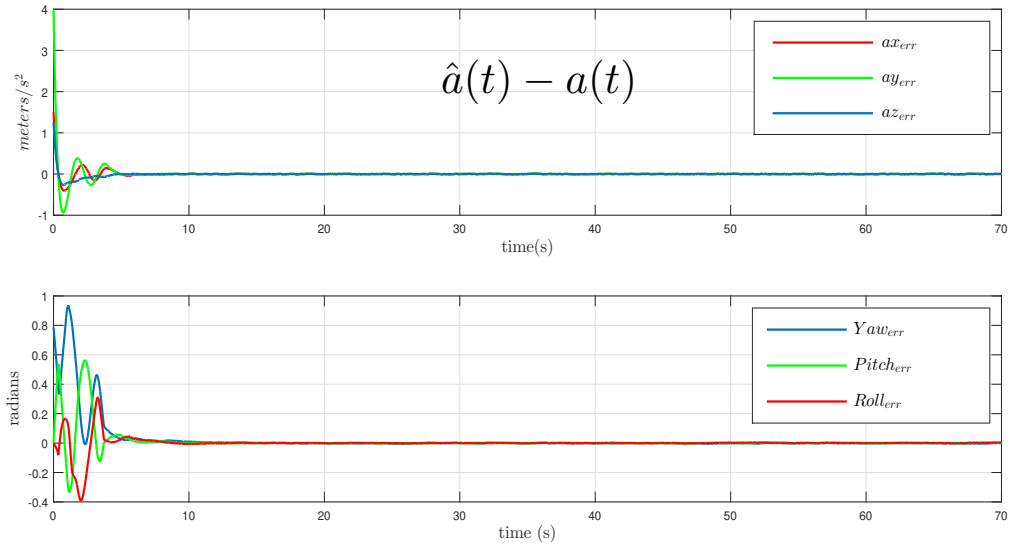


Figure 6.8: Attitude and acceleration estimation error versus time with the constant gain observer using 2 range measurements and an altimeter

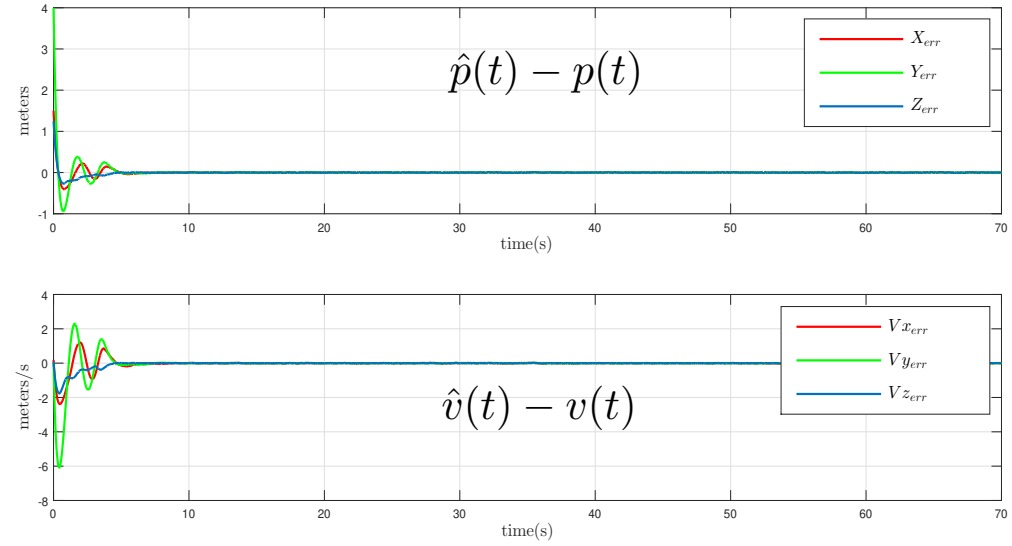


Figure 6.9: Position and velocity error versus time with the constant gain observer using 2 range measurements and an altimeter

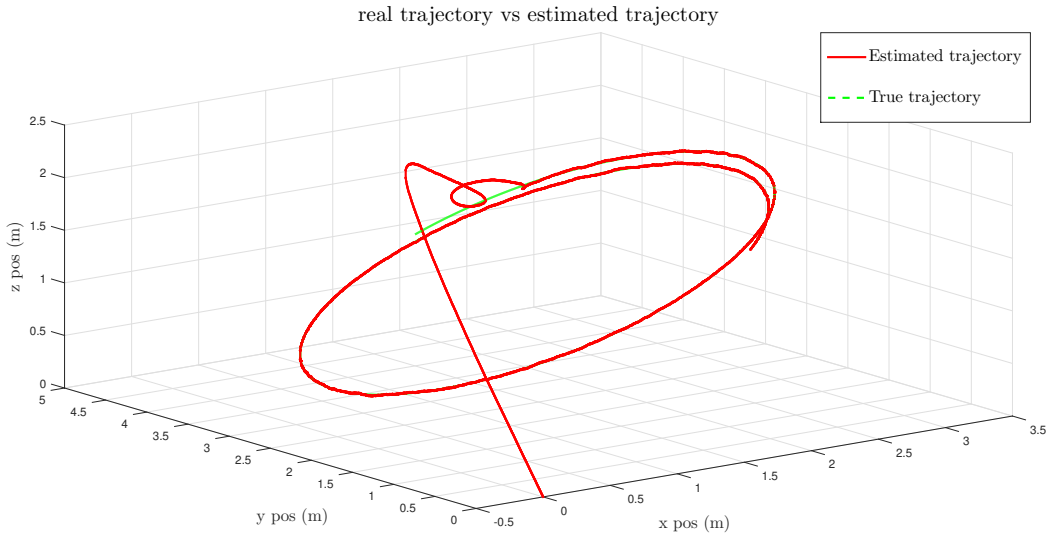


Figure 6.10: estimated trajectory with the constant gain observer using 2 range measurements and an altimeter

### 6.4.3 Comparison Study

In this section we will compare the converging speed of the two full state nonlinear observers defined in the previous section. Let us consider the same simulation scenarios with the same constants :

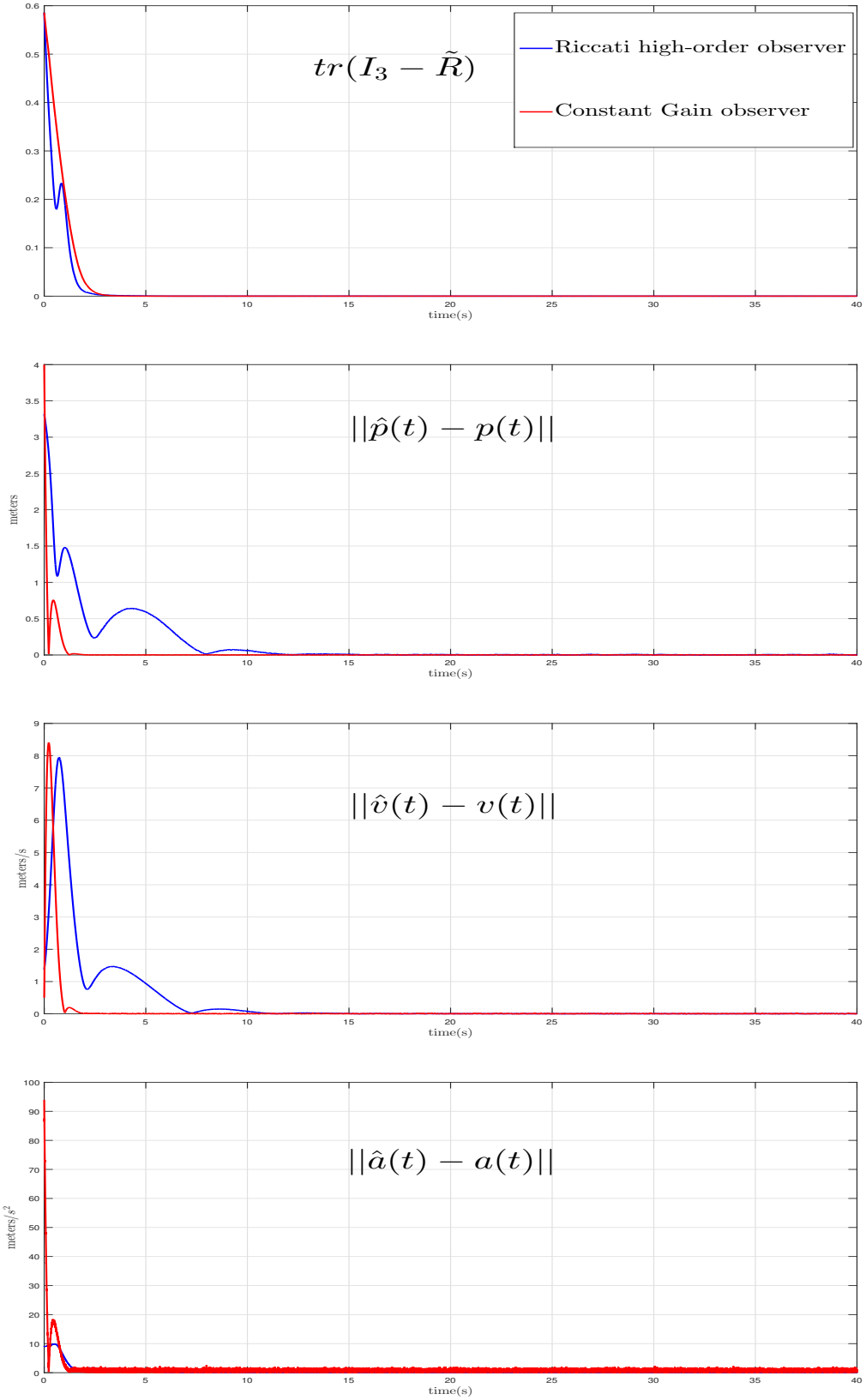


Figure 6.11: Comparison between the Riccati high-order observer and the modified constant gain observer

As we can see in thee figures the Riccati high-order observer showed very good result and a better noise filtering than the constant gain observer, but it is more computationally demanding due to the state augmentation. However, the modified constant gain observer with $\Psi$ function decreases the convergences time and insures a faster convergences than the other observers, still, chattering phenomenon occurs due to the sliding mode observer as shown in the numerical simulation section.

## 6.5 Full State Estimation Comparison Study

In this section, we will compare the full state estimation observers and methods in different simulation scenarios to prove the effectiveness of the nonlinear full state observers proposed and studied in chapter 6. In the first section, we will simulate the simple, yet ineffective way to obtain the position analytically directly from the UWB ranges measurements as shown in Chapter 4. In subsection 2, we will consider a scenario where the vehicle performs near to zero accelerations and compare the Complimentary-Kalman filter approach with the two nonlinear observers presented in Chapter 6. In subsection 3, we will consider an accelerated scenario and we will compare the three observers to demonstrate the limitations of the approaches presented in Chapter 5 and the effectiveness of the nonlinear deterministic observers presented in Chapter 6.

### 6.5.1 Position Reconstruction

In this subsection, we assume 4 non co-planar UWB anchors are deployed, and the position is reconstructed directly from the range measurements of the 4 anchors as shown in Chapter 4. Let us consider a vehicle navigating in inertial frame following this trajectory :

$$p(t) = \begin{bmatrix} 1.5 + \frac{1}{2}\sin\left(2\pi t/T\right) \\ 2.5 + \frac{1}{2}\cos\left(2\pi t/T\right) \\ 1.25 + \frac{1}{4}\cos(2\pi t/T) \end{bmatrix}, T = 30. \tag{6.63}$$

Note that the range measurements are corrupted by noise, modelled as a Gaussian white noise with variance $\sigma_{uwb} = 10cm$.

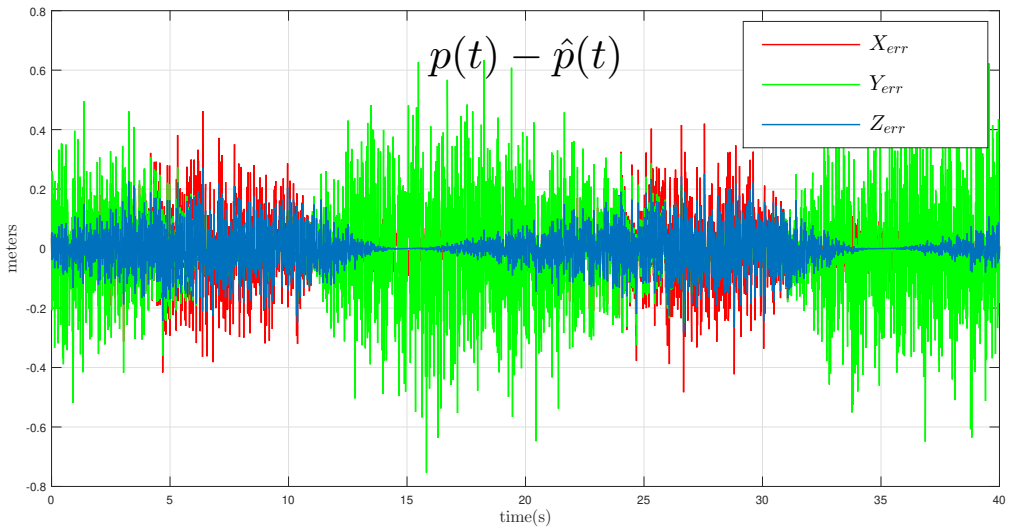


Figure 6.12: Position error versus time using position reconstruction directly from UWB

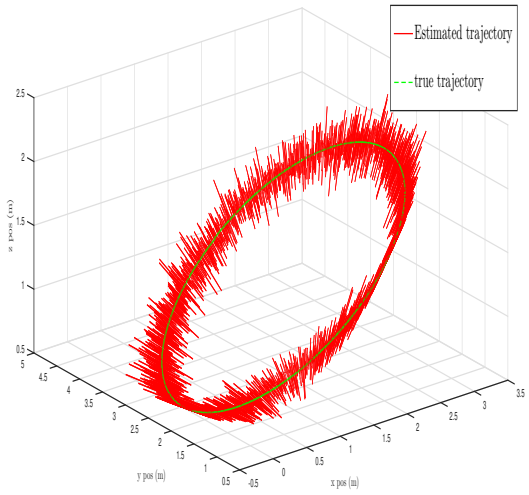


Figure 6.13: Reconstructed trajectory directly from UWB

Although this method seems simplistic, it offers no form of filtering for noisy measurements and as such will not produce reliable result as seen in the figure above. However, the output of this method are often used as input measurements for state observers to obtain a reliable filtered estimations as it is seen in chapter 5 and chapter 6.

### 6.5.2 Non Accelerated Trajectory

In this subsection, we assume a non accelerated scenario and compare the three full state observers :The complimentary-Kalman filter, the Riccati high-order observer and the constant gain observer. Let us consider a vehicle navigating in inertial frame following this low accelerated trajectory :

$$p(t) = \begin{bmatrix} 1.5 + \frac{1}{2}\sin(2\pi t/T) \\ 2.5 + \frac{1}{2}\cos(2\pi t/T) \\ 1.25 + \frac{1}{4}\cos(2\pi t/T) \end{bmatrix}, T = 100. \tag{6.64}$$

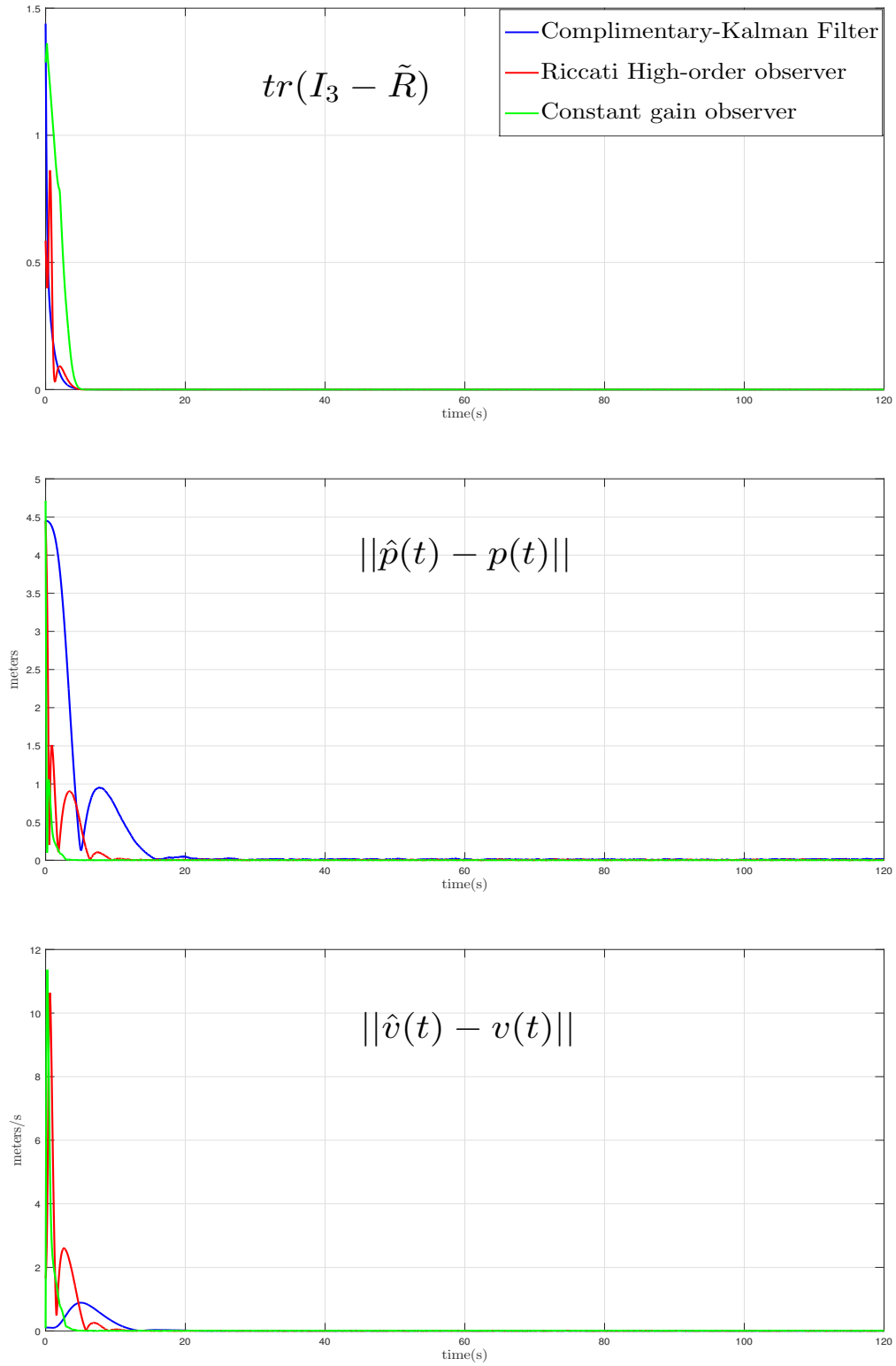


Figure 6.14: Comparison between the complimentary-Kalman filter, the Riccati high-order observer and the constant gain observer in the case of non accelerated vehicles

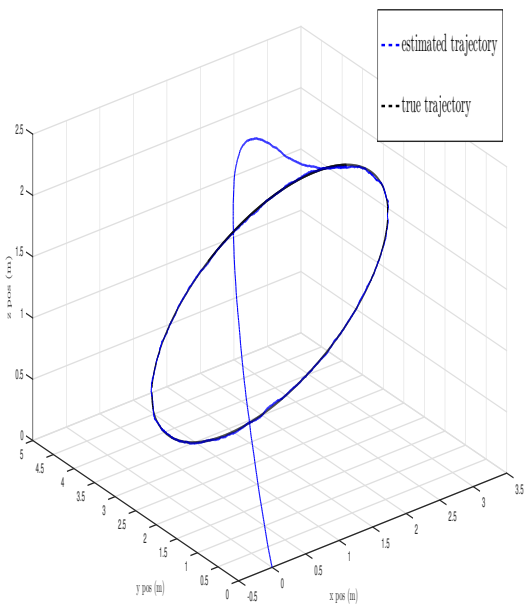


(a) Complimentary with Kalman

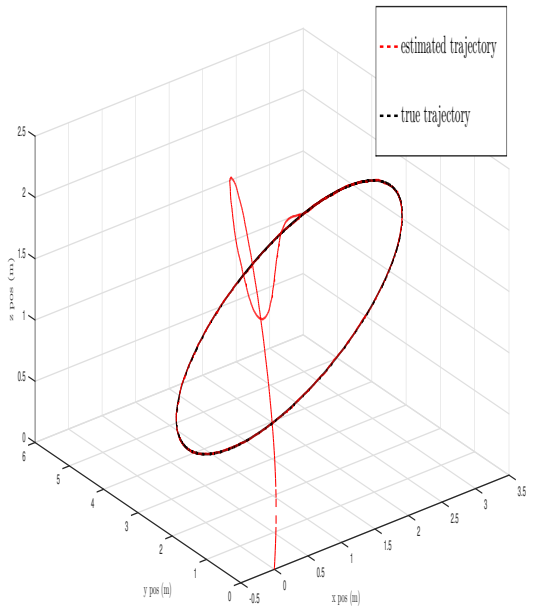


(b) Riccati High-order observer

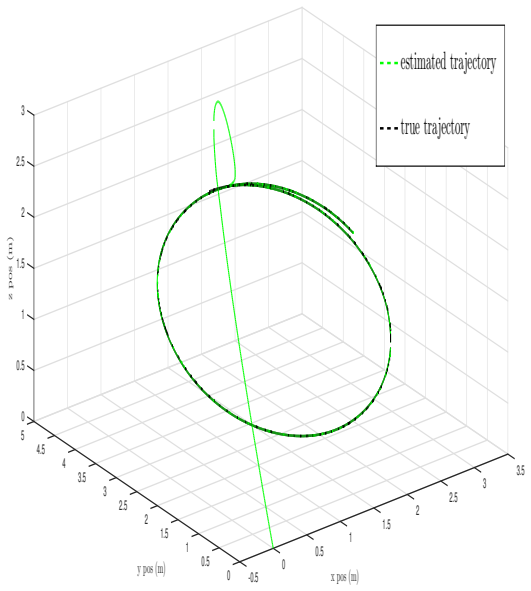


(c) Constant gain observer

Figure 6.15: Estimated trajectory vs real trajectory in the case of non accelerated vehicles

### 6.5.3 Accelerated Trajectory

In this subsection, we assume two accelerated scenarios and compare the three full state observers : The complimentary-Kalman filter, Riccati high-order observer and constant gain observer. In the first scenario, we consider a vehicle navigating in inertial frame following this accelerated trajectory :

$$p(t) = \begin{bmatrix} 1.5 + \frac{1}{2}\sin(2\pi tT/) \\ 2.5 + \frac{1}{2}\cos(2\pi t/T) \\ 1.25 + \frac{1}{4}\cos(2\pi t/T) \end{bmatrix}, T = 5. \tag{6.65}$$

The angular velocity applied to the vehicle is given by:

$$\omega(t) = \begin{bmatrix} 0.3\cos(\pi t/10) \\ 0.5\cos(2\pi t/10 + \pi/4) \\ 0.8\cos(4\pi t/10) \end{bmatrix}. \tag{6.66}$$

Second scenario, we will consider a case where the acceleration increases with time and the same angular velocity is applied :

$$p(t) = \begin{bmatrix} 1.5 + \frac{1}{2}\sin(2\pi tT/) \\ 0.4t^3/6 \\ 1.25 + \frac{1}{4}\cos(2\pi t/T) \end{bmatrix}, T = 25. \tag{6.67}$$

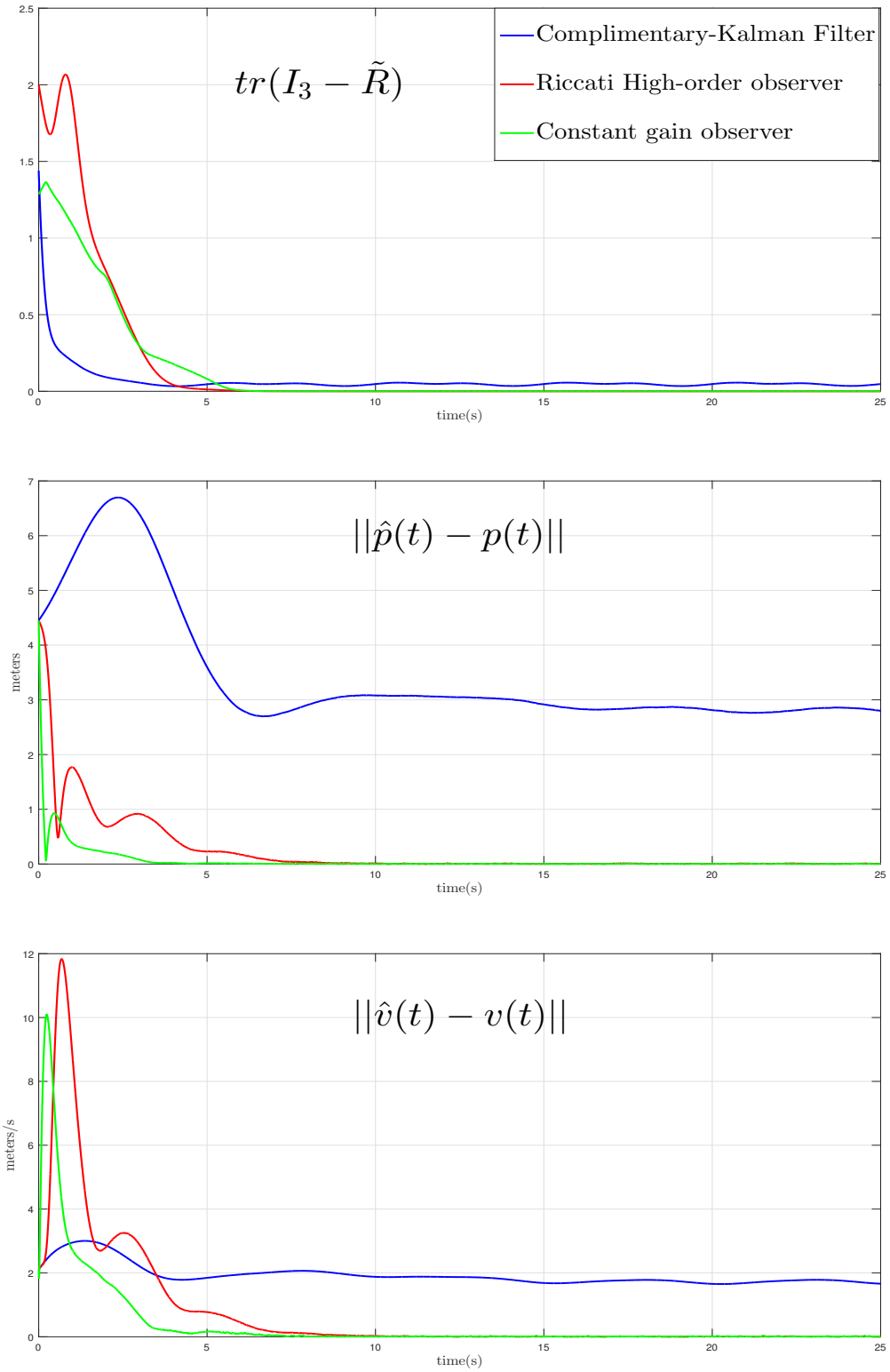


Figure 6.16: Comparison between the complimentary-Kalman filter, the Riccati high-order observer and the constant gain observer in the case of accelerated vehicles

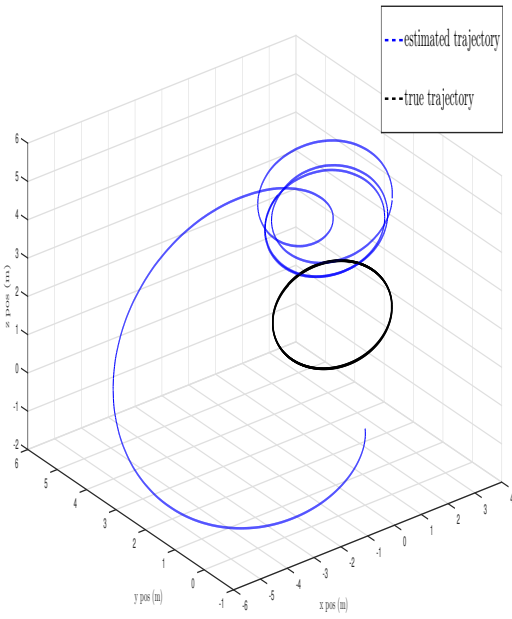


(a) Complimentary with Kalman

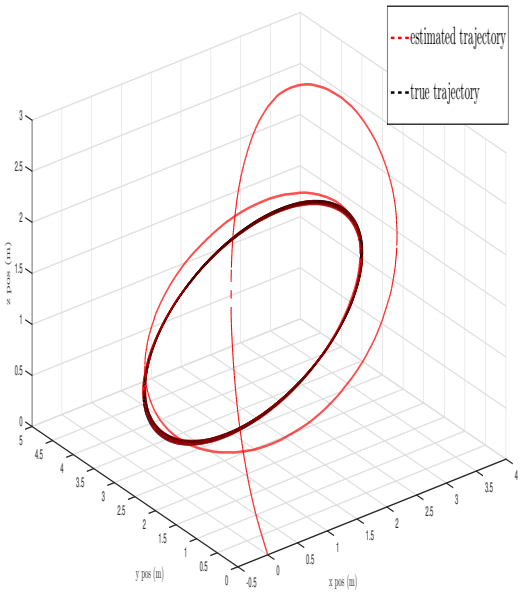


(b) Riccati High-order observer

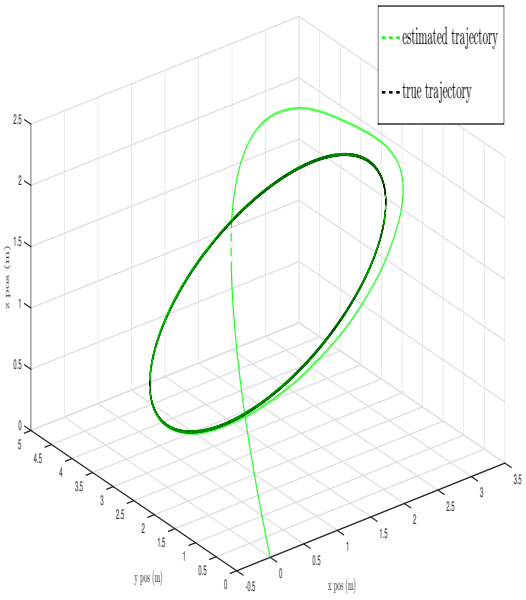


(c) Constant gain observer

Figure 6.17: Estimated trajectory vs real trajectory in the case of accelerated vehicles

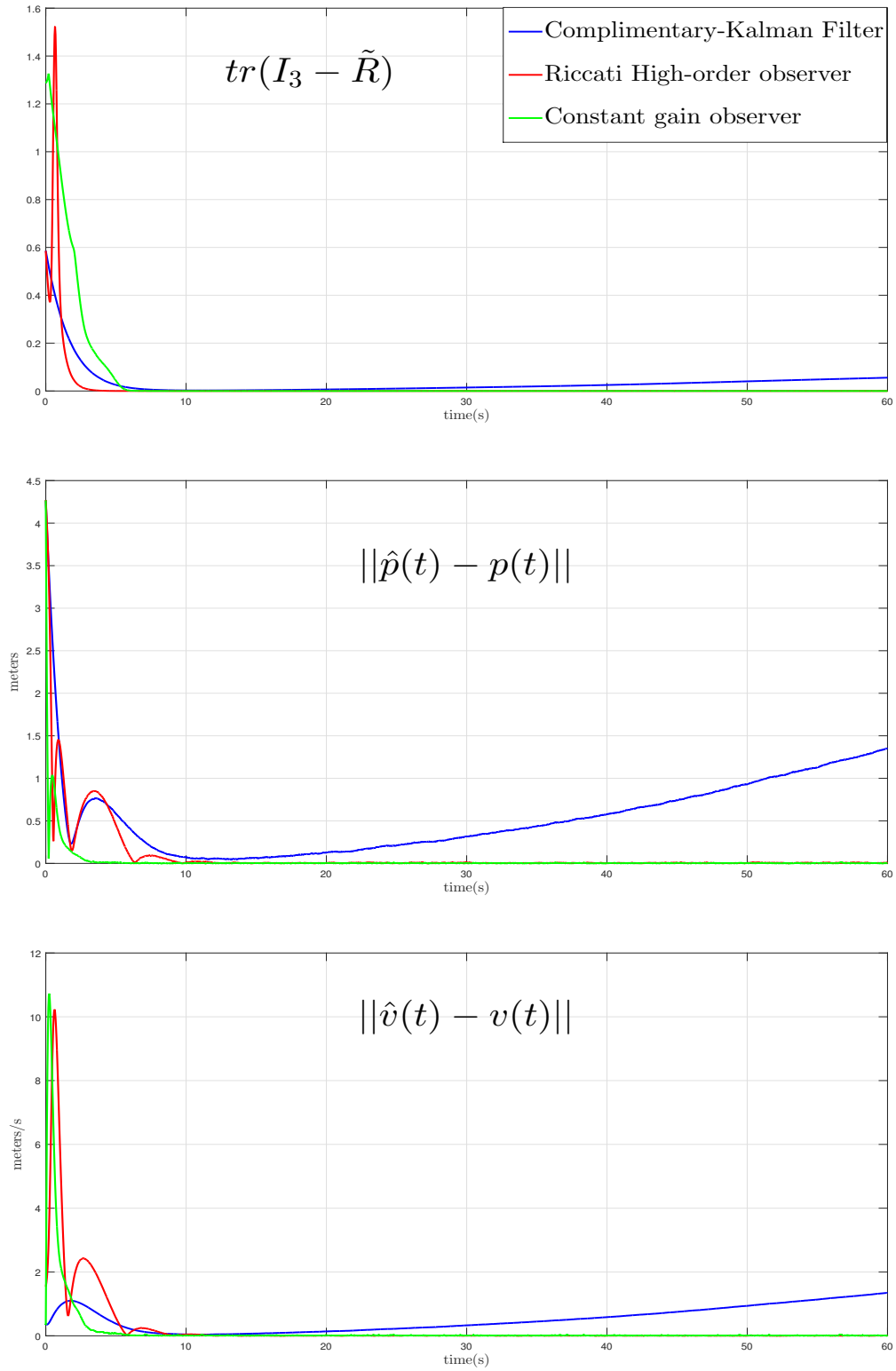


Figure 6.18: Comparison between the complimentary-Kalman filter, the Riccati high-order observer and the constant gain observer in the case where the acceleration increases with time

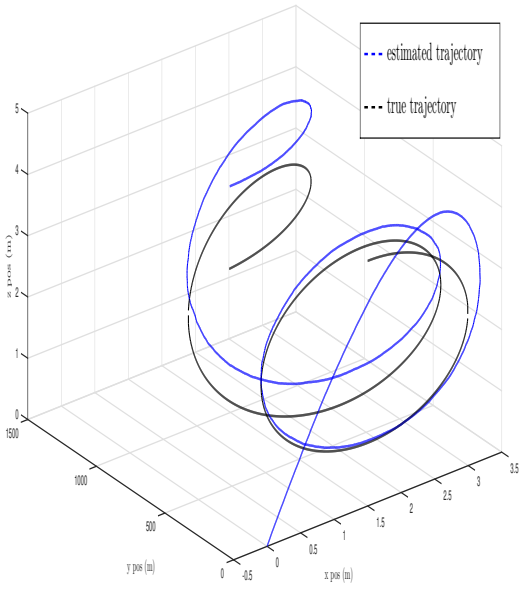


(a) Complimentary with Kalman

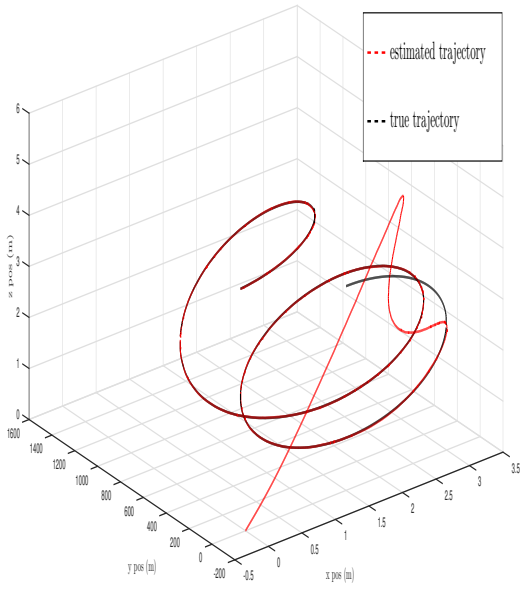


(b) Riccati High-order observer

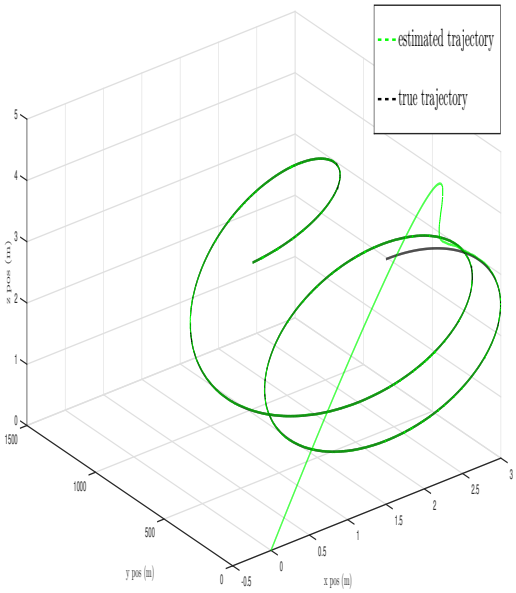


(c) Constant gain observer

Figure 6.19: Estimated trajectory vs real trajectory in the case where the acceleration increases with time

## 6.6 Conclusion

In this chapter, we proposed two nonlinear complete state observers. The proposed observers require the use of vector measurements from IMU and some position information from the UWB. The stability of the nonlinear Riccati high-order observer and the standard constant observer were discussed and proved. Furthermore, we compared these nonlinear full state observers with the complimentary-Kalman filter and a position reconstruction to show the advantages of these observers. All of the compared methods require also the use of UWB range measurements. The position reconstruction method proved to be unreliable as it contains no form of noise filtering as shown in the simulation. The other three observers were compared in different navigation scenarios as follows :

- First, by considering a low accelerated trajectory, all the three observers converged and gave good results and noise filtering. However, the converging speed of the complimentary-Kalman filter was slower then the two other deterministic nonlinear observers.
- Second, by considering an accelerated trajectory where the complimentary-kalman filter showed very poor unreliable results for attitude, position and velocity while the other two nonlinear observers gave excellent results in both convergence speed and noise filtering.
- Finally, we considered a trajectory that increases its acceleration with time, as shown in the simulation figures, the complimentary-Kalman filter converges at slow acceleration, then diverges and give poor results as the acceleration increases. The other two nonlinear observers gave excellent results in both convergence speed and noise filtering.

CHAPTER 7

# General Conclusion

State estimation for Unmanned Aerial Vehicles is a key step to achieve reliable control and autonomous flight. The use of nonlinear state observers that rely on the nonlinearity of the vehicle's model proved to be reliable and solved the problems encountered when using stochastic observers that rely on linearization assumptions. In this thesis, the full state estimation problem is considered when using IMU and UWB measurements.
As first, we presented the mathematical tools and background needed in this thesis. we defined then the mathematical model of rigid body in space.
After that, we studied and proposed different nonlinear attitude observers that gives the attitude estimation directly on the special orthogonal group $\mathbb{SO}(3)$, a comparison study between these observers in the case of measurement anomalies is done at the end of the chapter to illustrate the effectiveness of the proposed observers.
Furthermore, the UWB technology is presented and position measurements reconstruction methods are proposed in the case of using less than 4 UWB anchors.
Moreover, the full state estimation problem for non accelerated vehicles is considered and two estimation approaches are studied and compared in the case of vehicles performing near to hover accelerations.
Finally, two nonlinear observers are studied and discussed in the case of accelerated vehicles, a comparison study in different scenarios is done at the end to show the limitation of the classical non accelerated vehicles observers and the effectiveness of the two nonlinear observers.

**Futur Outlook**

As a future work, it would be interesting to implement these estimation methods with nonlinear control laws in a real physical system. Another interesting work would be to combine these estimation and control laws with obstacle avoidance algorithms and methods to achieve a fully autonomous navigation system for different aerial vehicles.

# Bibliography


[1] Benini, A., Mancini, A., and Longhi, S. An imu/uwb/vision-based extended kalman filter for mini-uav localization in indoor environment using 802.15.4a wireless sensor network. *J Intell Robot Syst 70* (2013), 461–476.

[2] Berkane, S. *Hybrid Attitude Control and Estimation On SO(3)*. PhD thesis, Electronic Thesis and Dissertation Repository. 5083, 2017.

[3] Berkane, S., and Tayebi, A. On the design of attitude complementary filters on SO(3). *IEEE Transactions on Automatic Control 63*, 3 (2018), 880–887.

[4] Berkane, S., and Tayebi, A. Position, velocity, attitude and gyro-bias estimation from imu and position information. In *2019 18th European Control Conference (ECC)* (2019), pp. 4028–4033.

[5] Berkane, S., and Tayebi, A. Navigation observers using imu and position information. In *Submitted, 2020.* (2030).

[6] Black, H. D. A passive system for determining the attitude of a satellite. *AIAA Journal 3*, 7 (1964), 1350–1351.

[7] d. Hua, M. Attitude estimation for accelerated vehicles using gps/ins measurements,. *Control Engineering Practic 18*, 7 (2010), 723–732.

[8] Farrell, J. L., Stuelpnagel, J. C., Wessner, R. H., Velman, J. R., and Brook, J. E. A least squares estimate of satellite attitude (grace wahba). *SIAM Review 8*, 3 (1965), 384–386.

[9] Foster, C. C., and Elkaim, G. H. Extension of a two-step calibration methodology to include nonorthogonal sensor axes. *IEEE Transactions on Aerospace and Electronic Systems 44*, 3 (2008), 1070–1078.

[10] Hua, M., Ducard, G., Hamel, T., Mahony, R., and Rudin, K. Implementation of a nonlinear attitude estimator for aerial robotic vehicles. *IEEE Transactions on Control Systems Technology 22*, 1 (2014), 201–213.

[11] Hua, M.-D., Ducard, K. R. G., Hamel, T., and Mahony, R. Nonlinear attitude estimation with measurement decoupling and anti-windup gyro-bias compensation. *IFAC Proceedings Volumes 44*, 1 (2011), 2972–2978.

[12] Jiménez, A., Seco, F., and Zampella, F. Indoor localization of persons in aal scenarios using an inertial measurement unit (imu) and the signal strength (ss) from rfid tags. in: Chessa s., knauth s. (eds) evaluating aal systems through competitive benchmarking. evaal 2012. *Communications in Computer and Information Science. Springer, Berlin, Heidelberg 362* (2013), 32–51|.

[13] Kalman, R. E. A new approach to linear filtering and prediction problems. *Journal of Basic Engineering 82*, 1 (1960), 35–45.

[14] Mahony, R., Hamel, T., and Pflimlin, J. Nonlinear complementary filters on the special orthogonal group. *IEEE Transactions on Automatic Control 53*, 5 (2008), 1203–1218.

[15] Mahony, R., Hamel, T., Trumpf, J., and Lageman, C. Nonlinear attitude observers on so(3) for complementary and compatible measurements: A theoretical study. In *Proceedings of the 48h IEEE Conference on Decision and Control (CDC) held jointly with 2009 28th Chinese Control Conference* (2009), pp. 6407–6412.

[16] Markley, F. L. Attitude error representations for kalman filtering. *Journal of guidance, control, and dynamics 26*, 2 (2003), 311–317.

[17] Martin, P., and Salaiin, E. Design and implementation of a low-cost observer-based attitude and heading reference system. *Control Engineering Practice 18*, 7 (2010), 712–722.

[18] Parv, L. *The Story Behind UWB Technology and Indoor Positioning*. Eliko, 2017.

[19] Pin, G., Chen, B., and Parisini, T. Robust finite-time estimation of biased sinusoidal signals: A volterra operators approach. *Automatica 77* (2019), 120–132.

[20] Rezaei, S., and Sengupta, R. Kalman filter-based integration of dgps and vehicle sensors for localization. *IEEE Transactions on Control Systems Technology 15*, 6 (2007), 1080–1088.

[21] Roberts, A., and Tayebi, A. On the attitude estimation of accelerating rigid-bodies using gps and imu measurements. In *2011 50th IEEE Conference on Decision and Control and European Control Conference* (2011), pp. 8088–8093.

[22] Titterton, D., Weston, J. L., , and Weston, J. *Strapdown inertial navigation technology*. IET, 2004.

[23] Woodman, O. J. An introduction to inertial navigation. Tech. Rep. UCAM-CL-TR-696, University of Cambridge, Computer Laboratory, Aug. 2007.

[24] y. Bar-Itzhack, I., and Oshman, Y. Attitude determination from vector observations: Quaternion estimation. *IEEE Transactions on Aerospace and Electronic Systems AES-21*, 1 (1985), 128–136.